Investigations of a Novel Manganite Oxyfluoride and Other Ceramic Materials

by

Ashley M. Wolf

Submitted in Partial Fulfillment of the Requirements

for the Degree of

Master of Science

in the

Chemistry

Program

YOUNGSTOWN STATE UNIVERSITY

December, 2011

Investigations of a Novel Manganite Oxyfluoride and Other Ceramic Materials

By

Ashley M. Wolf

I hereby release this thesis to the public. I understand that this thesis will be made available from the OhioLINK ETD Center and the Maag Library Circulation Desk for public access. I also authorize the University or other individuals to make copies of this thesis as needed for scholarly research.

Signature:

Ashley M. Wolf, Student Date

Approvals:

Dr. Timothy R. Wagner, Thesis Advisor Date

Dr. Daryl Mincey, Committee Member Date

Dr. Sherri Lovelace-Cameron, Committee Member Date

Dr. Peter J. Kasvinsky, Date
Dean of School of Graduate Studies and Research

Abstract

Perovskite-type compounds are among the most important of inorganic solid-state materials, and exist in a wide variety of compositions with related crystal structures. These variations allow perovskite-type materials to display many important and useful properties, such as superconductivity, dielectrics, and colossal magnetoresistance. A primary goal of this thesis is to prepare an oxyfluoride analog of (Ca, La)MnO_3, known for its colossal magnetoresistive properties, and determine the effect of anion substitution on the magnetic properties of this material. The novel compound targeted for synthesis in this study is $Ca_2Mn_2O_5F$, which achieves a mixed Mn^{+3}/Mn^{+4} oxidation in the lattice via anion rather than cation substitution, as is the usual case. This mixed oxidation is an important feature of manganite oxides displaying colossal magnetoresistance. A four-step process was proposed in order to synthesize the target oxyfluoride compound, and will be described in detail. While the first step was successfully completed, subsequent steps were not. These attempts will be summarized along with the conclusions from this study and suggestions for future work.

A second project discussed in this thesis is the Research Experiences to Enhance Learning (REEL) project, based on a state-wide initiative centered at the Ohio State University to introduce meaningful research experiences into the first and second year chemistry curriculum The YSU-developed REEL modules focus on perovskite-type compounds, and specifically for this study on solid solutions of $KCuF_3$ with $KNiF_3$ and $KMnF_3$. Thus the focus of the work was on the two series of compositions, $K(Cu_xNi_{1-x})F_3$ and $K(Cu_xMn_{1-x})F_3$ for $x = 0, 0.1, 0.2 \ldots 0.9, 1.0$. These two sets of compounds were prepared by students enrolled in the second semester general chemistry laboratory course during the Spring 2010 and Fall 2010 semesters. Students analyzed their compounds using X-ray Powder Diffraction (XRPD), UV-Vis Spectrometry, and X-ray Fluorescence (XRF) techniques under the guidance of this thesis author. The final data was then further analyzed and quantitatively refined in this study using Rietveld powder refinement methods. From the results, the solubilities of the cubic $KNiF_3$ and $KMnF_3$ phases in tetragonal $KCuF_3$ were determined, and compared to results of previous studies on the $K(Cu_xCo_{1-x})F_3$ and $K(Cu_xMg_{1-x})F_3$ systems.

Acknowledgements

To my advisor Dr. Timothy Wagner, I could never thank you enough for all of your guidance, patience and endless amounts of knowledge that you have given me during my time at YSU. To my committee members Dr. Daryl Mincey and Dr. Sherri Lovelace-Cameron, thank you for your time and input. A special thanks to Dr. Matthias Zeller for sharing your infinite amount of knowledge and spending countless hours teaching me how to analyze all of our data. I would like to thank the YSU Chemistry department and all of the faculty and staff at YSU for accepting me into your program and making YSU feel like a second home.

I would like to thank all of my peers that I meet at YSU who became my second family. Amanda Kotheimer and Travis Battiest, thank you so much for always being there and providing me with retail therapy when I needed it! To Dominic Loiacona, Chad Miller, Tom Rudnicki, Sherri Claypoole and Rick Cuckovich graduate school would not have been the same without all of you. To Caleb Tatebe, thank you for everything I could not have survived Project REEL without all of your help.

I would like to thank all of my family and friends. This thesis could not be possible without all of the love and support from my mom, dad, Walt and Barb. Thank you for being my rock, for always believing in me and pushing me to achieve all of my dreams, I love you all. To Alec, I could not ask for a more

supportive, loving, patient and encouraging boyfriend, thank you for everything I love you.

Finally I would like to dedicate this thesis to my niece and nephews, Justine, Frankie, Dakota and Aaron. I hope to be an inspiration to all of you and to help each of you achieve all of your dreams.

Table of Contents

CHAPTERS

List of Equations

List of Figures

Figure **Page**

List of Tables

Table **Page**

Chapter 1

Introduction to Concepts and Techniques

Solid State Introduction

A convenient way to describe solid-state materials chemistry is through the materials tetrahedron seen in Figure 1.1. This tetrahedron indicates that processing, structure, properties, and performance are all equally important to solid-state chemistry. During processing the compound is being synthesized and everything is important from the purity of the raw materials to the bond type of the product, and finally to the actual reaction that occurred. The structure of a solid-state compound is important because it describes the arrangement of the atoms in 3-dimensional space. Knowing the structure helps in analyzing the compound because one will surmise which properties may be important and therefore which techniques to use for further characterization of the materials. Magnetic, electrical, thermal and optical properties are all specific characteristics of a certain compound, and relate to its potential applications. Finally, the performance of a compound refers to how well the desired properties are maintained over time. In the center of the materials tetrahedron is characterization because this overlaps with each of the four other areas[1].

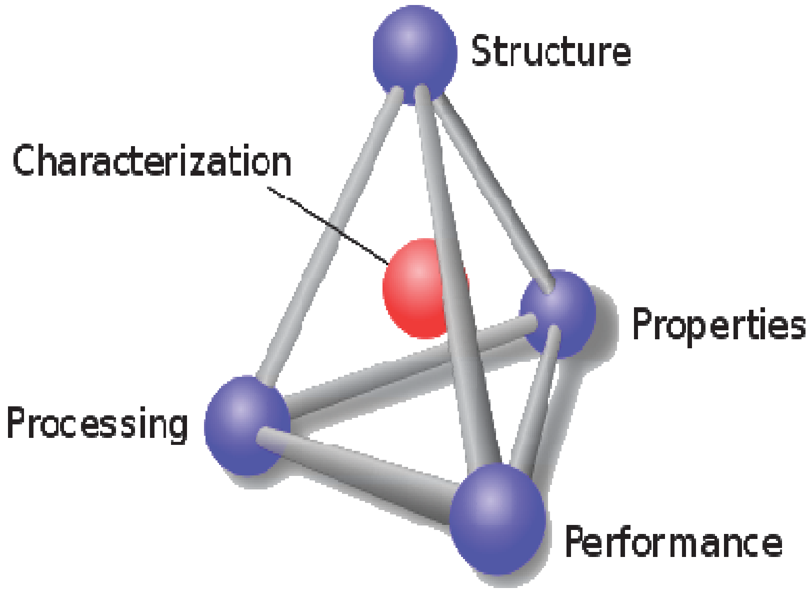

Figure 1.1: The materials tetrahedron[2]

Solid State Synthesis

There are many different methods that can be used to synthesize inorganic solid-state crystalline materials. All of the methods discussed in this introduction have been used in the research for this thesis. One common way to synthesize these materials is to use conventional ceramic methods. Conventional ceramic methods require starting materials to be weighed out in stoichiometric amounts, then thoroughly mixed together and then placed in a pellet press. The materials are thoroughly mixed to ensure that the reactants are in contact with each other during the reaction. A technique used in this research to ensure the compounds were adequately mixed was to create a slurry, which simply involves mixing the starting materials with a liquid that the materials are insoluble in. The slurry is left to evaporate, leaving a well-mixed powder, which can then be ground and made into pellets. The pellets are then typically placed into a crucible or metal boat, for example for this thesis project the pellets were usually placed into a nickel boat and then heated to various temperatures. Once heating is finished the sample is ground and then analyzed via X-ray powder diffraction. If the reaction was not complete the sample is re-pelletized and then reheated until the reaction is complete.

Another common synthesis technique is the sol-gel method, for which partial hydrolysis occurs to first form reactive monomers. These monomers then undergo polycondensation to form colloids. Finally, further hydrolysis occurs, leading to cross-linking and polymerization to form the final gel matrix[3]. The sol-gel method has been of recent interest in synthesizing solid-state materials, especially perovskites. It has been found that the sol-gel method can help synthesize perovskites at lower temperatures than previously reported[4]. Many factors can affect the result of a sol gel synthesis, such as choice of solvent and pH. Solvents typically used to carry out sol-gel reactions include citric acid, acetic acid, and malic acid. With the use of different starting materials and solvents, the pH of the solution may need to be adjusted before an optimal sol-gel can be achieved.

One issue that may arise when synthesizing solid-state inorganic materials is that many of them are air sensitive. When synthesizing such compounds it is very important to take every precaution to avoid air coming in contact with the reactants. This can be accomplished through the use of glove bags, glove boxes and Schlenk lines. Since non-volatile materials were used in this experiment a glove bag was used to create an inert atmosphere. If volatile materials were required then a glove box would have been the better option. A glove bag is a polyethylene bag that can be filled with gases such as argon or nitrogen to create the desired inert atmosphere, and permits all required materials to be placed inside thus ensuring the reaction remains air free from start to finish. A silica tube can also be placed in the glove bag to ensure that the air sensitive materials could be easily transferred to a tube furnace to be heated while still in the inert atmosphere.

Crystal Systems

In the solid state, crystalline materials take on a distribution of atoms in space called the unit cell, which contains the symmetry of the entire material and can be repeated and stacked in a three dimensional shape to give the crystal morphology. Every unit cell has lattice parameters, which are the angles between the edges of the unit cell and the lengths of these edges. The lengths are given by a, b, and c and the angles are given by α, β, and γ. Since every unit cell is not a perfect cube where $a = b = c$ and $\alpha = \beta = \gamma = 90°$ there are seven different crystal classes. These crystal classes account for the different lengths of the edges and the different angles. Other examples of the crystal classes are orthorhombic where $a \neq b \neq c$ and $\alpha = \beta = \gamma = 90°$ and hexagonal where $a = b \neq c$ and $\alpha = \beta = 90°$ and $\gamma = 120°$.

The lattice points that are contained in the unit cell can be arranged in four different ways; simple, body-centered, face-centered and base-centered. A simple lattice has only one lattice point whereas a face centered system has lattice points on all corners and on all face-centers of the unit cell. Combining these four lattice types with the seven crystal classes produces fourteen Bravais lattices, as shown in Figure 1.2.

All crystal structures have symmetry elements consisting of some combination of reflection, rotation, inversion and improper rotation. These symmetry elements operate on a point in the lattice, and for a crystalline substance there are only 32 different combinations of symmetry elements possible, or 32 possible point groups. Crystal structures, with the exception of quasicrystals, also require translational symmetry, meaning that it must be possible to merge unit cells into adjacent ones while leaving the system invariant. There are two translational symmetry operations, known as screw axes and glide planes, and combining these with the 32 point groups yields 230 possible space groups.

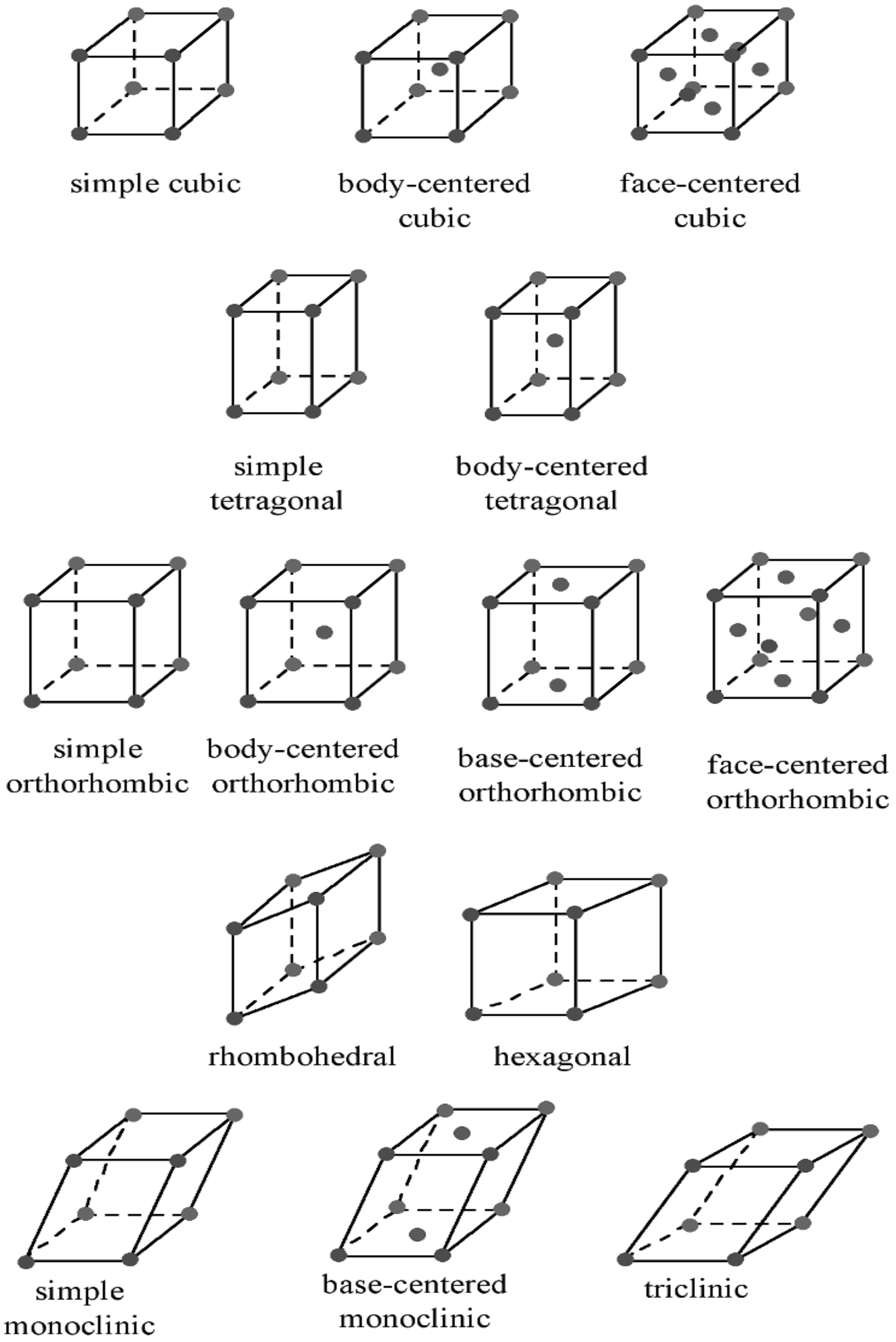

Figure 1.2: The 14 Bravais Lattices [5]

X-ray Powder Diffraction (XRD)

One of the most powerful techniques used to study crystalline materials is X-ray powder diffraction, which can be used to determine the unit cell parameter, phase, purity, or structure of powdered crystalline substances. X-rays are produced using a cathode ray tube, in which high-energy electrons emitted from a tungsten filament, strike a metal target resulting in a release of X-rays characteristic of the target. Typically metal targets used in X-ray powder diffraction are copper and molybdenum, although several others can be used. One way in which the resulting excess energy is relieved is through the release of X-ray radiation as an upper level electron drops to fill in the 1s vacancy. The X-ray energy released is characteristic of the metal target. For a copper target, if the electron from the 2p level replaced a hole in the 1s level, then Kα energy is produced. Kα actually consists of two sub-levels of energy, that is produced, $K\alpha_1$ with a wavelength of 1.54051 Ǻ and $K\alpha_2$ with a wavelength of 1.54433 Ǻ. If an electron from the 3p level dropped to fill the 1s vacancy, then Kβ energy is produced. However since Kα is more intense, Kβ is usually filtered out and in some diffractometers, $K\alpha_2$ is filtered out as well[7].

When the X-rays bombard the sample, the X-rays are diffracted in many directions, and constructive interference occurs when Bragg's Law is satisfied. Bragg's Law was developed by William Lawrence Bragg in an attempt to explain why X-ray beams appear to be reflected at certain angles. Bragg's Law is given in Equation 1.1.

$$2d\sin\theta = n\lambda \qquad \text{Eq. 1.1}^{6}$$

In Bragg's Law d is the distance between adjacent planes of atoms, θ is the angle of incidence of the X-ray beam, n is an integer that represents the order of the diffracted beam, and λ is the wavelength of the X-ray beam. Figure 1.3 depicts the constructive interference that occurs when Bragg's Law is satisfied. As seen in the figure the X-rays strike the sample and are "reflected" off the crystal plane. When Bragg's Law is satisfied these diffracted X-rays are in phase and interfere constructively, otherwise the X-rays interfere destructively and no "reflection" is observed.

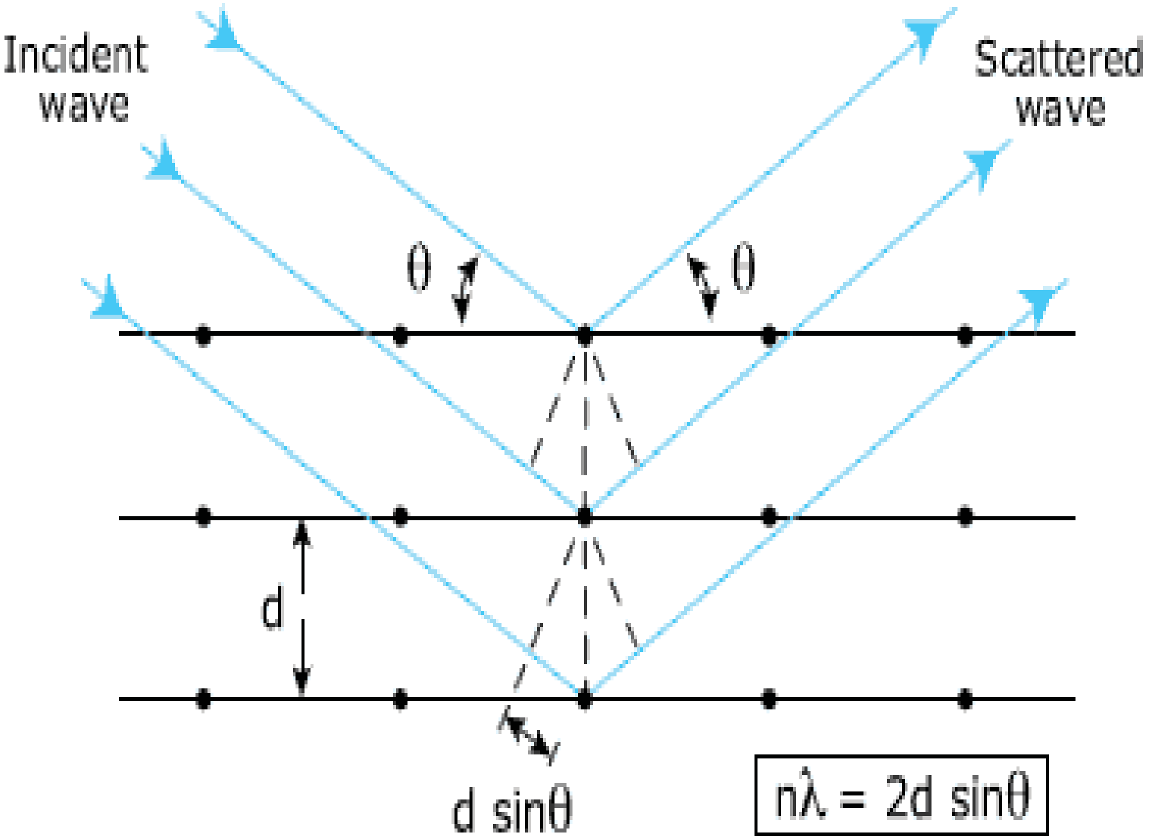

Figure 1.3: Representation of constructive interference that satisfies Bragg's Law[7]

When θ is at the Bragg angle and constructive interference occurs, the resulting peaks are plotted on an powder X-ray diffraction pattern consisting of a plot of peak intensity vs. 2θ. The powder pattern is unique to a sample, somewhat like a fingerprint, and thus can be matched to a database of known materials for identification of an unknown compound.

There are many advantages in using the XRD method for sample characterization. For example, it is a non-destructive technique. When a sample is subjected to the X-rays it is usually not altered in any way and can be used in other techniques after the analysis is complete. Another advantage of XRD is that it can be used to determine if there are any impurities in the sample and can match them to the database to determine what they are. Another advantage is that it does not require a large quantity of sample, which helps in low yield reactions. One disadvantage is that XRD is actually best for identifying single phase materials because if there are multiple phases the 2θ? peaks can overlap and identification can become complicated. However, it is often at least qualitatively possible to identify the phases present in a mixed sample, and in fact perform quantitative refinements in some cases using Rietveld analysis[6]

Rietveld Refinement

Rietveld refinement was developed by Hugo Rietveld as a way to quantitatively analyze X-ray and neutron diffraction patterns. In these patterns there are peaks of intensity that are characteristic of a specific sample. Each of these peaks has a width, shape and position that can be modeled with the least squares approach to refine the pattern. The width of a peak is known to depend on the Bragg angle; at higher Bragg angles peaks are wider. The shape of a peak is manipulated by many factors; the sample size and shape, the beam and arrangement. Rietveld refinement corrects for many factors that affect peak shapes, such as the way the crystals are arranged, the calibration of the instrument, the broadness of peaks, etc. Rietveld refinement is very useful for obtaining a quantitative match of a single-phase pattern to a known compound, or it can be used to determine the percent compositions of phases in a mixture[9].

Thermal Gravimetric Analysis (TGA)

Another technique that was implemented in this thesis was Thermal Gravimetric Analysis (TGA). TGA is an analytical technique used to determine the rate and amount of change in the mass of a material as a function of time or temperature in a controlled atmosphere. Samples analyzed via TGA usually weigh between 5 and 500mg and can be either a liquid or a solid. The sample is heated to a desired temperature up to 1200°C at a desired rate, and can be held constant for a given time at the target temperature. The mass of the sample is recorded at all temperatures and a spectrum of mass versus temperature or mass versus time at a constant temperature is given. A sample can lose or gain weight due to dehydration, oxidation or decomposition when heated. Also different sample environments can be used, such as heating the sample in air, nitrogen or argon to determine how the atmosphere and temperature affect the sample. TGA is a very useful analytical tool because it gives information about the stability of a sample, and can be used to learn how samples decompose and at what temperature the reaction occurs[10].

Chapter 2

Perovskites

Perovskite was discovered in 1839 by Gustav Rose and is named after the Russian mineralogist L.A. Perovski. The first perovskite to be found was $CaTiO_3$. Perovskites are materials that all share related crystal structures and general formulas, although there are many layered type of perovskites that have a different formula. The ideal general formula for perovskites is ABX_3, where A is the larger cation coordinated by 12 anions, B is the smaller cation that is enclosed by an octahedron of anions and X is the anion that bonds A and B together[11]. The ideal cubic pervoskite structure can be seen in Figure 2.1, where A is represented by the red sphere in the center, B are the green spheres on the corners, and X are the blue spheres. Different ions can be readily substituted on each site, which makes the perovskite structure a common type in solid state inorganic chemistry. These substitutions can be made by most of the metallic ions in the periodic table and many different anions[12]. In the research projects discussed in this thesis, A is Ca or K, B is Mn, Cu, or Ni, and X is O or F.

Perovskites have been widely studied over the past several decades because of their many important properties. Since A, B and X can be readily substituted, the ion sizes can be varied and the symmetry reduced. The reduction of the symmetry leads to several important properties that perovskites can possess, including ferroelectricity, superconductivity[13], microwave dieletric properties[14], optical[15] and magnetic properties. In this particular research we are exploring the property of colossal magnetoresistance that had been discovered in manganese-based perovskite oxides. Having properties such as these make perovskites important in fuel cells, memory devices and optoeletronic devices[16].

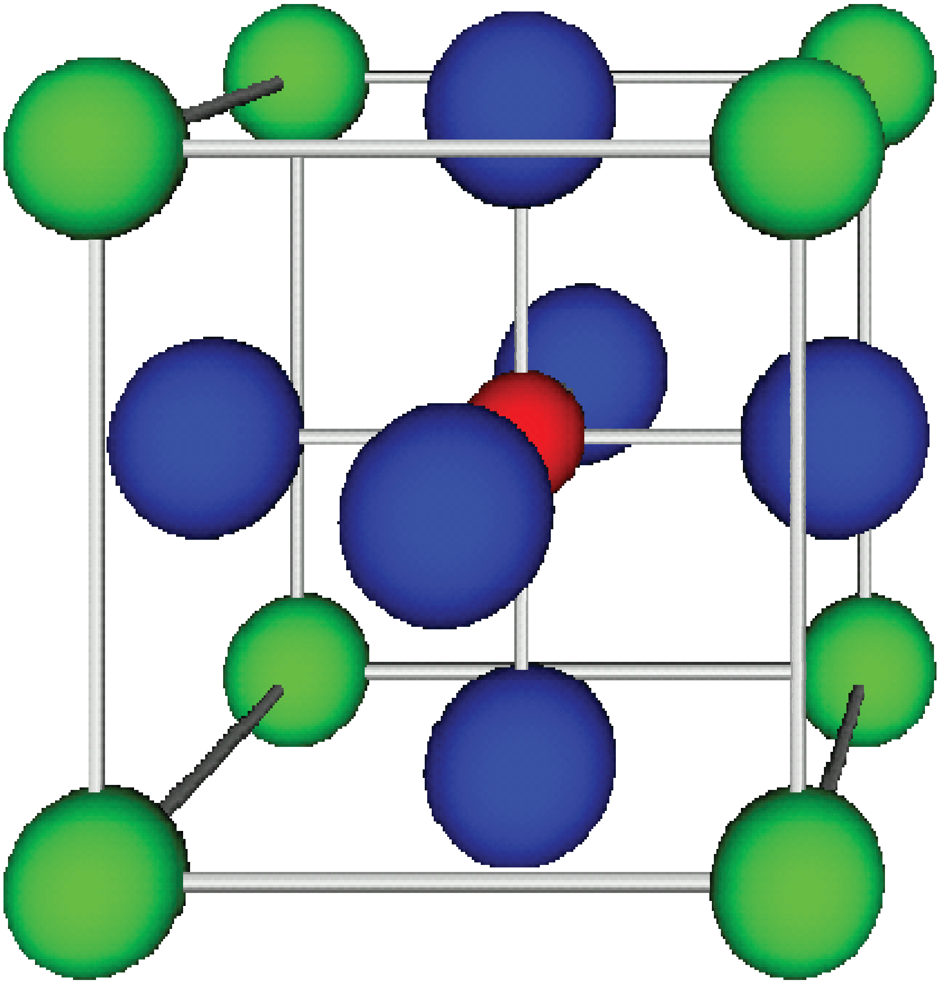

Figure 2.1: Ideal cubic perovskite structure where the red sphere in the center is the A type atoms in 12-fold coordination, the green spheres on the corner are the B-type atoms and the blue spheres are the X-type anions[17].

Tolerance Factor

Since the perovskite structure is a corner sharing framework, the structure can accommodate partial substitution and non-stoichiometry, and since the ions can be of different size-ratios, a certain perovskite phase may not always have the ideal cubic structure. To determine the degree of distortion, the Goldschmidt tolerance factor (*t*) is used, which is given in Equation 2.1

$$t = \frac{\text{radius(A)} + \text{radius(O)}}{\sqrt{2}[\text{radius(B)} + \text{radius(O)}]} \qquad \text{Equation 2.1}^{18}$$

The ideal t to maintain the cubic structure can be determined from this equation and should be $0.89 < t < 1^2$. If the size of A and B cations gives a tolerance factor below 0.90, such as $CaTiO_3$, tilting and other distortions can alter the symmetry from its ideal cubic structure and reduces the symmetry of the structure. The octahedral will tilt if not ideal to optimize the bond distances. Therefore many perovskite structures appear to have tetragonal or orthorhombic symmetry as seen in Figure 1.5 instead of the ideal cubic symmetry[11].

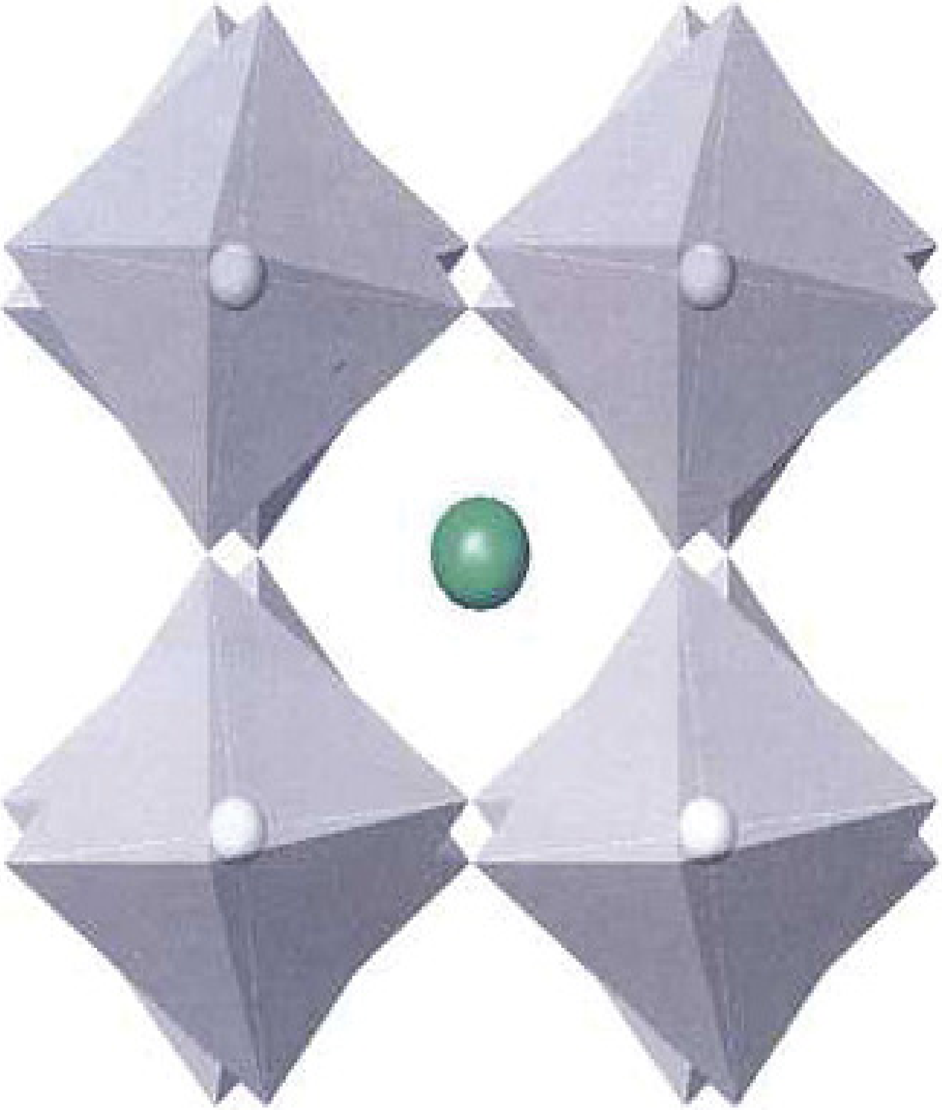

Figure 2.2: View of the othorhombic perovskite structure of $CaMnO_3$ to illustrate the out-of-phase tilting of the MnO_6 octahedra[11]

Colossal Magnetoresistance

When most conventional materials are exposed to a magnetic field, their change in resistivity is approximately 5%. However when materials that display colossal magnetoresistance (CMR) are exposed to a magnetic field, their change in resistivity is orders of magnitude, as seen in Figure 2.3. Mixed cation manganite perovskites are well-known materials that are found to display CMR. For example, while $CaMnO_3$ does not display CMR, partial substitution of Ca^{+2} for La^{+3} ions yields a mixed-cation phase with CMR behavior for the range x = 0.25 in $(Ca_xLa_{1-x})MnO_3$[19]. The extra charge introduced into the formula as La^{3+} replaces Ca^{2+} is compensated by the reduction of some Mn^{+4} to Mn^{+3}, and in previous studies it has been found that the manganites displaying colossal magnetoresistance tend to have mixed Mn^{+3}/Mn^{+4} ions present in the lattice[19]. This is because both Mn^{+3} and Mn^{+4} are needed to satisfy the double exchange mechanism (see next section) and produce the Jahn-Teller effect, which are each thought to be a component of CMR observed in manganite perovskites[8]. As will be noted later, however, this is not always the case for manganites in general.

It is also thought that this effect observed through cation substitutions could be achieved by introducing mixed Mn^{3+}/Mn^{4+} ions in the lattice through anion substitutions like N^{-3} and/or F^-. Anita Dasu attempted to synthesize an oxynitride material of composition $Ca_2Mn_2O_4N$, but all attempts were unsuccessful[18]. As repeated trials for producing manganite oxynitrides in these previous studies failed, a goal of this thesis project was to synthesize the oxyfluoride material of composition $Ca_2Mn_2O_5F$, which would also necessarily require the presence of mixed Mn^{3+}/Mn^{4+}.

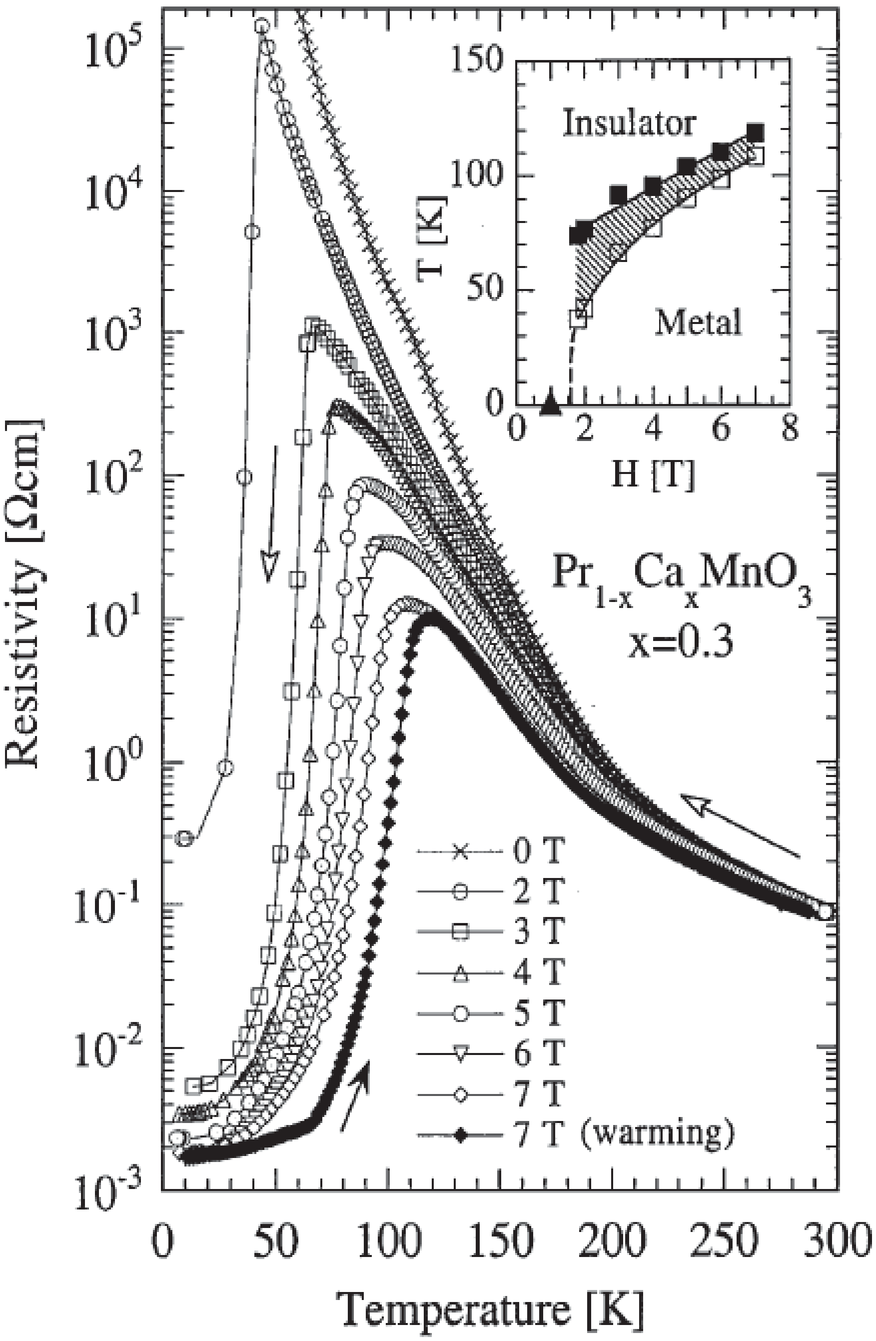

Figure 2.3: Depicts the change in resistivity of $(Pr_{1-x}Ca_x)MnO_3$[19]

Double Exchange Mechanism

As mentioned, La-doped $CaMnO_3$ is a manganite perovskite that displays CMR but $CaMnO_3$ itself does not. One reason for this is thought to be the Mn^{+3}-O-Mn^{+4} double exchange interaction made possible by introducing mixed Mn^{+3}/Mn^{+4} ions through La-doping. The double exchange interaction is a ferromagnetic interaction that occurs between two atoms having different oxidation states, like Mn^{+3} and Mn^{+4}, in a configuration such that the itinerant electron does not have to change spin[12,19]. As explained by Zener[20], the double exchange mechanism is a process that contains two simultaneous motions, namely the electron moving from the Mn^{+3} to the oxygen and the electron moving from the oxygen to the Mn^{+4} and this is depicted in Figure 2.4 [19]. Another key factor is that the itinerant electron obeys Hund's rules when it moves to the atom that is accepting it.

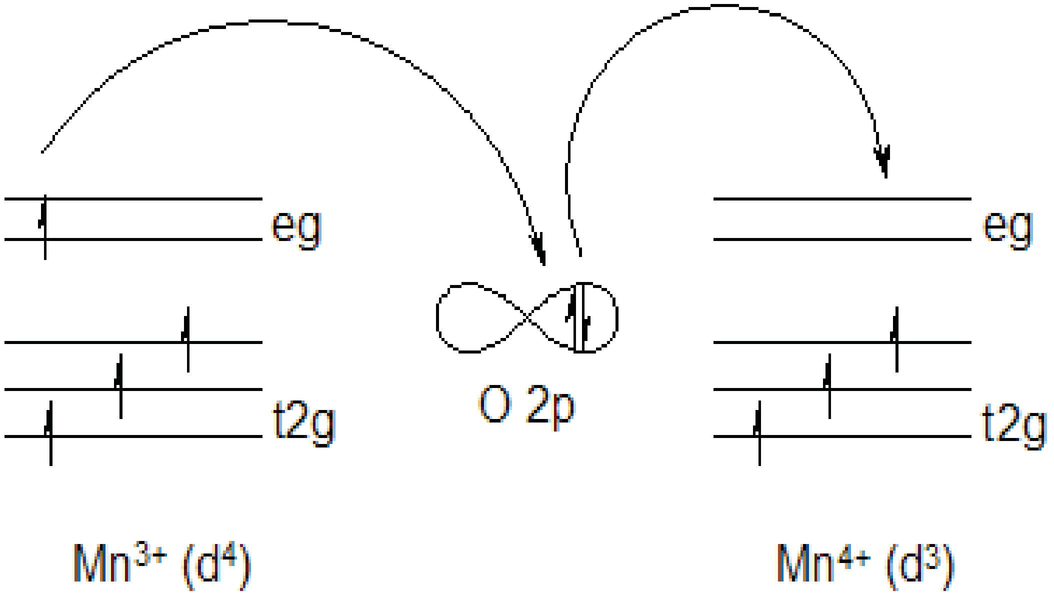

Figure 2.4: Depiction of the double exchange mechanism[21]

It is important to note that while double-exchange appears to be a component contributing to CMR in several materials, it is not present in all cases when CMR is observed. For example, the pyrochlore-type compound $Tl_2Mn_2O_7$, with Mn present only as Mn^{4+}, displays CMR behavior with magnetic ordering driven by superexchange rather than the double exchange mechanism[23]. Superexchange is typically described as the antiferromagnetic (AFM) coupling between neighboring cations through an anion that is non-magnetic, and with a metal-o-metal bond angle of 180° as shown in Figure 2.5. In the pyrochlore structure, Mn-O-Mn angles are closer to 134° such that superexchange can be ferromagnetic rather than AFM, however CMR behavior requires the alignment of electron spin on the metals. In superexchange interactions, it is the coupling between electrons on the oxygen and manganese atoms that results in alignment of electrons. Double exchange is different from superexchange because in double exchange the electrons actually move from Mn^{+3} to the oxygen and from the oxygen to the Mn^{+4}, whereas in superexchange the electrons do not actually move between the Mn and the O and usually the occupancy of the d-shell of the Mn is the same.

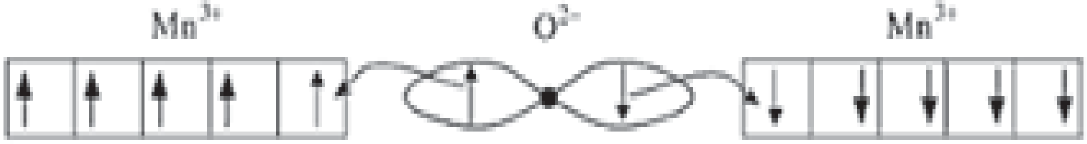

Figure 2.5: Depiction of a typical superexchange mechanism in which the Mn-O-Mn bond angle is 180°, resulting in antiferromagnetic behavior[24].

Mixed Anion Substitution

As mentioned, this thesis work attempts to synthesize a mixed oxidation Mn^{+3}/Mn^{+4} perovskite through anion rather than cation substitution, namely, via F^{-} anion substitution to give the product $Ca_2Mn_2O_5F$. There have been a few research studies discussing oxyfluoride perovskites. In 1998 R.L. Needs and M.T. Weller reported for the first time a compound with the cubic perovskite-type composition $BaScO_2F$. Before this there were two other materials reported as having ABO_2F perovskite-type stoichiometry, $KNbO_2F$ and $KTiO_2F$[25]. In 2005 Frank J. Berry et al. published a paper on the fluorination of $SrFeO_3$. Much of the other work before and around this time focused on cuprate perovskites because $Sr_2CuO_2F_{2+x}$ was found to become superconductive at 46 K. The paper by *Berry et al* [26] showed that the fluorination of a perovskite significantly increases cell parameter because with the substitution of some O^{2-} for F^{-} results in longer bond distances and therefore a larger unit cell. Also this compound was analyzed with Mössbauer spectroscopy and it was found to exhibit magnetic ordering. Most recently, *W. Tong et al*. in 2009 published a paper discussing a silver molybdenum oxyfluoride (SMOF) perovskite, and its use as a cathode in rechargeable lithium batteries[27]. This is of interest because of the recent rise in use of rechargeable batteries in such things as biomedical devices and portable electronics. One other advantage that has been found by fluorinating perovskites is that they can be synthesized at relatively low temperatures and a number of different fluorinating agents are available, such as F_2 gas, NH_4F, XeF_2, CuF_2, NiF_2 and ZnF_2[26].

Chapter 3

Statement of the Problem

The goal of this research is to synthesize $Ca_2Mn_2O_5F$ for the first time, and investigate its magnetic properties. It is well known that some perovskite oxides display Colossal Magnetoresistance (CMR) behavior, such as La-doped $CaMnO_3$. Although a theoretical basis for the CMR phenomenon is not well established, some features, such as ferromagnetic double exchange, do appear to be a common ingredient for CMR behavior and can be used as a guiding hypothesis in the design of new materials. For example, in order for the double exchange mechanism to work in manganites there must be a presence of mixed Mn^{3+}/Mn^{4+} in the material. In this research we aim to incorporate mixed Mn^{3+}/Mn^{4+} ions by using anion substitution instead of cation substitution. Specifically, the composition $Ca_2Mn_2O_5F$ is targeted and we propose to prepare it by first synthesizing $Ca_2Mn_2O_5$ followed by fluorination to give $CaMnO_2F$, which contains Mn^{3+}. The $CaMnO_2F$ phase will then be reacted with $CaMnO_3$ to give the $Ca_2Mn_2O_5F$ target compound that contains both Mn^{3+} and Mn^{4+} ions. Once $Ca_2Mn_2O_5F$ is successfully prepared it will be tested to determine if it does indeed display CMR.

Another goal of this thesis study is related to Project REEL (Research Experience to Enhance Learning), which is a state-wide initiative funded through the National Science foundation, and centered at the Ohio State University. The overall goal of the project is to incorporate a meaningful research experience into the first two years of the undergraduate chemistry curriculum in order to increase retention and enrollment in STEM-related disciplines. At YSU, the REEL modules are implemented into the second semester general chemistry laboratory course, and the goal is to prepare perovskite fluorides as potential pigment materials that are relatively environmentally benign, particularly compared to some inorganic red and yellow pigments in use that contain heavy toxic metals like Cd, Hg, and Pb. More specifically, for the present study we aim to direct students to prepare the unreported compounds of the series of $K(Cu_xM_{(1-x)})F_3$ with M = Ni & Mn ($0 \leq x \geq 1.0$) and to show that the sample color and unit cell dimensions can be tuned by varying Cu vs. Ni/Mn content. Furthermore, as $KMnF_3$ and $KNiF_3$ are cubic and $KCuF_3$ is tetragonal, we intend to establish the solubilities of the cubic KMF_3 (M = Mn & Ni) phases into the tetragonal $KCuF_3$ lattice. This will require the use of more quantitative techniques than are typically completed in the general chemistry lab, in particular, high resolution PXRD data will be acquired for each sample and the data will be refined using Rietveld analysis methods.

Chapter 4

Synthetic Methods

The objective of this research project was to synthesize and investigate the magnetic properties of $Ca_2Mn_2O_5F$ and ultimately determine if it displays CMR behavior. Before any synthesis was started all the furnaces used in this research were calibrated with Chromel-Alumel thermocouples to ensure that all reactions were occurring at the correct temperatures.

Proposed synthesis of $Ca_2Mn_2O_5F$

In order to synthesize $Ca_2Mn_2O_5F$ the following reaction scheme was initially proposed:

$$(1)\ MnO_2 + CaCO_3 \rightarrow CaMnO_3 + CO_2$$

$$(2)\ 2CaMnO_3 + 2/3\ NH_3 \rightarrow Ca_2Mn_2O_5 + H_2O + 1/3\ N_2$$

$$(3)\ Ca_2Mn_2O_5 + NH_4HF_2 \rightarrow 2CaMnO_2F + NH_3 + H_2O$$

$$(4)\ CaMnO_2F + CaMnO_3 \rightarrow Ca_2Mn_2O_5F$$

Modifications to this procedure will be introduced at appropriate points in the following discussion. As much of the effort of this project focused on optimizing the first two steps, unfortunately no attempts could be make herein to achieve the end target compound.

Step One: Synthesis of $CaMnO_3$

Trial One

In the proposed reaction scheme the first step involves the synthesis of $CaMnO_3$, which is not commercially available. The first synthesis trial that was attempted used the procedure from Zhou *et al*.[11] For this first synthesis 3.850g of $CaCO_3$ and 3.390g of MnO_2 were weighed out and placed in a mortar and mixed thoroughly together with a pestle until a dark grey powder was achieved. Then the mortar was filled half way with acetone and mixed to form a slurry to ensure complete mixture of the starting materials. This slurry was left overnight to allow evaporation of acetone. After complete evaporation the resulting powder was pressed into three pellets and placed into a nickel boat, which was placed into a Thermolyne 59300 tube furnace and reacted according to the following program; where R = heating or cooling rate; L = temperature level; and D = dwell time or time spent at each temperature level.

Step 1: R1: Step function; L1: 28°C; D1: 0.0 hours

Step 2: R2: 60°C/hr; L2: 800°C; D2: 48.0 hour

Step 3: R3: 60°C/hr; L3: 1150°C; D3: 72.0 hours

Step 4: R4: 40°C/hr; L4: 200°C; D4: 0.0 hours

Step 5: R5: Step function; L5: 28°C; D5: End function

It should be noted that the dwell times used in this reaction were double from what the procedure in the article proposed in order to ensure completion of the reaction. The final product was analyzed using X-ray Powder diffraction and indicated the reaction to be unsuccessful as discussed in the next chapter.

Trial Two

The second synthesis trial for preparation of $CaMnO_3$ that was attempted was adapted from article by *C.* Monesi *et al.*[28] In this procedure stoichiometric amounts of $Ca(NO_3)_2 \cdot 4H_2O$ and $MnCO_3$ were weighed out and mixed together. This mixture was then saturated with a citric acid solution and left to evaporate over night to produce a sol-gel. The sol-gel was then placed in a muffle furnace at 700º C for 7 days, after which the sample was found to be a mixture of $CaMnO_3$ and $CaMn_2O_4$. The sample was then placed back into the furnace at 900º C for an additional 3 days. At this point the product still contained $CaMn_2O_4$, so the sample was placed back into the furnace at 900º C for an additional three days to complete the oxidation of $CaMn_2O_4$ to $CaMnO_3$.

This synthesis trial was successful so the step two of the reaction scheme was attempted. The procedure for this step was adapted from Poeppelmeier *et al.*[29] who was able to reduce $CaMnO_3$ to $Ca_2Mn_2O_5$ using ammonia according to the following reaction:

$$2CaMnO_3 + 2/3\ NH_3 \rightarrow Ca_2Mn_2O_5 + H_2O + 1/3\ N_2.$$

A total of 3.195g of $CaMnO_3$ was weighed out and placed into a nickel boat, which was then placed into a silica tube located within a Thermolyne 21100 Tube Furnace. Ammonia gas was flowed through the tube into a bubbler filled with deionized water for 48 hours at 350° C. After 48 hours the sample was removed from the furnace and analyzed using X-ray powder diffraction as discussed in the next chapter.

Trial Three

The ammonolysis of the product in Trial Two was unsuccessful and with the $CaMnO_3$ used up, the same procedure as in Trial Two was followed to prepare additional $CaMnO_3$. This attempt used the same starting materials but was heated at different temperatures for different increments of time in an effort to shorten the duration of the reaction. The sample was placed in the muffle furnace at 500º C for 3 days, then 1000º C for 4 days and finally at 1100º C for another 4 days. After the completion of this reaction it was found to be unsuccessful. Therefore new routes were explored, and a procedure published by Longo *et al.*[30] was followed that reported the use of freshly precipitated $MnCO_3$ instead of the commercially available reagent grade to prepare $CaMnO_3$. Thus, as the first step in the next synthesis trial, $MnCO_3$ was freshly made according to the reaction:

$$Mn(NO_3)_2 + (NH_4)_2CO_3 \rightarrow MnCO_3 + 2NH_4NO_3$$

To perform this synthesis, 10.2 grams of $Mn(NO_3)_2$ was dissolved in 40 ml of DI water in a glove bag filled with Argon. Once completely dissolved this mixture was precipitated with an excess amount (approximately 450 mL) of 0.5M $(NH_4)_2CO_3$ producing a thick white precipitate. This precipitate was filtered using a vacuum pump until it was dry. The precipitate was then placed into a nickel boat, which in turn was inserted into a silica tube prior to being heated at 100°C under argon for approximately 18 hours. The sample was then removed from the silica tube and placed into a sealed container. A small sample was analyzed via PXRD and verified to be pure $MnCO_3$.

One last attempt to prepare $CaMnO_3$ was made using the *C.* Monesi *et al.* procedure[28]. For this synthesis the freshly precipitated $MnCO_3$ was used as well as a slight excess of $Ca(NO_3)_2 \cdot 4H_2O$. This attempt was also unsuccessful with the product containing a mixture of CaO, $CaMnO_3$, $CaMn_2O_4$ and Ca_2MnO_4.

Trial Four

In order to decrease the time required to prepare $CaMnO_3$, as described in Trials Two and Three, a fourth trial was attempted to produce $CaMnO_3$ involving a citrate sol-gel process that was adapted from *M.E.* Melo Jorge *et al.*[4] For this synthesis stoichiometric amounts of $CaCO_3$ and $Mn(NO_3)_2 \cdot 4H_2O$ were weighed out and dissolved in a slight excess of nitric acid (approximately 250 mL). Then a 0.14 M citric acid solution was prepared and added to the solution. The amount of citric acid added must be sufficient to replace all of the nitrate ions with citrate ions. This solution was then evaporated in a muffle furnace at 110°C for 24 hours to form a yellow sol-gel. This sol-gel was then heated to approximately 400º C in a beaker that was submerged into a sand bath in a fume hood. At first the sample bubbled and a large amount of gases were released. Once all of the gases were released, the sample glowed and autoignition occurred, and the sample reacted to form a dark brown/black material. This material was then transferred to a porcelain crucible and placed back into the muffle furnace and heated in air at 600°C for 6 hours, followed by heating to 850°C for 3 days. The final product was analyzed using XRD and was found to be $CaMnO_3$.

Step 2: Synthesis of $Ca_2Mn_2O_5$

With successful products of $CaMnO_3$ made, a new synthesis route for Step 2 of the reaction scheme was attempted. In an article by Schaber *et al*. it was reported that when urea is heated to 160°C, ammonia gas is released as a byproduct which can then be used *in situ* as a reactant in a desired reaction. We therefore decided to mix $CaMnO_3$ with urea as a potential route to the desired $Ca_2Mn_2O_5$ target material[31]. To verify the decomposition temperature for our mixture of interest, a sample size of 7.3190 mg of urea was placed in a sample pan for TGA analysis and first ramped at 2°C per minute from 50°C to 600°C in air. Next $CaMnO_3$ and urea were mixed in a 1:24 ratio and a 7.2360mg sample was ramped 2°C per minute from 50°C to 600°C in air. The remaining 1:24 mixture of $CaMnO_3$ and urea that was not sacrificed to the TGA was placed into a muffle furnace at 500°C for 30 minutes. After 30 minutes the sample was analyzed using XRD. This final attempt was unsuccessful. This was the last reaction performed for this experiment.

Chapter 5

Results and Discussion

The first trial for the synthesis of $CaMnO_3$ was performed using conventional ceramic methods. This method was chosen due to the ease of mixing compounds and placing them in a furnace for an extended period of time. The final product of Trial One was analyzed using powder X-ray diffraction; which indicated and that the reaction was unsuccessful and produced a mixture of $CaMnO_3$, $CaMn_2O_4$ and MnO_2 as seen in Figure 5.1. It should be noted however that the identities of the unwanted $CaMn_2O_4$ and MnO_2 phases may be somewhat ambiguous, because the best ICDD database card match is marked as 'Deleted', meaning the database sample could be from an impure sample.

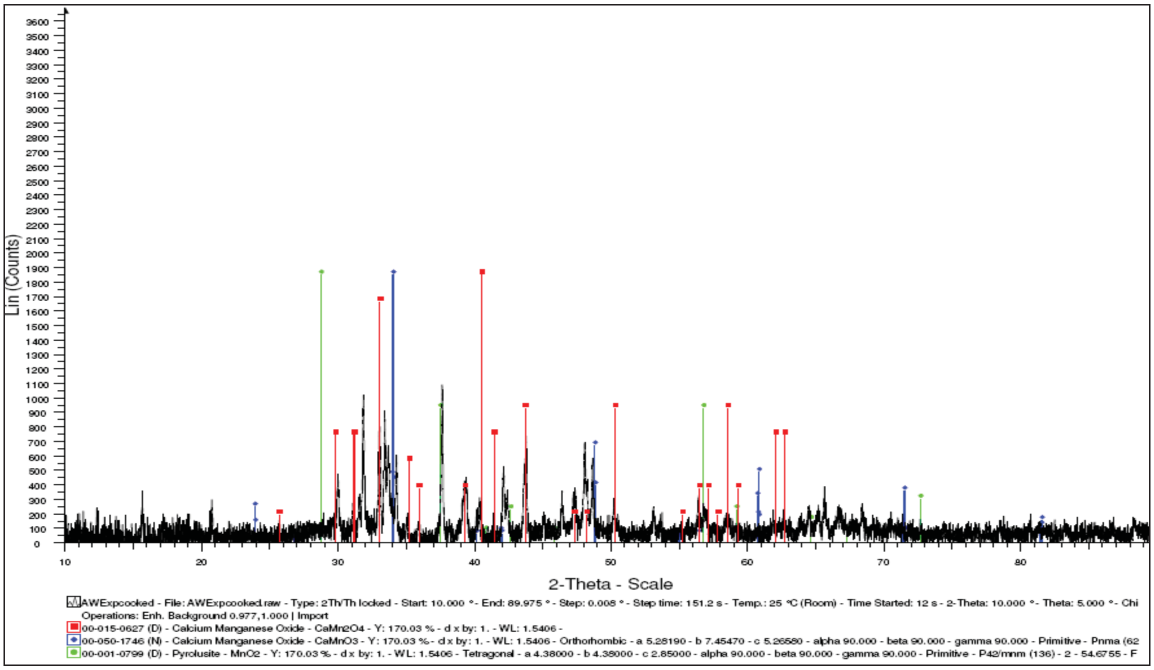

Figure 5.1: Unsuccessful first trial of CaMnO3

Following this first unsuccessful trial a sol-gel method adapted from an article by *C.* Monesi *et al.* was used[28]. The sol-gel method was attempted because of its ability to produce a pure homogeneous mixture of the starting materials in solution at low temperatures. When using the sol gel method, the gel is initially heated at a relatively low temperature for a period of time to remove all of the liquid that was added in order to form the sol gel, which is then heated at a temperature and time frame dependent on the sample. The PXRD pattern of the final product from the first sol-gel preparation attempt is shown in Figure 5.2 and indicates that $CaMnO_3$ was successfully prepared.

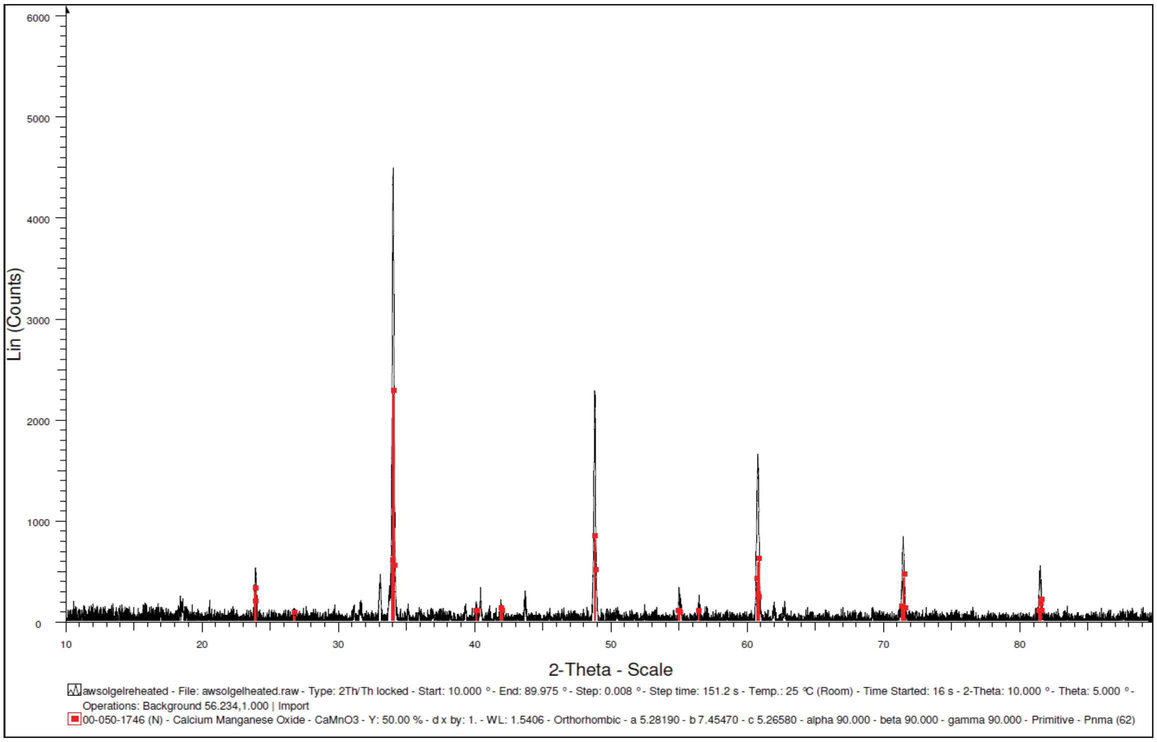

Figure 5.2: X-ray powder diffraction pattern of the product from the sol gel synthesis of $CaMnO_3$.

Using the $CaMnO_3$ material synthesized in Trial Two, Step 2 of the proposed reaction scheme from page 28 was attempted. The purpose of this step is to use ammonia to reduce Mn from Mn^{+4} in $CaMnO_3$ to Mn^{+3} in $Ca_2Mn_2O_5$. The procedure for this step was adapted from Poeppelmeier *et al.*[29] This particular procedure was used because it can be run at a low temperature although over a long duration in time. According to Poeppelmeier *et al.*, the procedure is to be performed between 300°C and 350°C for approximately 100 hours. For our experiment, the sample was heated at 350°C for 48 hours as an initial attempt[29]. After the sample was analyzed using PXRD, it was found that the final product contained different MnO phases, such as MnO_2 and Mn_2O_3 as seen in Figure 5.3, while the desired $Ca_2Mn_2O_5$ product was present only as a minor compound. The mixture was not placed back in the furnace for additional heating because it was determined that the manganese had already been reduced enough that additional phases of the desired $Ca_2Mn_2O_5$ product could not be obtained.

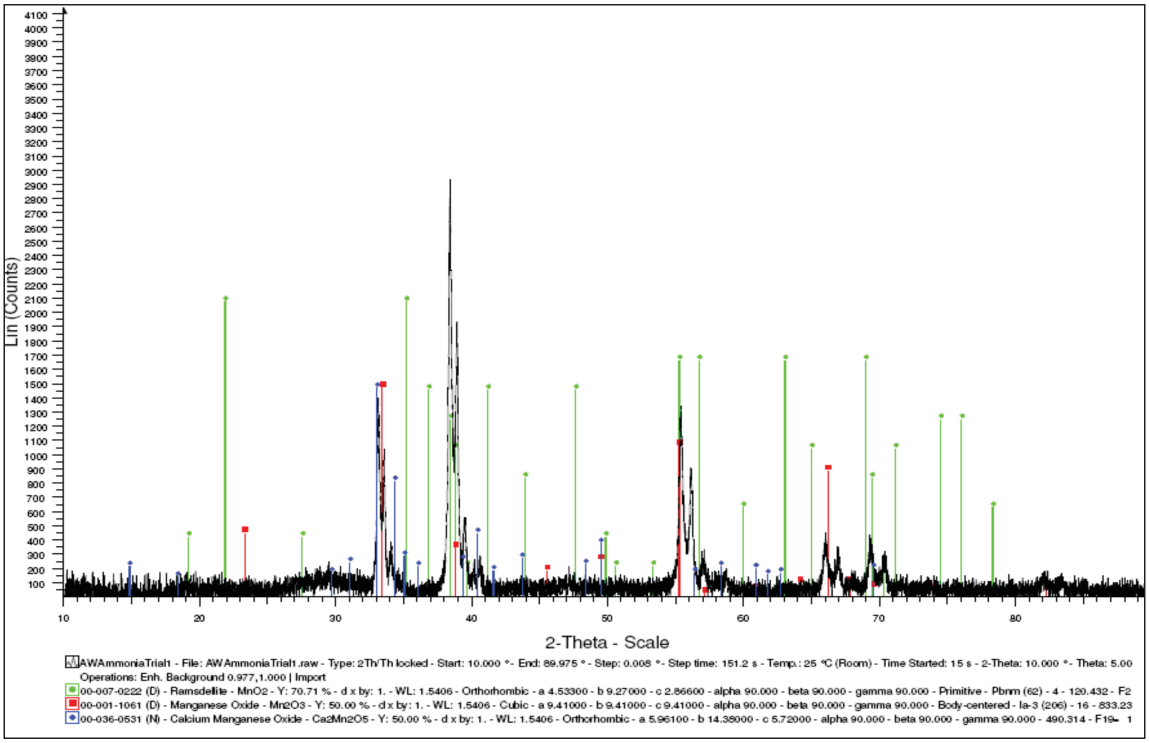

Figure 5.3: First unsuccessful attempt at ammonolysis. The blue lines represent $Ca_2Mn_2O_5$, which was the desired product.

After the majority of the $CaMnO_3$ precursor sample was used up in the initial Step Two ammonolysis trial, other trials were attempted to produce $CaMnO_3$. These trials used different heating temperature and times to determine if $CaMnO_3$ could be made at higher initial temperatures for a shorter time period. Initially Trial Three was to take 7 days unlike Trial Two's 13 day duration; however after 7 days it was found that the sample was still a mixed phase material. The temperature was then ramped up 100°C for an additional 4 days. However after this additional heating the sample was found to be a mixture of $CaMnO_3$ and possibly $CaMn_2O_4$ as seen in the PXRD pattern in Figure 5.4.

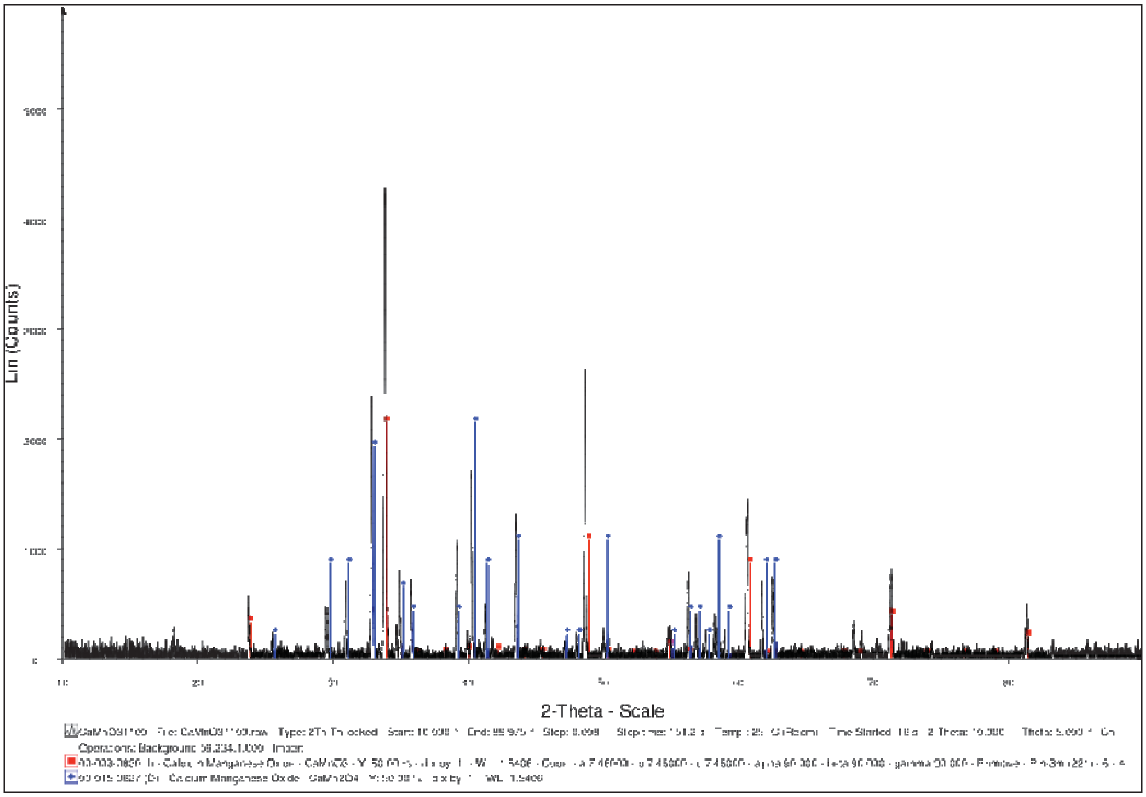

Figure 5.4: X-ray powder diffraction pattern of the product from the sol gel synthesis. The experimental peaks best match the database pattern for $CaMn_2O_4$ (blue lines) and $CaMnO_3$ (red lines).

Following these unsuccessful attempts to reproduce synthesis routes for $CaMnO_3$, a phase diagram (Figure 5.5) published by Longo *et al.* was examined to determine why our sample contained mixtures of $CaMnO_3$ and $CaMn_2O_4$[30]. From this phase diagram it was inferred that if a slight excess of Mn is present in the sample then the product would consist of the desired phase $CaMnO_3$ mixed with $CaMn_2O_4$. Thus, in order to obtain a pure sample of $CaMnO_3$, subsequent synthesis trials were adjusted to contain a slight excess of Ca to help ensure that the product mixture containing $CaMn_2O_4$ would not be observed.

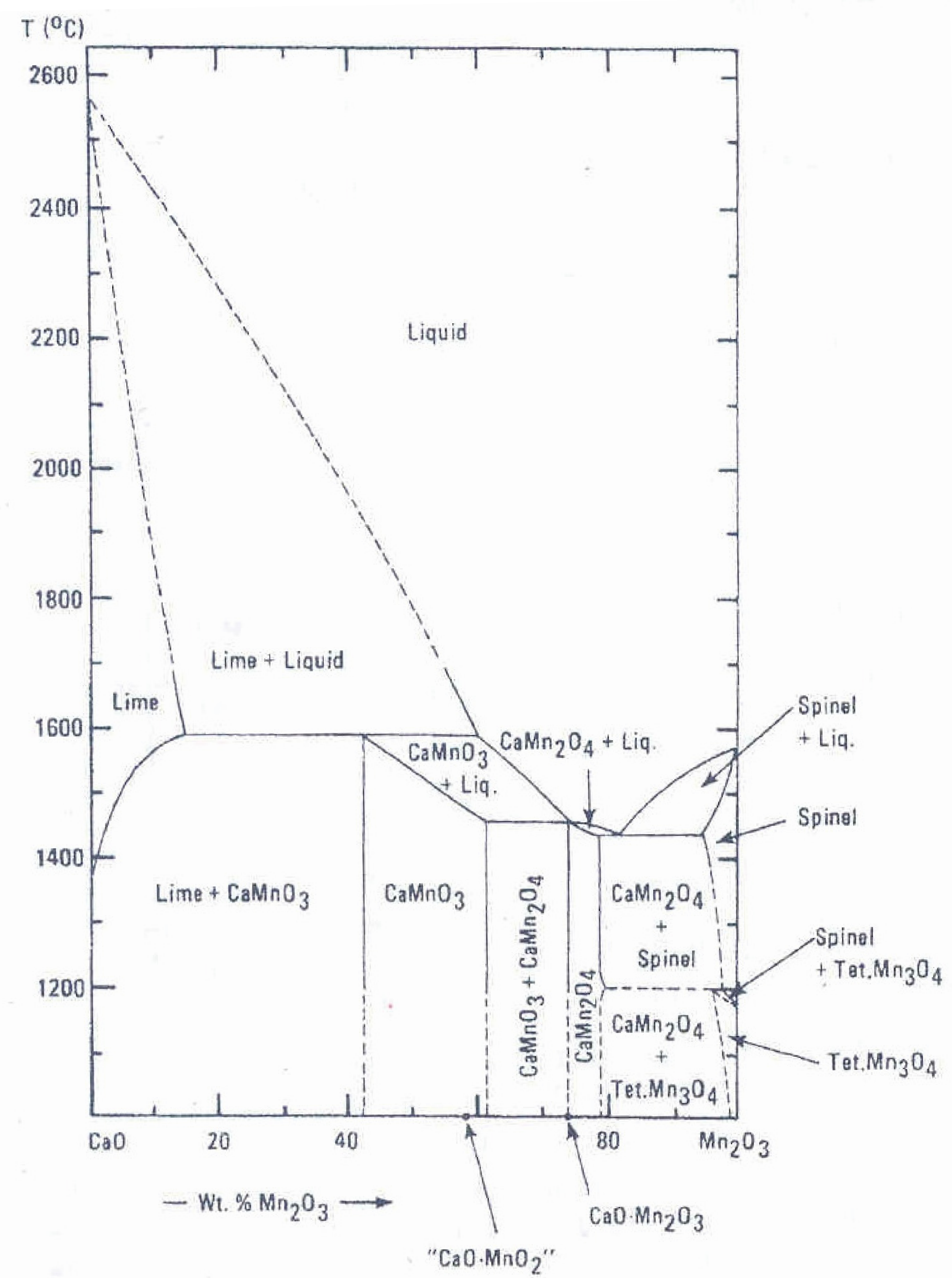

Figure 5.5: Ca-Mn-O phase diagram. The position of the target $CaMnO_3$ phase is marked as 'CaO·MnO_2', and it can be seen that a slight excess of Mn could lead to a product mixed with $CaMn_2O_4$[30].

Also, in addition the Longo *et al.* paper reported the use of freshly precipitated $MnCO_3$ rather then commercially available reagents, as these often have a brown color indicating that the manganese has been oxidized[30]. Close examination of the $MnCO_3$ used in these procedures showed the presence of some oxidation so the Longo procedure was used to make $MnCO_3$, and the PXRD of the final product can be seen in Figure 5.6.

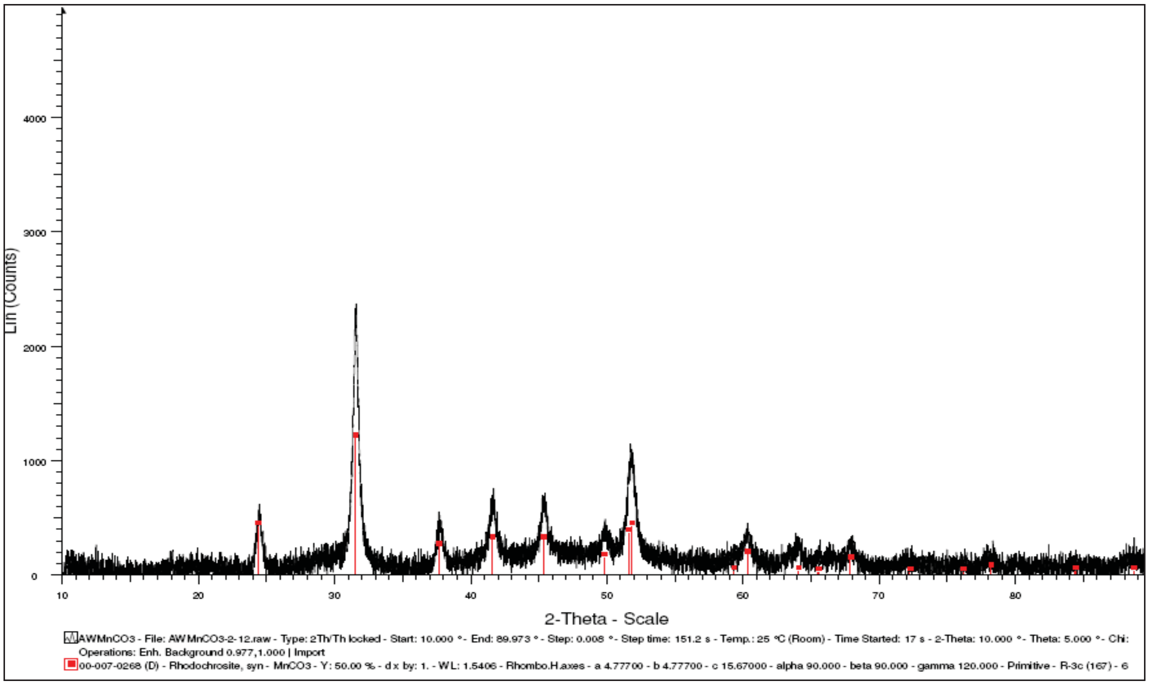

Figure 5.6: XRD pattern of $MnCO_3$. The relatively broad peaks likely indicate small particle sizes in the sample, which could also be the reason the best database match is from a card marked as ‘Deleted’.

The final attempt using the *C.* Monesi *et al.* procedure was performed using the freshly precipitated $MnCO_3$ along with a slight excess of $Ca(NO_3)_2 \cdot 4H_2O$[28]. As seen in Figure 5.7, this attempt was also unsuccessful with the product containing a mixture of CaO, $CaMnO_3$, $CaMn_2O_4$ and Ca_2MnO_4.

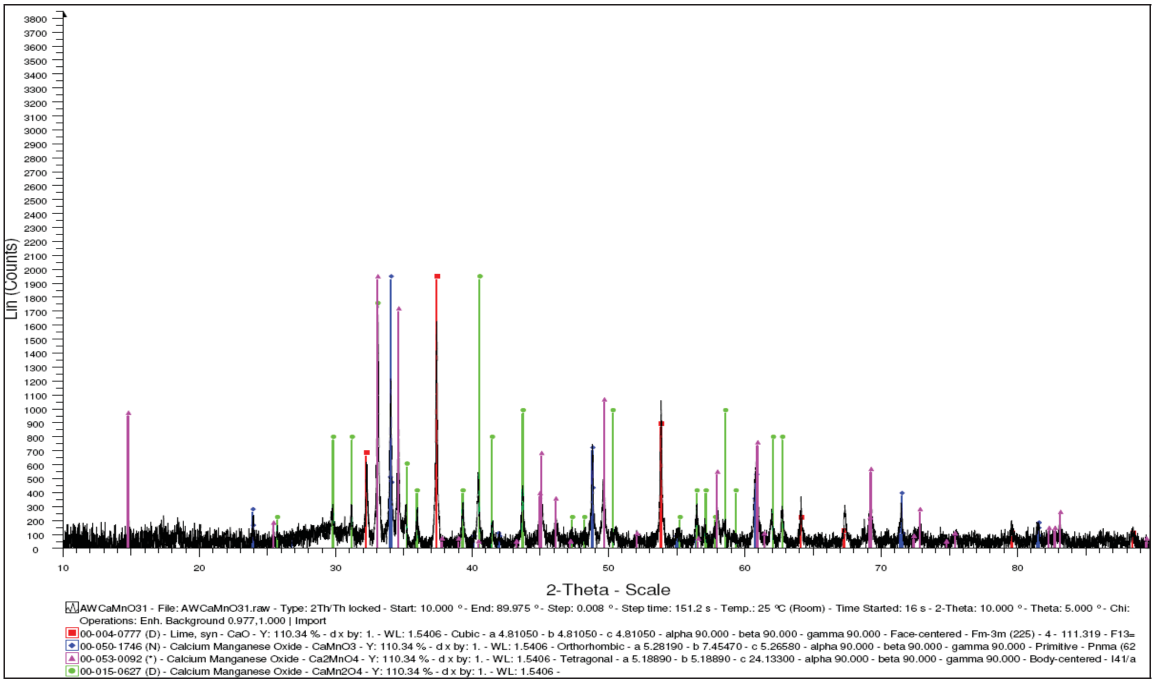

Figure 5.7: XRD pattern of final product containing mixture of CaO, $CaMnO_3$, $CaMn_2O_4$ and Ca_2MnO_4.

Next, a different type of sol-gel technique was used to decrease the time required to prepare $CaMnO_3$ as described in Trials Two and Three. This synthesis approach was adapted from M.E. Melo Jorge *et al.*[4]. In this process a sol-gel was made and then heated on a sand bath to release all of the gases. A sand bath is used because it can be easily monitored and can uniformly heat the sample. During reaction in a sand bath, gases are given off as the reaction occurs and the temperature at this point can be monitored. Thus the use of a sand bath allows the time duration of the experiment to decrease, since it is evident when the reaction has completed and can be halted. This process was successful in making $CaMnO_3$ as seen in Figure 5.8.

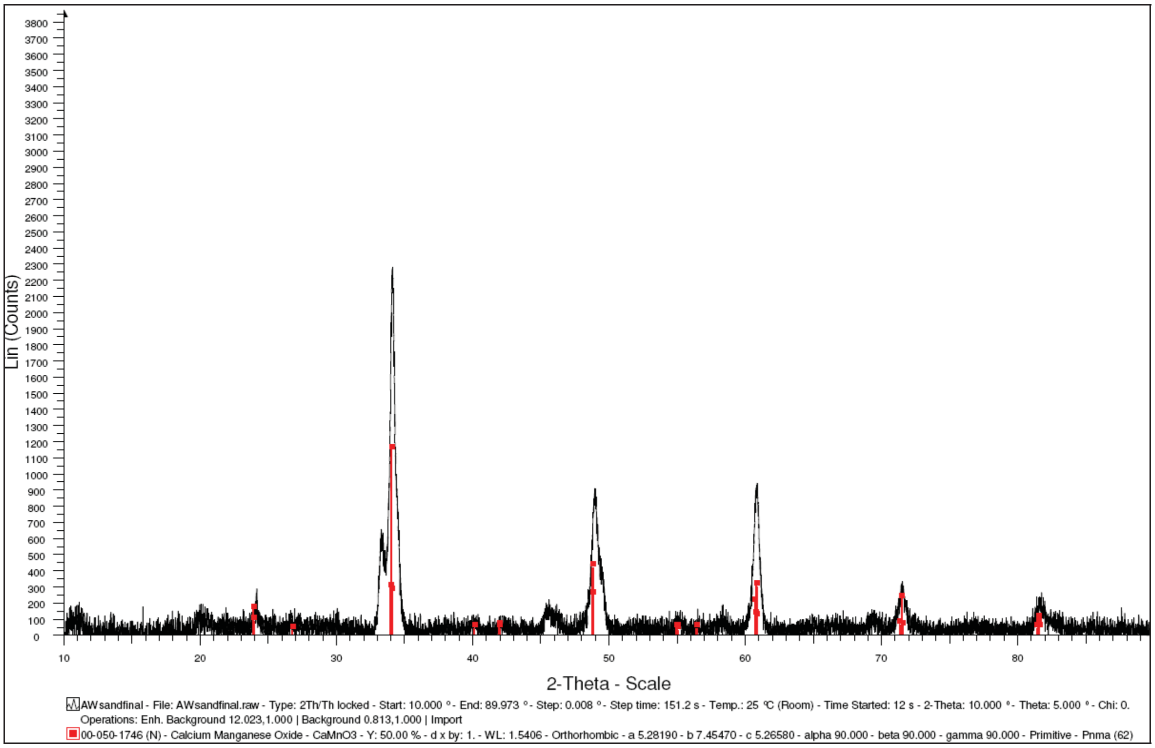

Figure 5.8: XRD pattern of $CaMnO_3$ successfully made using the citrate sol-gel process

With another successful $CaMnO_3$ sample, Step 2 (reaction 2) of the reaction scheme was again performed. Since the previous attempt at Step 2 was unsuccessful, a new technique was found. In an article by Peter M. Schaber *et al.* 2004 it was discovered that when urea is heated to 160°C, ammonia gas is released as a byproduct[31]. The decomposition temperature of urea has to first be verified to determine at what temperature urea will completely decompose. If urea completely decomposes at a relatively low temperature, then there is the possibility that it can be mixed with $CaMnO_3$ such that the ammonia gas byproduct can react with the $CaMnO_3$ to give $Ca_2Mn_2O_5$, while the urea completely decomposes and leaves no trace in the sample. To verify the decomposition temperature for our mixture of interest, a Thermogravimetric analysis (TGA) was first run for a sample of urea, with the results shown in Figure 5.9.

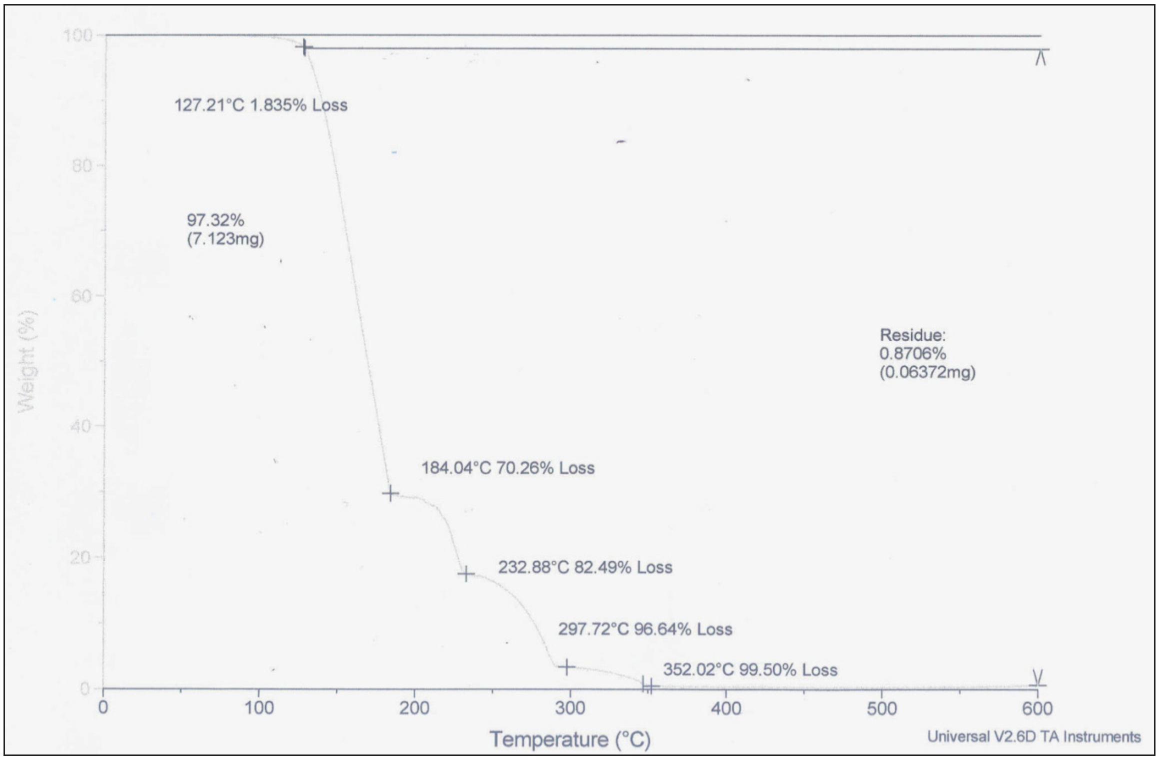

Figure 5.9: TGA of urea in air

From Figure 5.9 it can be seen that at approximately 360°C there is a 99.50% loss of urea. Therefore it is found that the majority of the urea has decomposed at 360°C, which is very close to the 350°C temperature that was previously used for ammonolysis. The next thing to determine was what a TGA would look like with a 1:24 mixture of $CaMnO_3$, as that is the ratio that the reported synthesis route specifies[31]. The results are shown in Figure 5.10, where it is apparent that at approximately 450°C most of the urea has decomposed.

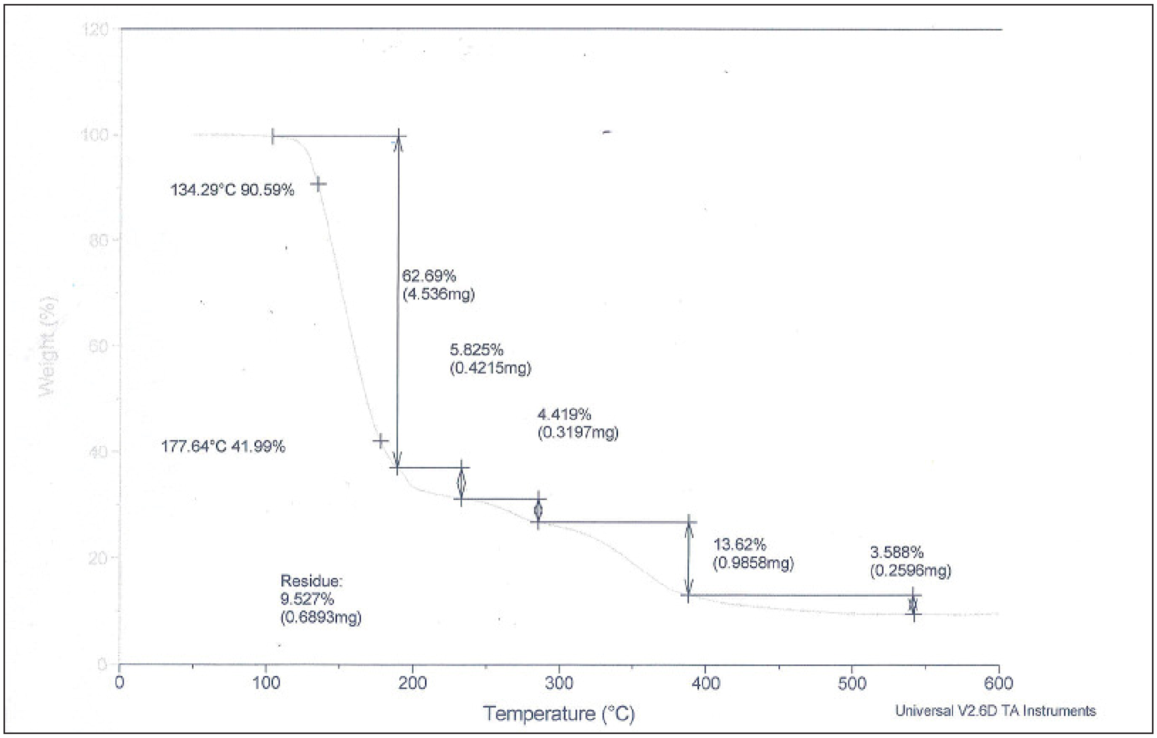

Figure 5.10: TGA of 1:24 mixture of $CaMnO_3$ and urea in air.

From this TGA data it was determined that this reaction could potentially work to synthesize $Ca_2Mn_2O_5$ without using a dynamic stream of ammonia gas. The portion of the 1:24 mixture that was not sacrificed for the TGA experiment was then sintered in a furnace at 500°C and the PXRD pattern of the product from this synthesis can be seen in Figure 5.11.

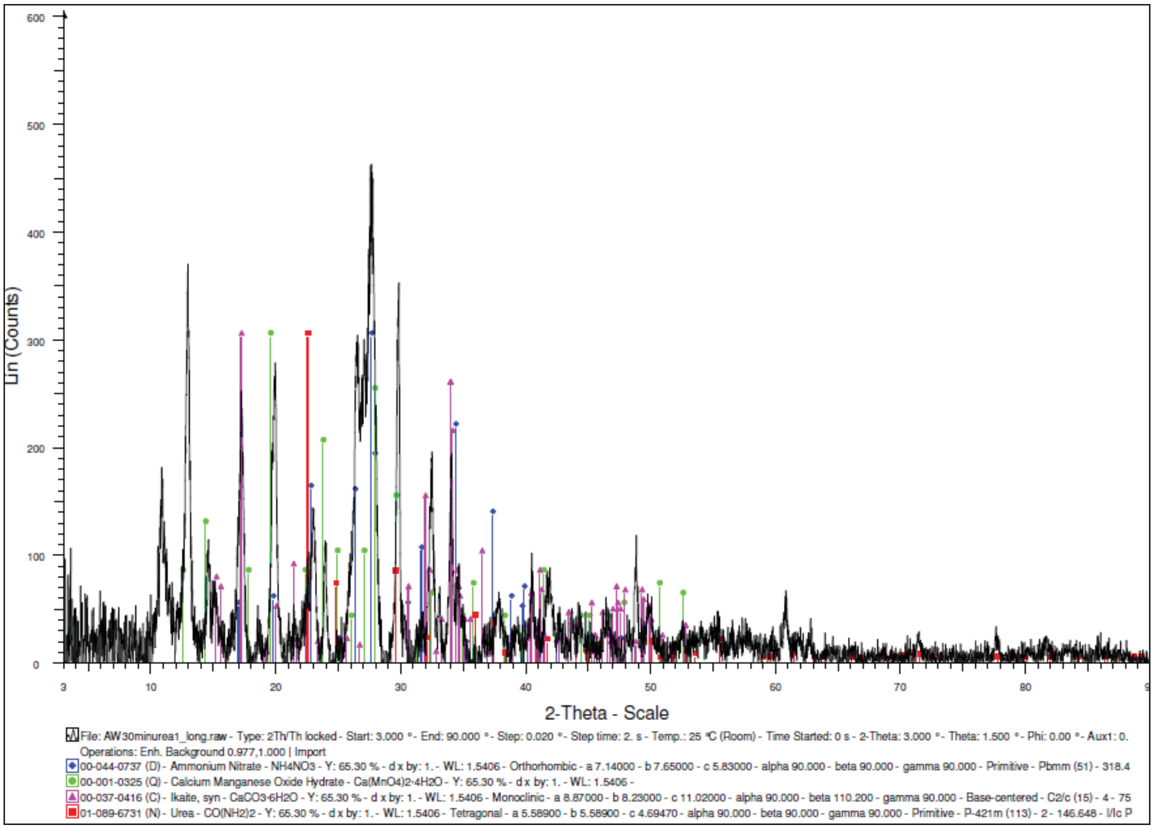

Figure 5.11: XRD pattern of 1:24 mixture of $CaMnO_3$ and urea

From Figure 5.11 it can be seen that the ammonia produced from the urea in the 30 minutes of heating was too much and reduced the $CaMnO_3$ sample past the desired point. Urea was viewed as a desirable method but failed because it was too reactive and also the ammonia reacted with some excess nitrate from the starting material $Mn(NO_3)_2 \bullet 4H_2O$ to produce NH_4NO_3.

Chapter 6

Project REEL Analysis

Introduction

The Research Experiences to Enhance Learning (REEL) project is implemented only in Ohio and is funded through the National Science Foundation Undergraduate Research Centers Program(NSF-URC). The Ohio REEL project is centered at Ohio State University and 15 colleges and universities throughout Ohio participate. The goals of this project are to increase the retention and graduation rates in science fields by introducing research into first and second year chemistry laboratories, as well as to generate new knowledge in the chemical sciences. These goals have been adopted for the YSU implementation of Project REEL, which is designed for students enrolled in the second semester general chemistry laboratory course. In further support of the project, YSU received NSF-CCLI funding to purchase sophisticated instrumentation for use by students completing appropriate modules in the course. The major instrumentation funded consists of a Rigaku Miniflex II benchtop X-ray Powder Diffractometer and an Ocean Optics QE65000 UV-Vis Spectrometer, and hands-on access of such equipment has better enabled YSU to achieve its goal of incorporating meaningful research experiences into the General Chemistry curriculum. The overall research goal of the YSU project REEL modules is to synthesize more environmentally benign materials, such as KMF_3 compounds, that can be used to replace certain inorganic red and yellow pigments containing heavy toxic metals like Cd, Hg, and Pb. To date, Project REEL has impacted approximately 560 participants at YSU.

The REEL modules of particular relevance to this thesis project focus on the perovskite structure. The ideal general formula for perovskite-related compounds is ABX_3, and the ideal cubic structure was depicted in Fig. 2.1, where is it seen that A is the larger cation coordinated by 12 anions, B is the smaller cation enclosed by an octahedron of anions and X is the anion that bonds A and B together[11]. The specific perovskite systems that this YSU project REEL study focuses on are $KCuF_3$, $KMnF_3$ and $KNiF_3$, with the latter two compounds having the ideal cubic perovskite structure. $KCuF_3$ is a type of distorted perovskite and has a tetragonal lattice due to the presence of the Cu^{2+} ion, which undergoes Jahn-Teller distortion within the octahedral field of fluoride ions present in the structure[32]. The Jahn-Teller distortion occurs wherever further splitting (i.e. in addition to normal ligand-field splitting) of the degeneracy of the d-orbitals in a transition metal yields additional stabilization energy. Fig. 6.1 depicts typical splitting of d-orbitals in a uniform octahedral ligand field, while Fig. 6.2 shows further splitting for a d^9 ion such as Cu^{2+}, for the case in which the ligand-metal distance along the z-axis has been elongated. As seen in Fig. 6.2, the loss in degeneracy in the e_g orbitals results in some energy stabilization due to the placement of two electrons in the lower energy dz^2 orbital vs. one in the higher energy $d_{x^2-y^2}$ orbital.

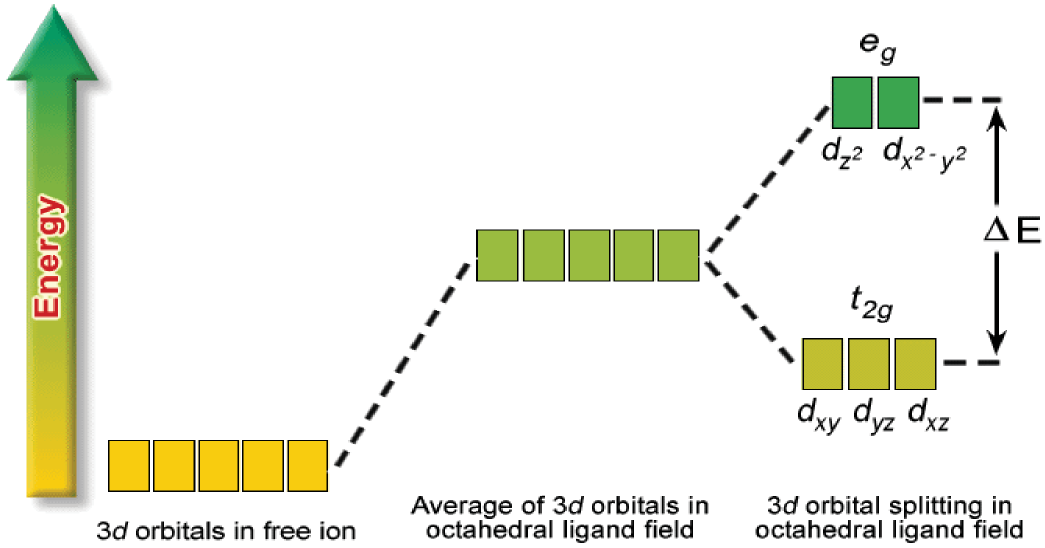

Figure 6.1: Energy diagram of the splitting of the d orbitals in an octahedral field[33].

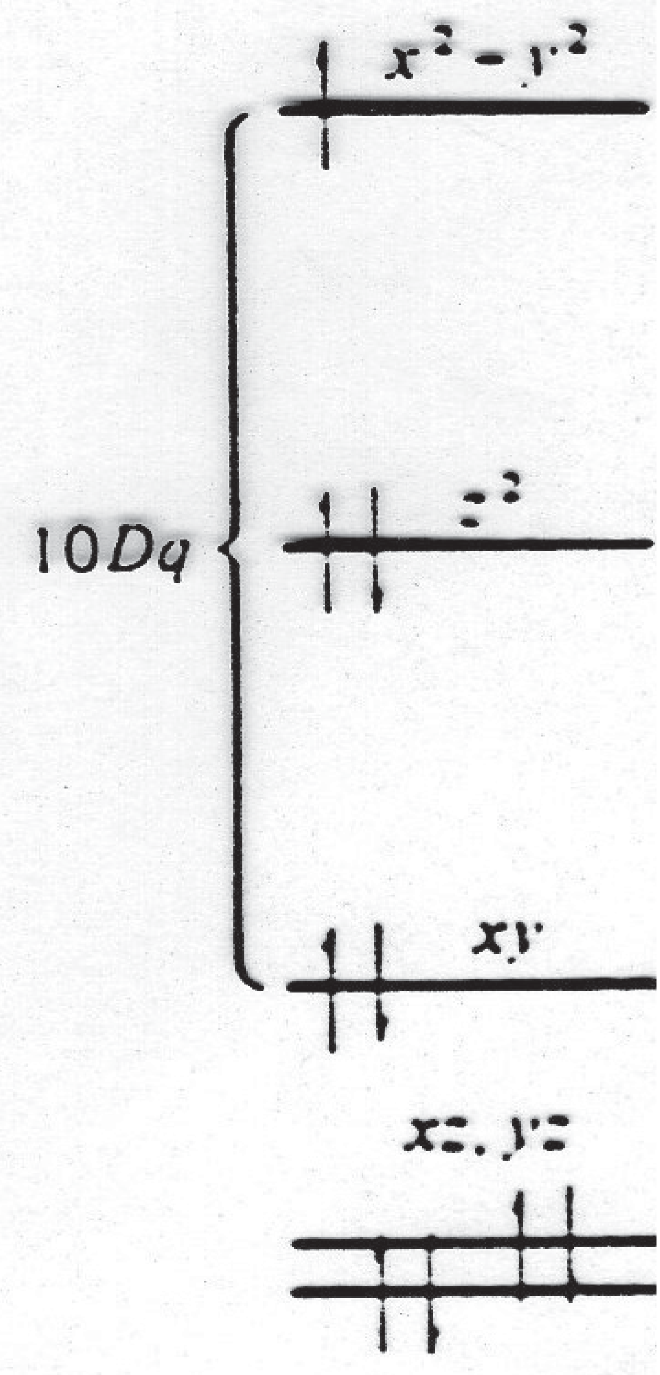

Figure 6.2: Jahn-Teller distortion of Cu[34]

The actual structure for $KCuF_3$ is shown in Fig. 6.3 where it is seen that there are actually three different Cu-F bond lengths in the lattice, rather than two as might be expected from a typical Jahn-Teller 4+2 distortion. The two different Cu-F bond lengths in the a-b plane are due to a shift of F atoms from the midpoint between adjacent Cu atoms. It is also clear from the figure how the tetragonal unit cell of $KCuF_3$ is related to the ideal cubic perovskite structure. Thus, for the unit cell shown with a = b = 5.857 Å and c = 7.859 Å,[35] this tetragonal cell can be related to the ideal cubic perovskite setting shown in Fig. 2.1 by: $a_{cubic} = a_{tet}/\sqrt{2} = 4.142$ Å and $c_{cubic} = c_{tet}/2 = 3.929$ Å. Note that these are the cell parameters chosen for the Rietveld refinements described shortly, as they are more readily related to the KMF_3 (M = Ni, Mn) cubic lattices that Cu was essentially dissolved in for our experiments. The reason for the displacement of F atoms off-center in the a-b plane of the $KCuF_3$ lattice is due to a cooperative Jahn-Teller interaction between Cu atoms, leading to the alternating long and short Cu-F bonds observed.[35,36] This in turn leads to two possible unit-cell types for $KCuF_3$, depending upon whether or not the long and short Cu-F bonds are staggered along the c-axis, as depicted in Fig 6.4. Note that in most samples of $KCuF_3$, these two unit cell types coexist.

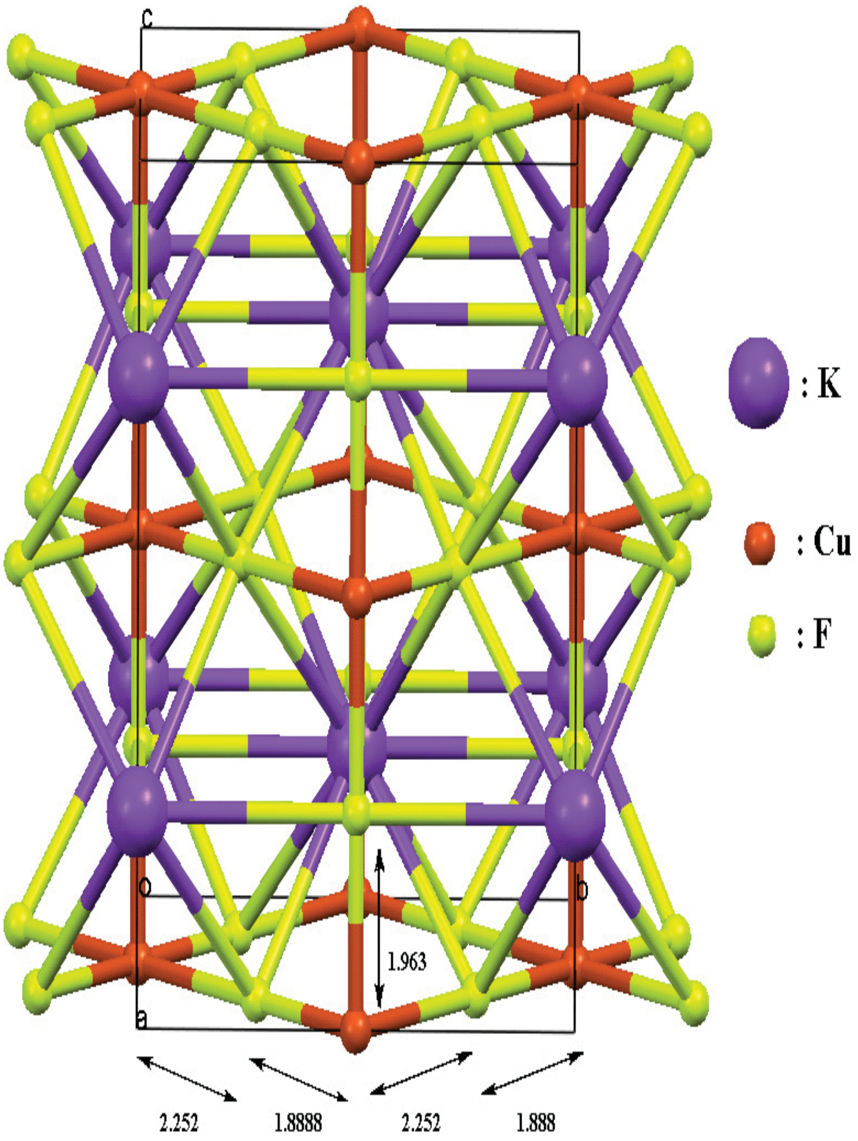

Figure 6.3: Model of the tetragonal unit-cell of $KCuF_3$. (Cu-F bond distances given are in Å)[36] The unit cell outlined in black lines has parameters a = b= 5.857 Å and c = 7.849 Å, S.G. = I4/mcm.[37] The relation between this cell and the ideal cubic perovskite structure is evident from the shape defined by Cu-F bonds (yellow/orange lines) in the lattice. The cubic (c) and tetragonal (t) cell parameters are related by $a_t = \sqrt{2}(a_c)$ and $c_t = 2c_c$.

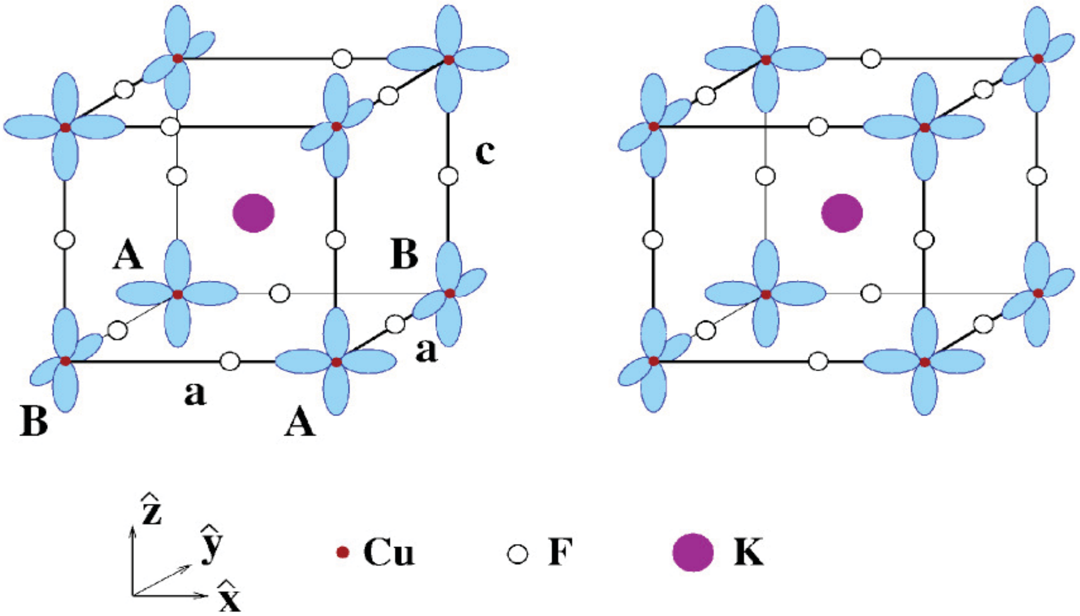

Figure 6.4: The two polytypes of $KCuF_3$, taken from Binggeli and Altarelli.[36] The figure on the left shows long and short Cu-F bonds staggered along the c-axis, while the stacking is ordered in the polytype on the right. It is seen that the different stacking schemes arise from different possible orientations of d-orbitals in the a-b planes, in turn caused by cooperative Jahn-Teller interactions between adjacent Cu atoms.[35,36]

With the goal of this project being able to make safe inorganic pigments, perovskite fluorides were chosen as the materials of choice for study since they can be relatively easily synthesized in the general chemistry laboratory, and their colors can be tuned via substitutions of transition metals at the B-site in the ABX_3 formula. The source of color in the pervoskite fluorides is d-to-d transitions. As was shown in Fig. 6.1, in an octahedral field the degeneracy of the five d-orbitals splits into two sets, specifically a relatively stabilized t_{2g} set and destabilized e_g set, where the t_{2g} set consists of the d_{xy}, d_{xz}, and d_{yz} orbitals and the e_g set consists of the $d_{x^2-y^2}$ and d_{z^2}. The energy difference between the t_{2g} and e_g orbitals lies in the visible region for these materials, and the color observed is the complement of the color absorbed when electrons get excited and jump from a t_{2g} to an e_g orbital.

Knowing the colors of ternary end members KMF_3 (M = 1st row transition element) from the literature, students are asked to make (usually previously unpublished) new compositions by combining two different transition metals at the M site. Thus KMF_3 could be one end member and KNF_3 the other. A new composition would then be $K(M_xN_{1-x})F_3$, with $0 < x < 1$. In project REEL the students are asked to predict the color of their target compound. To do this they consult a color wheel such as that shown in Figure 6.5.

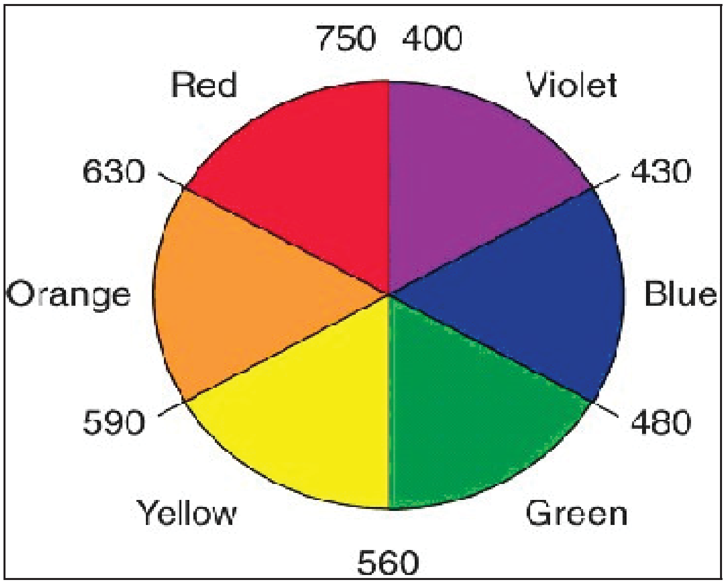

Figure 6.5: A color wheel. Numbers represent wavelengths in nm[37].

For example, knowing that one end member is a yellow compound and the other is red, students would predict the composition $KM_{0.5}N_{0.5}F_3$ to be orange in color. Also seen in Figure 6.5 are the wavelengths associated with each color and its complement on the opposite side of the wheel. With this information the students can also predict what wavelength of light their final target compound should absorb on the UV-Vis spectrum they will collect in lab.

Experimental Methods

For the YSU project REEL the novel perovskite-related series $K(Cu_XMn_{1-X})F_3$ and $K(Cu_XNi_{1-X})F_3$ (x = 0, 0.1, 0.2, …0.9) were synthesized and characterized along with their ternary end-members by students in a General Chemistry II course. Two sets of each series were analyzed in this study; one set was prepared during the Spring 2010 term, and the other during Fall 2010.

For the Spring 2010 term, samples were prepared by two General Chemistry II classes using a general procedure adapted from R.H. Langley[39] *et al* as represented in Eq. 6.1:

$$3KF + MCl_2 \rightarrow KMF_3 + 2KCl_{aq} \text{ ; M=Mn, Ni and/or Cu} \qquad \text{Eq. 6.1}$$

For the ternary end-members the students dissolved 0.12 moles of potassium fluoride dihydrate in 30-40 mL of deionized water with three drops of nitric acid. A stir bar was placed into this solution, which was then heated and stirred on a hot plate until boiling. A solution of a divalent metal chloride was then prepared by dissolving 0.04 moles of either Mn(II), Ni(II) or Cu(II) chloride hydrate in 30-40 mL of deionized water. This solution was also placed on the hot plate with a stir bar next to the potassium fluoride solution, where it was stirred and heated. Once both solutions were boiling, the divalent metal solution was added to the potassium fluoride solution dropwise until the transfer was completed; then the solution was stirred and heated for another five minutes. At this point the beaker was removed from heat and 30 milliliters of cool deionized water was added. Within a short time a precipitate formed and settled to the bottom, and the solution was filtered. The solid precipitate was next washed twice with ethanol and then twice with acetone. Finally, the sample was dried by placing it in a microwave oven at 30% power for one minute increments for a maximum of five minutes. These samples were then analyzed using X-ray powder diffraction, UV-Vis spectroscopy and X-ray fluorescence.

To synthesize the target quaternary compounds, the students followed the identical procedure as used for the ternary compounds, except for modifying the composition of the divalent metal chloride solution added. For example, preparation of a $K(Cu_{0.5}Ni_{0.5})F_3$ sample would require that 0.02 moles of $CuCl_2$ and 0.02 moles of $NiCl_2$ be weighed out and placed in the sample beaker, and then dissolved in 30-40 mL of deionized water for use in the remainder of the synthesis procedure.

Results and Discussion

As mentioned, the primary goal of project REEL is to synthesize environmentally safe inorganic pigments that can be used to replace pigments containing harmful metals such as Cd, Hg and Pb. During two of the Spring 2010 laboratory classes, each group, consisting of two or three students, synthesized $KCuF_3$, $KMnF_3$ or $KNiF_3$ and their mixed-metal target compound. The resulting pigments that were synthesized by two laboratory classes are shown in Figures 6.6 and 6.7.

Each sample was analyzed using Powder X-ray Diffraction (PXRD) and X-ray Fluorescence (XRF). Students collected X-ray powder diffraction data on a Rigaku MiniFlex Bench Top XRD, and as an exercise, calculated cell parameters by hand.

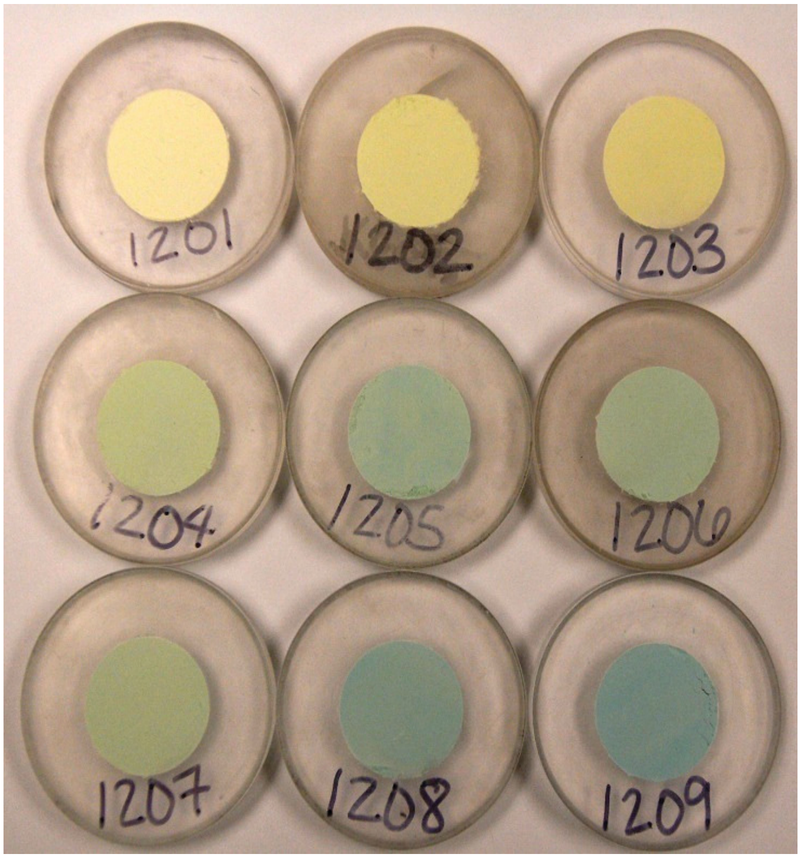

Figure 6.6: Depiction of Project REEL samples of the series $K(Cu_xNi_{1-x})F_3$ from Spring 2010 with x = 0.1 at upper left (sample 1201) and increasing to x = 0.9 at the lower right (sample 1209).

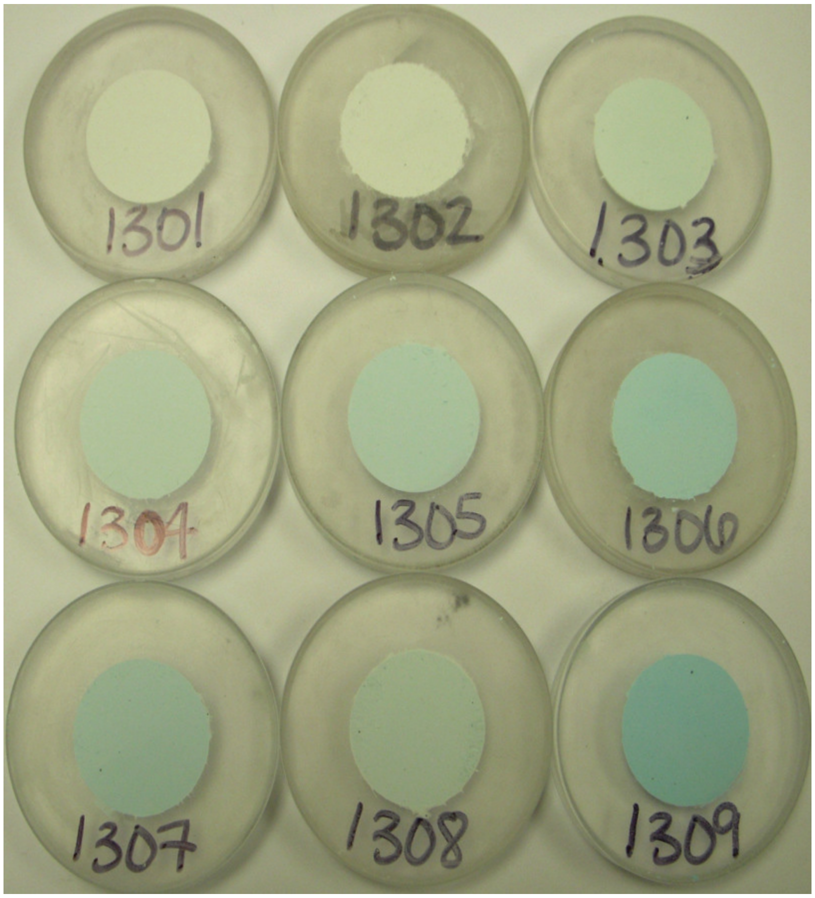

Figure 6.7: Depiction of Project REEL samples of the series $K(Cu_xMn_{1-x})F_3$ from Fall 2010 with x = 0.1 at upper left (sample 1301) and increasing to x = 0.9 at the lower right (sample 1309).

For the quantitative work presented in this thesis, data was also collected on a Bruker D8 powder XRD with a Cu source. Diffraction data was analyzed and fitted to the database patterns using EVA, and Rietveld powder refinement was performed using TOPAS.[40] The Rietveld calculations were performed by using structures of $KNiF_3$, $KMnF_3$ and/or $KCuF_3$ from the Inorganic Crystal Structure Database (copyrighted by Fachinformationszentrum Karlsruhe, Germany, and the U.S. Department of Commerce) as a starting point. These structures were then used to refine the cell parameters (but not the atomic positions or occupancies) by treating the sample as a mixture of either $KNiF_3$ and $KCuF_3$ or $KMnF_3$ and $KCuF_3$ to determine the percent compositions of cubic vs. tetragonal phases. Note that the impurity phases claringbullite and KCl or KBr were refined in a similar fashion, simultaneously with the perovskite phases. X-ray fluorescence data was collected using a Bruker S2 XRF spectrometer. Results are summarized in Table 6.1 for the $K(Cu_xNi_{1-x})F_3$ data and in Table 6.2 for the $K(Cu_xMn_{1-x})F_3$ data both from Spring 2010; X-ray diffraction patterns and Rietveld refinements are shown in Figs. 6.8-6.16 and Figs. 6.17-6.25, respectively. In each of the PXRD patterns, the blue curve is the experimental pattern and the red one is the pattern calculated using TOPAS. The line below the pattern represents the difference curve between experimental and calculated patterns, with a flatter line representing a better fit.

Table 6.1

Summary of Spring 2010 $KCu_xNi_{1-x}F_3$ Class Results

Group	Target Composition $KCu_xNi_{1-x}F_3$		Actual Composition (from X-ray Fluorescence data) $KCu_xNi_{1-x}F_3$		Crystal system	Refined Unit Cell Lengths Determined from X-ray Powder Diffraction Data	% Match
	x	1-x	x	1-x		a (Å)	
1201	0.1	0.9	0.11	0.89	Cubic	4.0169	98.16*
1202	0.2	0.8	0.21	0.79	Cubic	4.02180	100
1203	0.3	0.7	0.32	0.68	Cubic	4.02775	94.23*
1204	0.4	0.6	0.42	0.58	Cubic	4.02718	98.16*
1205	0.5	0.5	0.56	0.44	Cubic	4.03286	96.45*
1206	0.6	0.4	0.64	0.36	Cubic	4.03512	98.31*
1207	0.7	0.3	0.71	0.29	Cubic	a = 4.03757	95.98
					Tetragonal	a = 4.13 c = 3.92	4.02
1208	0.8	0.2	0.82	0.18	Cubic	a = 4.0371	18.95*
					Tetragonal	a = 4.0771 c = 3.9759	76.44*
1209	0.9	0.1	0.91	0.09	Cubic	a = 4.05848	25.12*
					Tetragonal	a = 4.11140 c = 3.94135	67.88*

*These samples contain impurities of either KCl and/or claringbullite

Table 6.2

Summary of Spring 2010 $KCu_xMn_{1-x}F_3$ Class Results

Group	Target Composition $KCu_xMn_{1-x}F_3$		Actual Composition (from X-ray Fluorescence data) $KCu_xMn_{1-x}F_3$		Crystal system	Refined Unit Cell Lengths Determined from X-ray Powder Diffraction Data	% Match
	x	1-x	x	1-x		a (Å)	
1301	0.1	0.9	0.07	0.93	Cubic	4.18205	100
1302	0.2	0.8	0.18	0.82	Cubic	4.17349	88.62*
1303	0.3	0.7	0.15	0.85	Cubic	4.17924	100
1304	0.4	0.6	0.33	0.67	Cubic	4.15437	100
1305	0.5	0.5	0.44	0.56	Cubic	a = 4.13338	85.81*
					Tetragonal	a = 4.11433 c = 4.07093	10.13*
1306	0.6	0.4	0.57	0.43	Cubic	a = 4.14374	41.82*
					Tetragonal	a = 4.12403 c = 4.10766	50.72*
1307	0.7	0.3	0.67	0.33	Cubic	a = 4.11238	49.71*
					Tetragonal	a = 4.10356 c = 4.07879	44.75*
1308	0.8	0.2	0.78	0.22	Cubic	a = 4.09575	56.98*
					Tetragonal	a = 4.12729 c = 3.95173	39.74*
1309	0.9	0.1	0.88	0.12	Tetragonal	a = 4.09839 c =4.06571	85.14*

*These samples contain impurities of either KCl and/or claringbullite

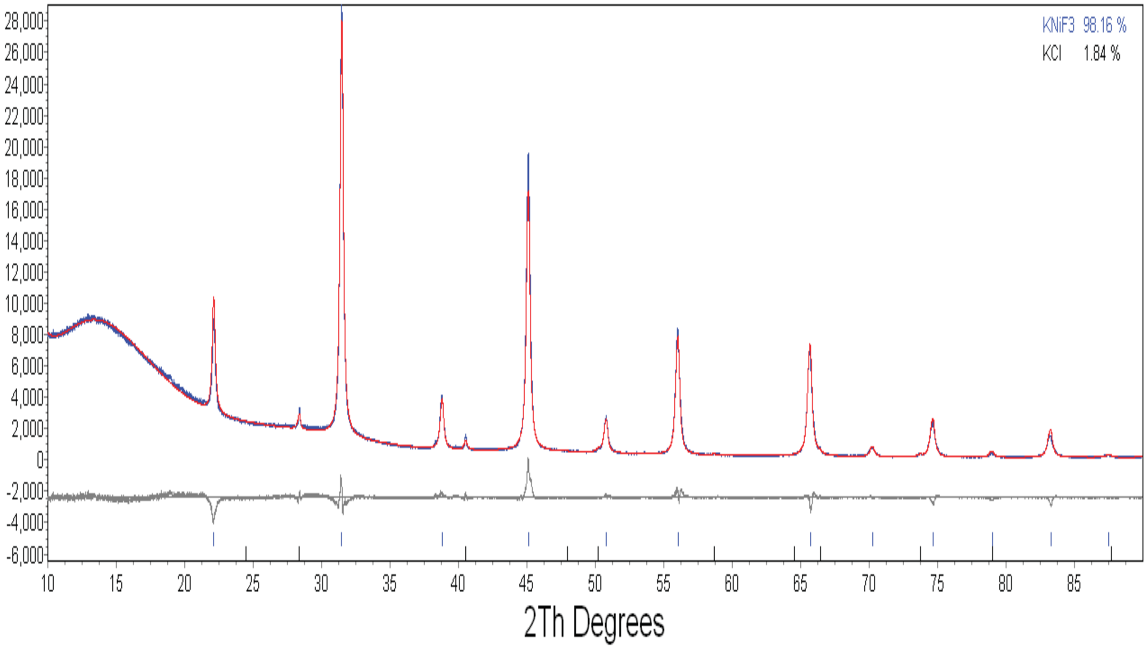

Figure 6.8: Powder X- ray diffraction data and Rietveld refinement for 1201 $KCu_{0.1}Ni_{0.9}F_3$. Blue curve is experimental, red curve is calculated.

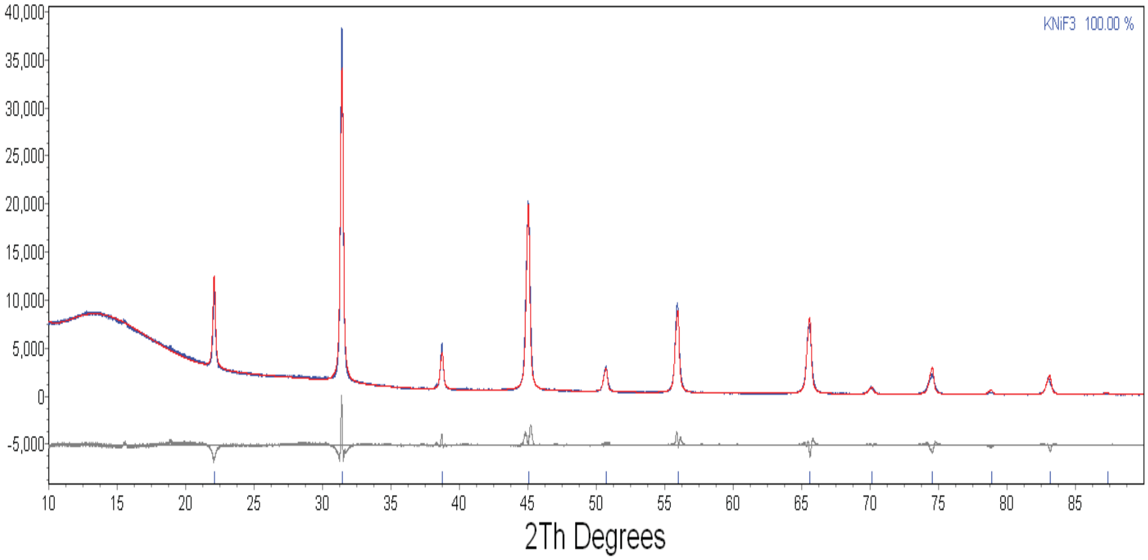

Figure 6.9: Powder X- ray diffraction data and Rietveld refinement for 1202 $KCu_{0.2}Ni_{0.8}F_3$

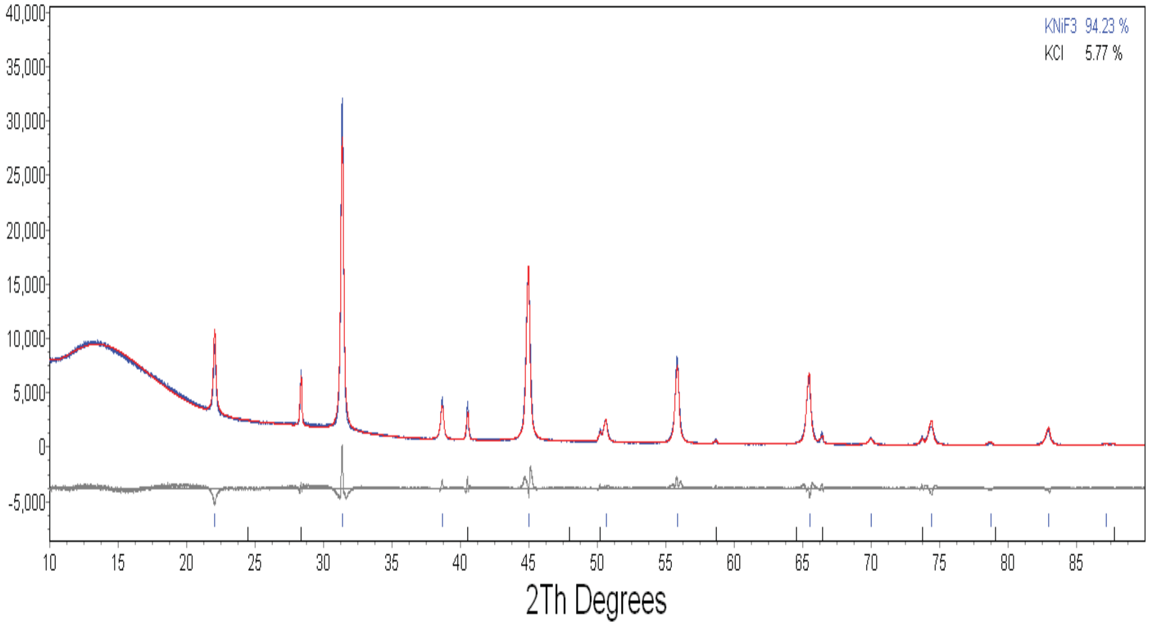

Figure 6.10: Powder X- ray diffraction data and Rietveld refinement for 1203 $KCu_{0.3}Ni_{0.7}F_3$. Blue curve is experimental, red curve is calculated.

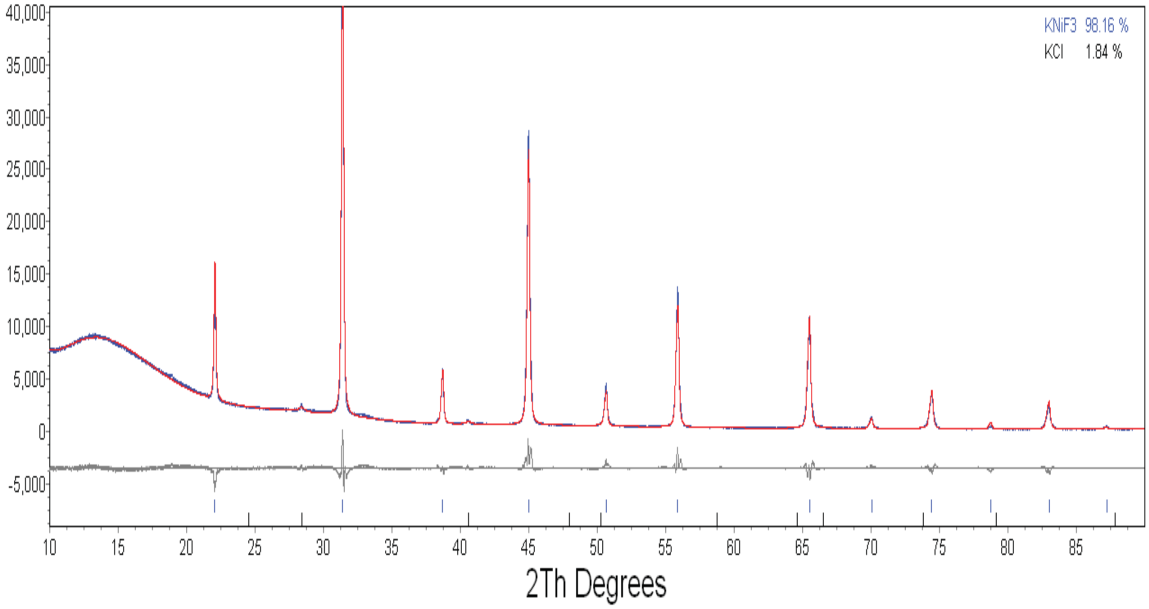

Figure 6.11: Powder X-ray diffraction data and Rietveld refinement for 1204 $KCu_{0.4}Ni_{0.6}F_3$

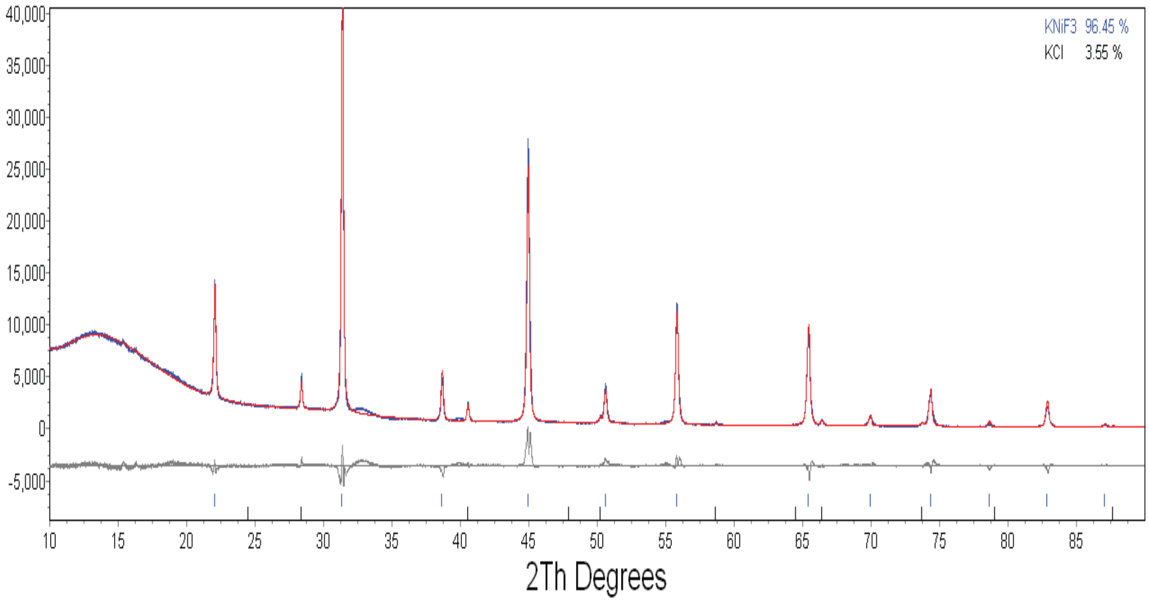

Figure 6.12: Powder X- ray diffraction data and Rietveld refinement for 1205 $KCu_{0.5}Ni_{0.5}F_3$. Blue curve is experimental, red curve is calculated.

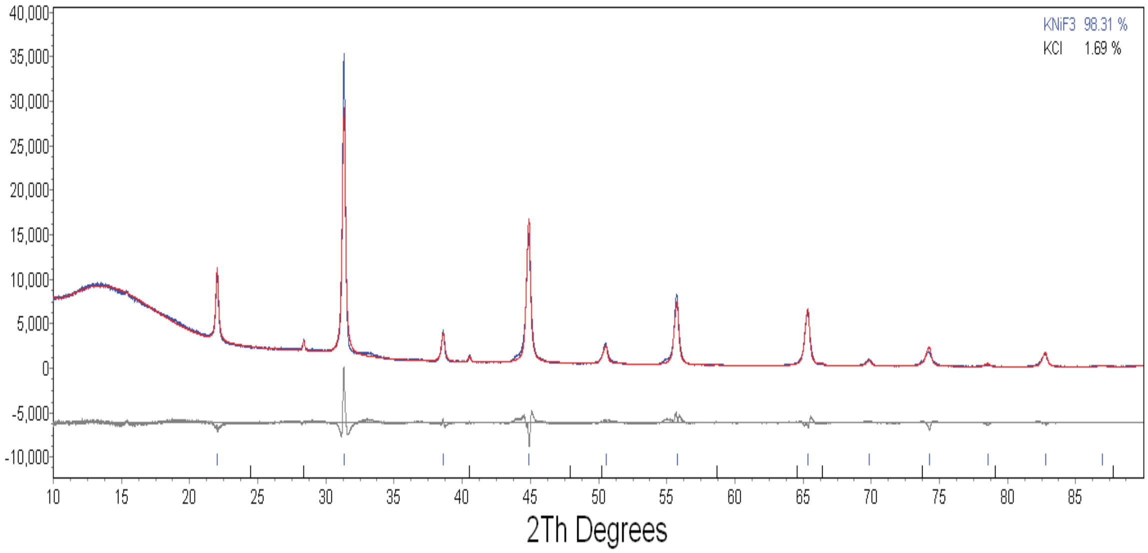

Figure 6.13: Powder X- ray diffraction data and Rietveld refinement for 1206 $KCu_{0.6}Ni_{0.4}F_3$

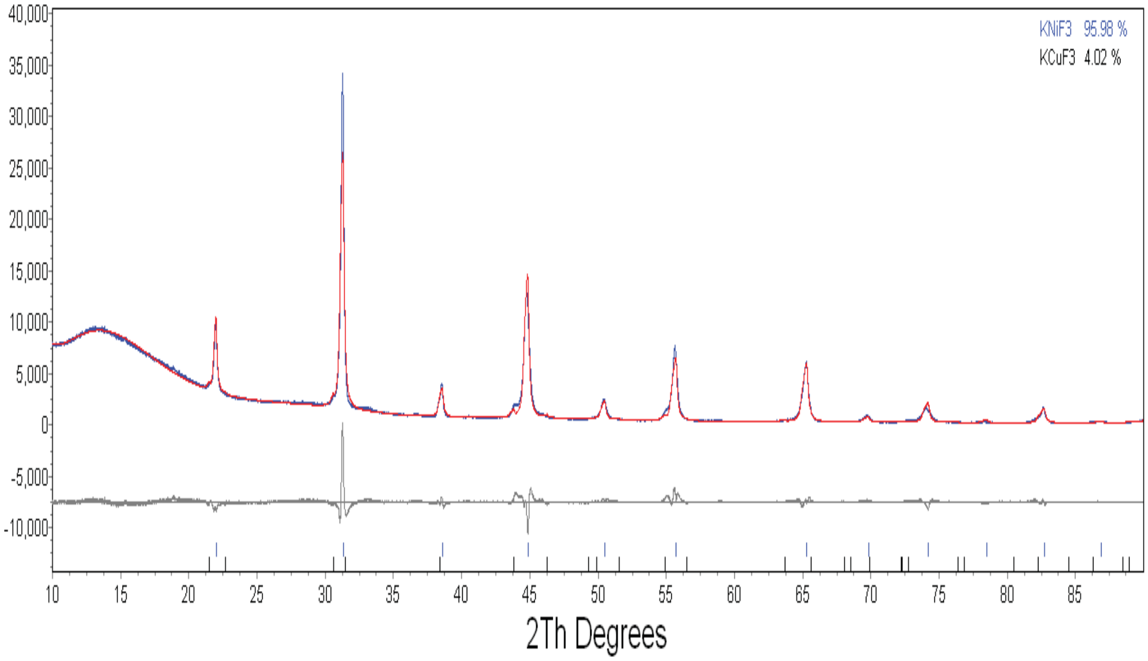

Figure 6.14: Powder X- ray diffraction data and Rietveld refinement for 1207 $KCu_{0.7}Ni_{0.3}F_3$. Blue curve is experimental, red curve is calculated.

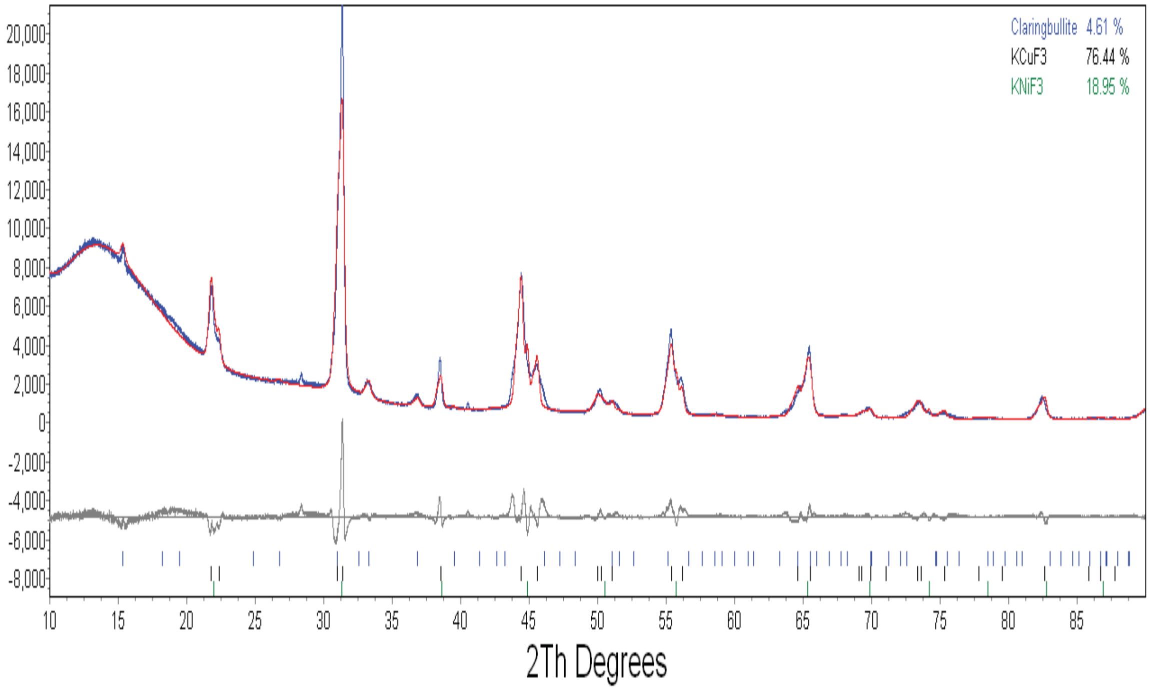

Figure 6.15: Powder X- ray diffraction data and Rietveld refinement for 1208 $KCu_{0.8}Ni_{0.2}F_3$

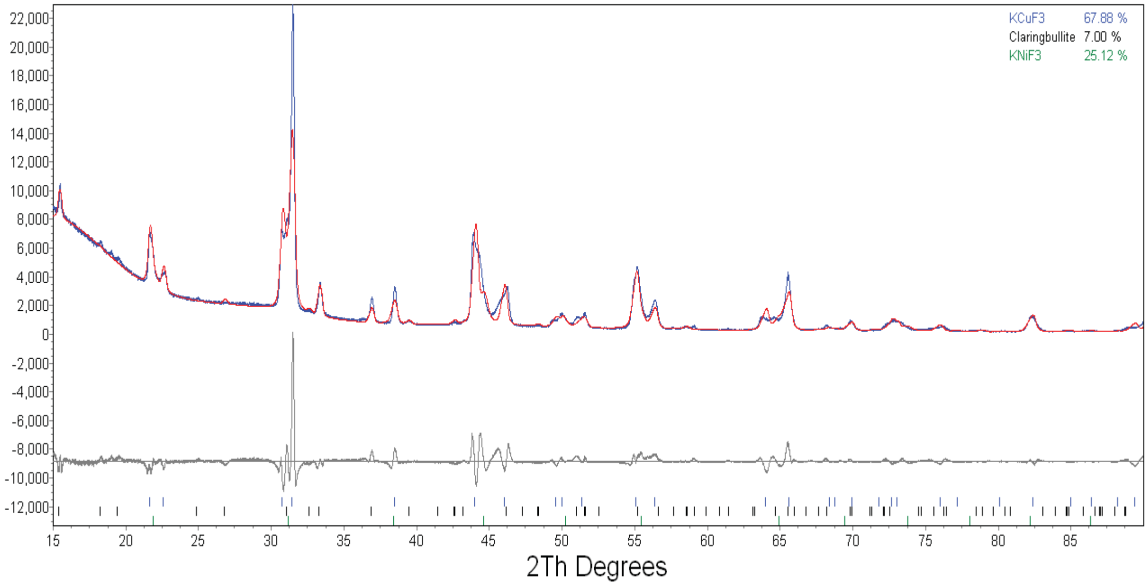

Figure 6.16: Powder X- ray diffraction data and Rietveld refinement for 1209 $KCu_{0.9}Ni_{0.1}F_3$. Blue curve is experimental, red curve is calculated.

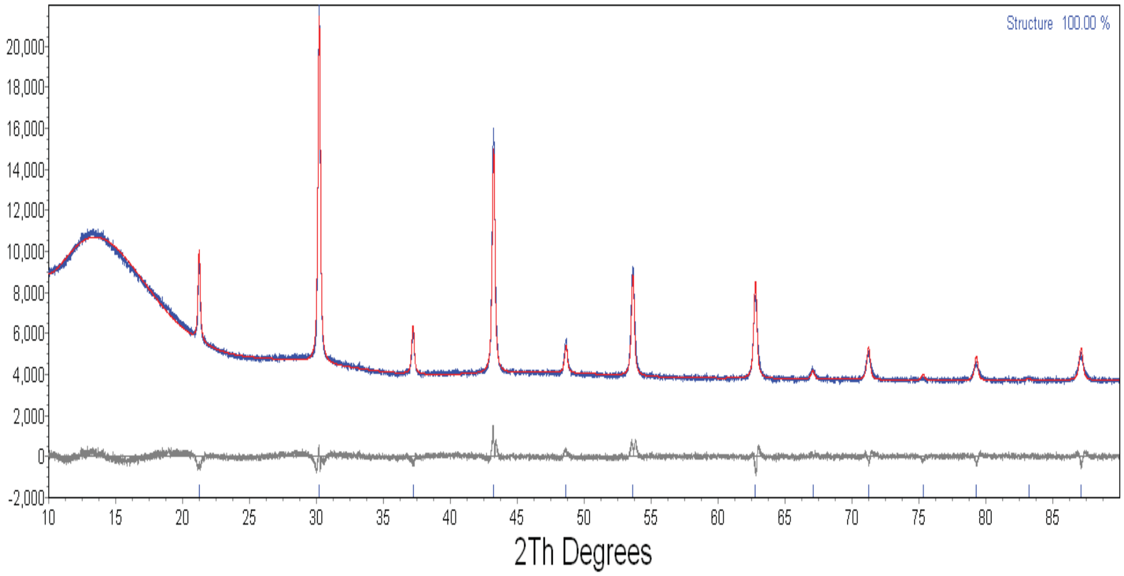

Figure 6.17: Powder X- ray diffraction data and Rietveld refinement for 1301 $KCu_{0.1}Mn_{0.9}F_3$. Blue curve is experimental, red curve is calculated.

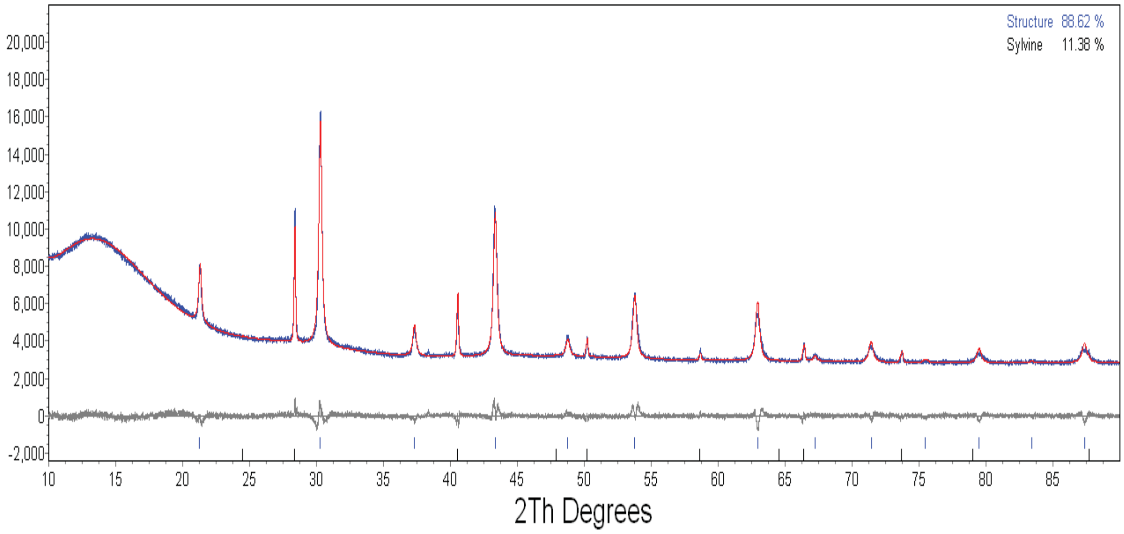

Figure 6.18: Powder X- ray diffraction data and Rietveld refinement for 1302 $KCu_{0.2}Mn_{0.8}F_3$

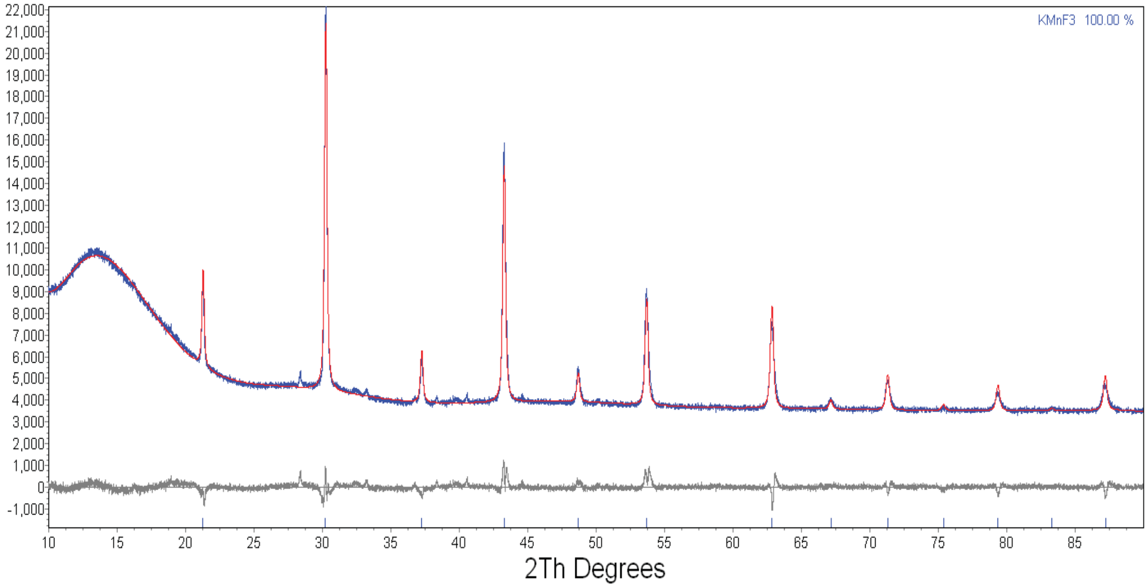

Figure 6.19: Powder X- ray diffraction data and Rietveld refinement for 1303 $KCu_{0.3}Mn_{0.7}F_3$. Blue curve is experimental, red curve is calculated.

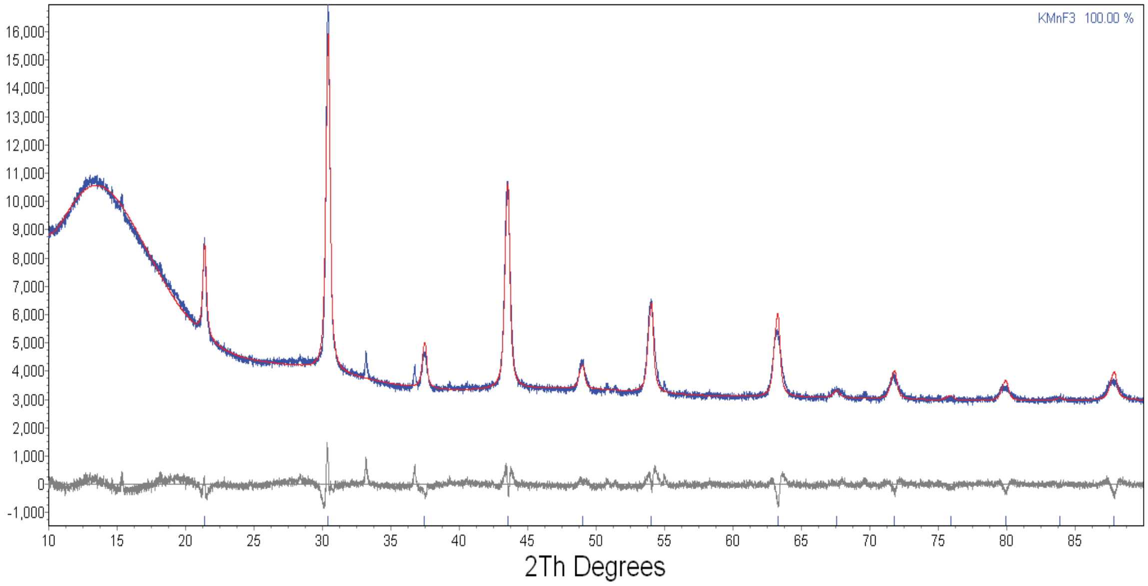

Figure 6.20: Powder X- ray diffraction data and Rietveld refinement for 1304 $KCu_{0.4}Mn_{0.6}F_3$

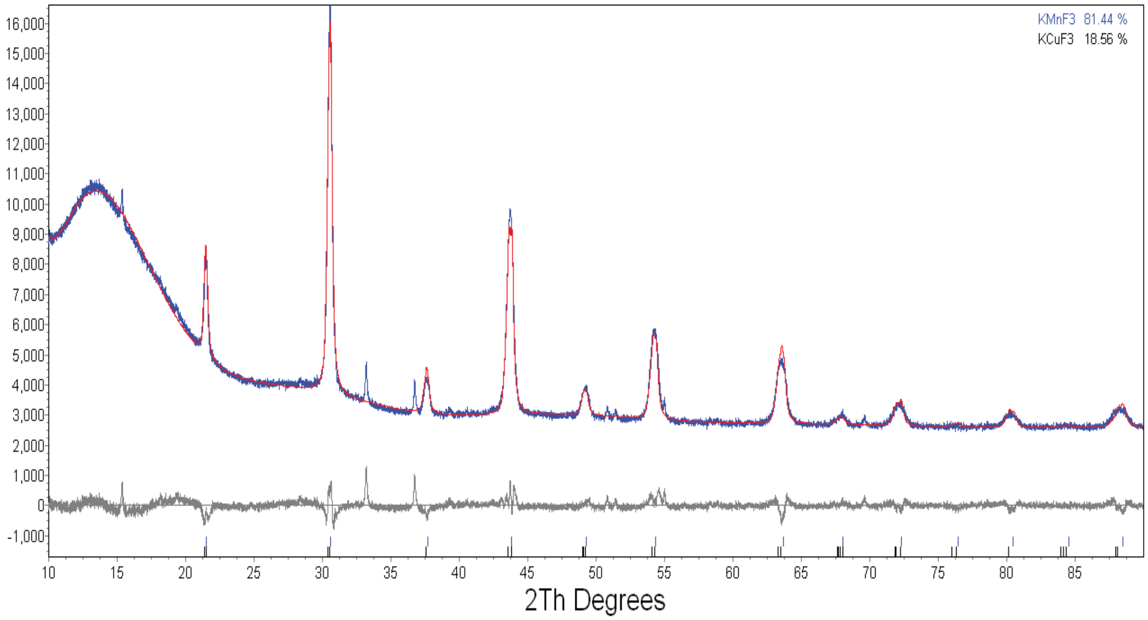

Figure 6.21: Powder X- ray diffraction data and Rietveld refinement for 1305 $KCu_{0.5}Mn_{0.5}F_3$. Blue curve is experimental, red curve is calculated.

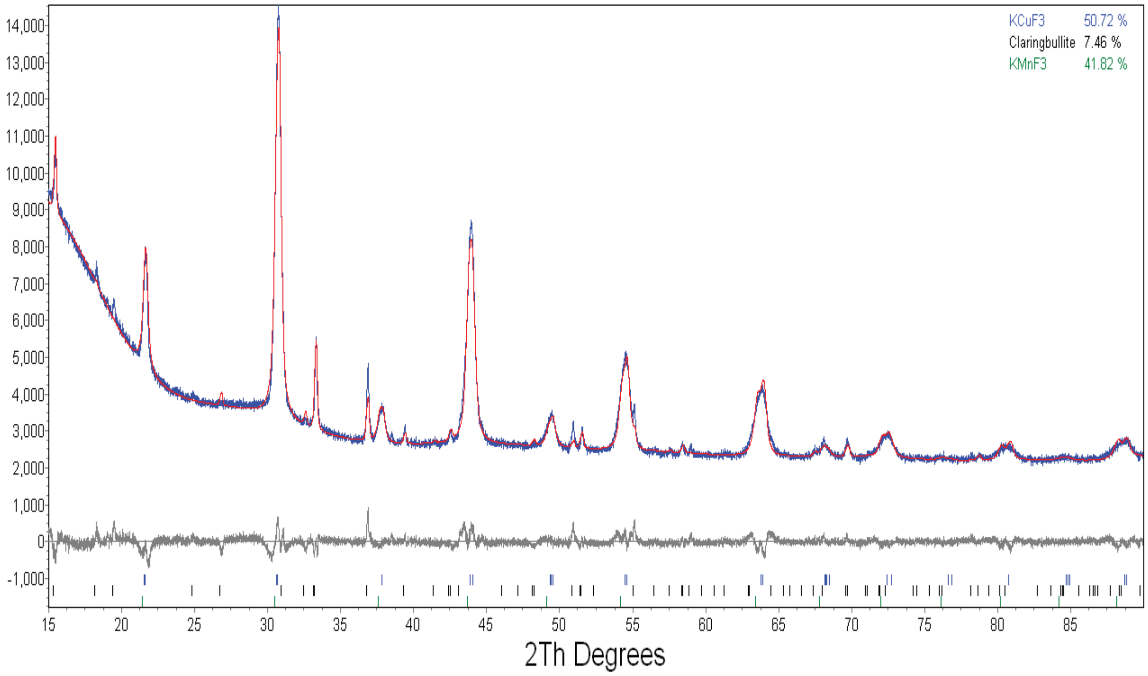

Figure 6.22: Powder X- ray diffraction data and Rietveld refinement for 1306 $KCu_{0.6}Mn_{0.4}F_3$

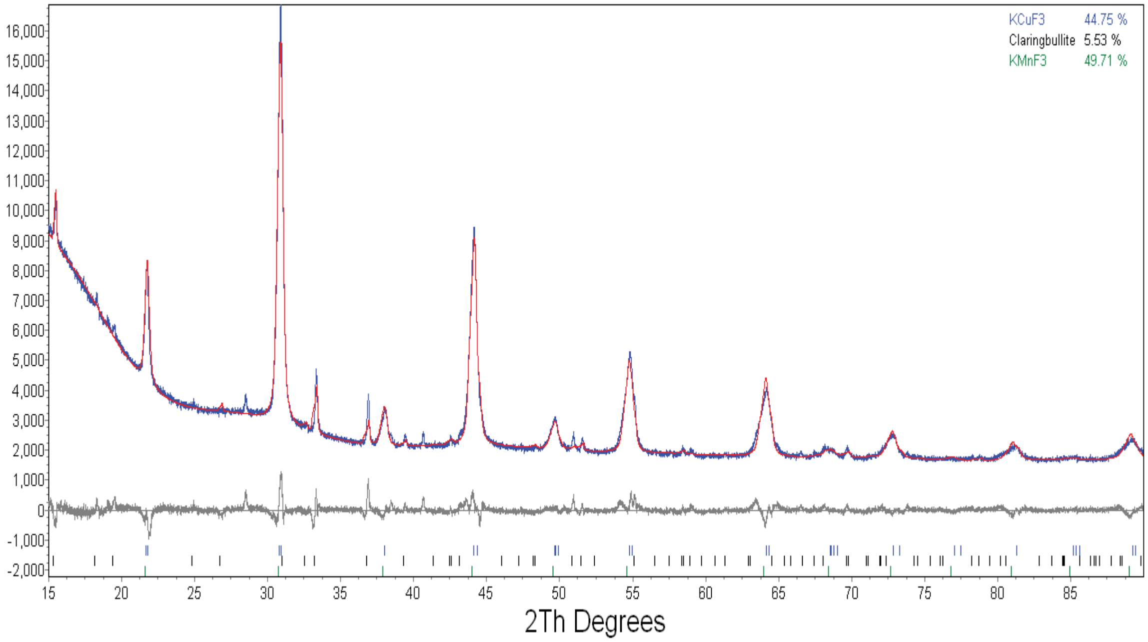

Figure 6.23: Powder X- ray diffraction data and Rietveld refinement for 1307 $KCu_{0.7}Mn_{0.3}F_3$. Blue curve is experimental, red curve is calculated.

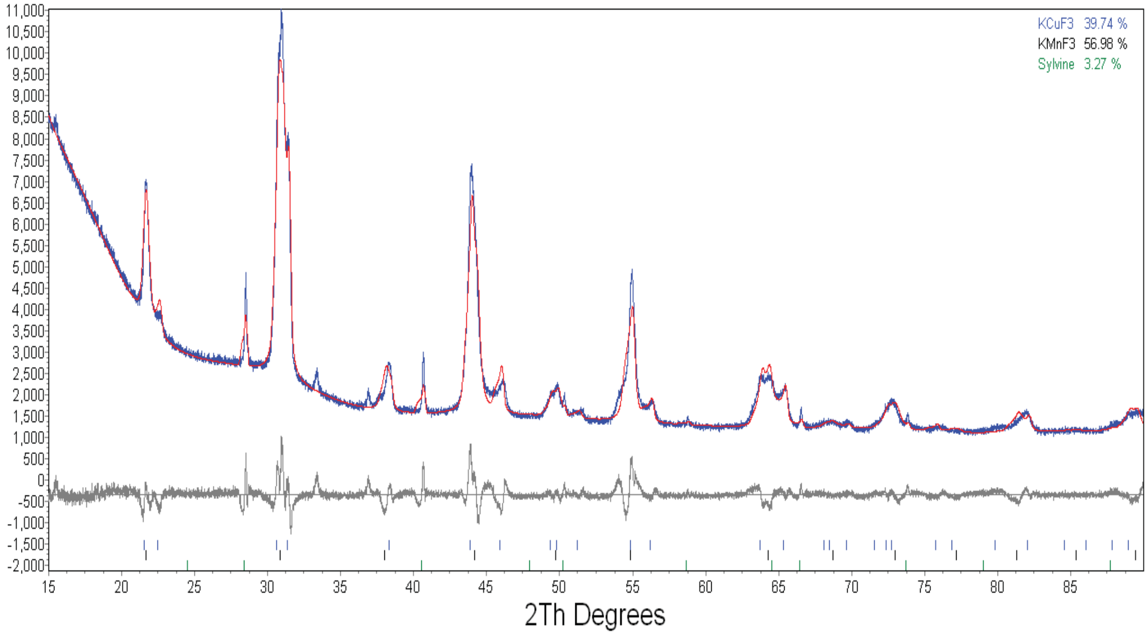

Figure 6.24: Powder X- ray diffraction data and Rietveld refinement for 1308 $KCu_{0.8}Mn_{0.2}F_3$

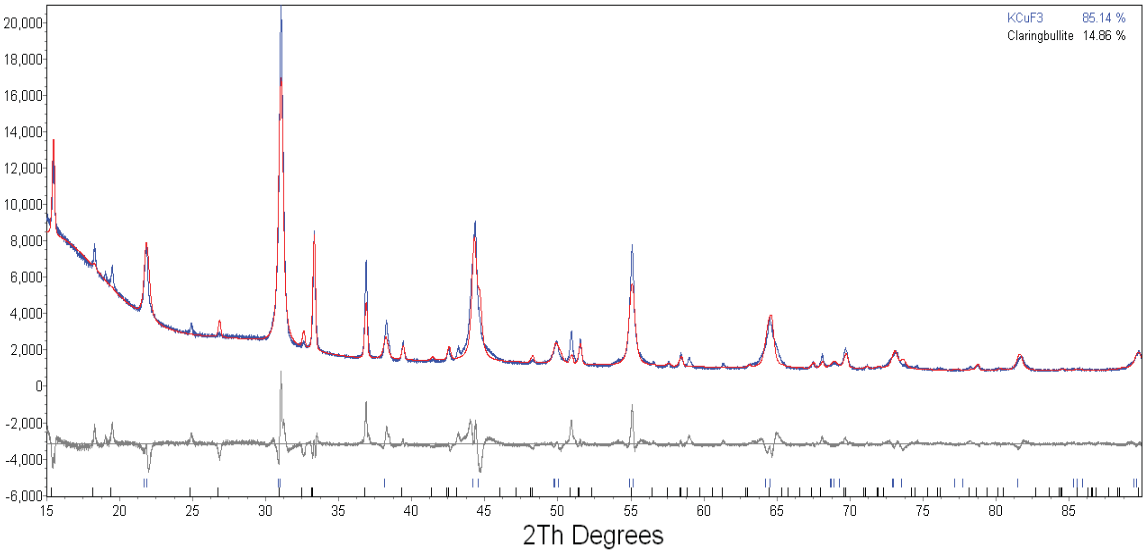

Figure 6.25: Powder X-ray diffraction data and Rietveld refinement for 1309 $KCu_{0.9}Mn_{0.1}F_3$. Blue curve is experimental, red curve is calculated.

From the XRF data shown in Table 6.1, it can be seen that the target compositions $K(Cu_xNi_{1-x})F_3$ were for the most part accurately prepared by the students. The students' work was taken to the next step by performing Rietveld refinements of the data, with the results indicating that for the $K(Cu_xNi_{1-x})F_3$ series, the cubic formation can only be held through the x = 0.64 sample as seen in Figure 6.13 We see that when x = 0.71, 0.82 and 0.91 there is a two phase region of both the cubic and tetragonal phases as seen in Figures 6.14, 6.15 and 6.16 respectively.

For the $K(Cu_xMn_{1-x})F_3$ series the Rietveld refinements show that the cubic formation can only be sustained up to x = 0.33 as seen in Figure 6.20. The two-phase region is observed when x = 0.44, 0.57, 0.67 and 0.78 as seen in Figures

6.21, 6.22, 6.23 and 6.24, respectively. For the Cu-Mn system the tetragonal formation takes over at x = 0.88 as seen in Figure 6.25.

As stated, the cubic formation can be sustained in the $K(Cu_xNi_{1-x})F_3$ system up to x = 0.64, but can only be sustained in the $K(Cu_xMn_{1-x})F_3$ system up to x = 0.33. For these systems in general, as Cu^{2+} ions are dissolved in the KMF_3 host lattice, the Jahn-Teller distorted Cu^{2+} sites are oriented randomly, and the cubic phase is sustained until the system is Cu-rich enough for cooperative J-T interactions to occur. At this point, either one or both polytypes of KCuF3 (see Fig. 6.4) could appear in the sample. Shannon-Prewitt[41] ionic radii for Ni^{2+}, Mn^{2+}, and Cu^{2+} are 69 pm, 83 pm, and 73 pm, respectively, and for $KNiF_3$ and $KMNF_3$, the cell parameters are 4.020 Å and 4.193 Å[39], respectively. Given that the unit cell parameters for pure KCuF3 are a = 4.14 Å and c = 3.93 Å[39], it might be expected that as Cu is dissolved in a cubic lattice, and as the cubic cell dimension approaches the value of 4.14 Å, then conditions may become optimal for the cooperative J-T interactions to occur. Thus as Cu is added to the $KNiF_3$ lattice, the lattice expands to 4.035 Å at X = 0.64, and the cubic structure is sustained until at x = 0.71 the system becomes Cu rich enough such that a larger tetragonal cell crystallizes with lattice dimensions to accommodate the cooperative interactions. For the $KMnF_3$ system, addition of Cu decreases the cell (already closer to the 4.14 Å value) until at X = 0.44 the lattice dimensions are optimized and a tetragonal cell crystallizes which is Cu-rich enough for cooperative interactions to occur. Erratic trends in relative percents of cubic vs.

tetragonal phase found as a function of x may reflect both the inaccuracy of compositional data, as well as the findings of subsequent studies (discussed later) that certain compositions may actually have precipitated as a range of coexisting tetragonal cells.

As noted from the Rietveld data discussed above, it was found that in the majority of compounds with cubic formations there was a KCl impurity, while in the tetragonal formations there was a claringbullite ($Cu_4(OH)_7Cl$) impurity. To attempt to purify the tetragonal formations it was proposed to use metal(II) bromide precursors instead of metal(II) chlorides, such that the chemical reaction shown in Eq. 6.1 was modified as follows:

$$3KF + MBr_2 \rightarrow KMF_3 + 2KBr_{aq} \text{ ; M=Mn, Ni and/or Cu} \qquad \text{Eq. 6.2}$$

These series of compounds were prepared by students during the Fall 2010 term, and the results from this study are summarized in Tables 6.3 and Table 6.4.

Table 6.3

Summary of Fall 2010 $K(Cu_xNi_{1-x})F_3$ Results

Group Number	Target Composition $KCu_xNi_{1-x}F_3$		Actual Composition (from X-Ray Fluorescence data) $KCu_xNi_{1-x}F_3$		Crystal System	Refined Unit Cell Lengths Determined from X-ray Powder Diffraction Data	% Match
	x	1-x	x	1-x		a (Å)	
1401	0.1	0.9	0.21	0.79	Cubic	4.01945	100%
1402	0.2	0.8	0.27	0.73	Cubic	4.02328	98.59*
1403	0.3	0.7	0.34	0.66	Cubic	4.02086	96.14*
1404	0.4	0.6	0.49	0.51	Cubic	a = 4.02400	87.87*
					Tetragonal	a = 4.1 c = 3.99	6.55*
1405	0.5	0.5	0.57	0.43	Cubic	a = 4.02584	81.938
					Tetragonal	a = 4.09422 c = 3.96925	13.18*
1406	0.6	0.4	0.89	0.11	Tetragonal	a = 4.1 c = 3.94	93.06*
1407	0.7	0.3	0.86	0.14	Tetragonal	a = 4.09364 c = 3.94719	88.06*
1408	0.8	0.2	0.96	0.04	Cubic	a = 4.08024	6.14*
					Tetragonal	a = 4.12299 c= 3.93166	83.62*

* These samples contain impurities of either KBr and/or claringbullite

Table 6.4

Summary of Fall 2010 $K(Cu_xMn_{1-x})F_3$ Results

Group Number	Target Composition $KCu_xMn_{1-x}F_3$		Actual Composition (from X-Ray Fluorescence data) $KCu_xMn_{1-x}F_3$		Crystal System	Refined Unit Cell Lengths Determined from X-ray Powder Diffraction Data a (Å)	% Match
	x	1-x	x	1-x			
1501	0.1	0.9	0.09	0.91	Cubic	a = 4.16770	100
1502	0.2	0.8	0.16	0.84	Cubic	a = 4.15526	100
1503	0.3	0.7	0.22	0.78	Cubic	a = 4.15346	88.44*
1504	0.4	0.6	0.32	0.68	Cubic	a = 4.14929	30.36*
					Tetragonal	a = 4.12687 c = 4.10464	64.30*
1505	0.5	0.5	9.45	0.55	Cubic	a = 4.13938	72.46*
					Tetragonal	a = 4.11121 c = 4.08914	17.44*
1506	0.6	0.4	0.56	0.43	Cubic	a = 4.10657	62.77*
					Tetragonal	a = 4.09424 c = 4.02871	31.25*
1507	0.7	0.3	0.66	0.34	Cubic	a = 4.10134	40.54*
					Tetragonal	a = 4.12550 c = 3.94380	48.94*
1508	0.8	0.2	0.78	0.22	Cubic	a = 4.09217	45.40*
					Tetragonal	a = 4.11454 c = 3.96752	46.93*
1509	0.9	0.1	0.90	0.10	Tetragonal	a = 4.09694 c = 4.05963	89.63*

* These samples contain impurities of either KBr and/or claringbullite

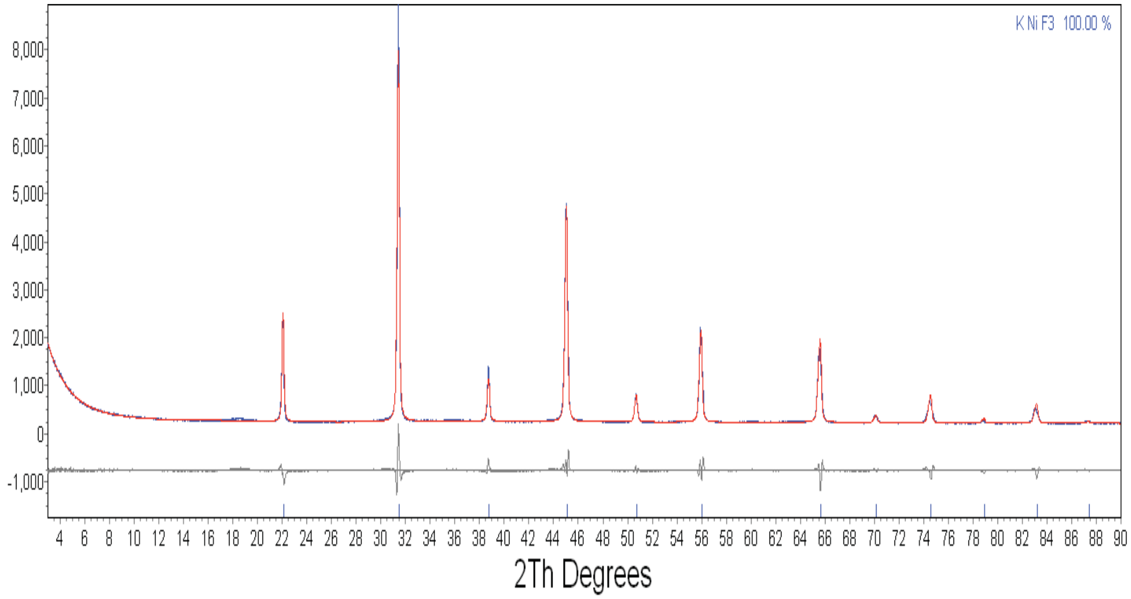

Figure 6.26: Powder X- ray diffraction data and Rietveld refinement for 1401 $KCu_{0.1}Ni_{0.9}F_3$. Blue curve is experimental, red curve is calculated.

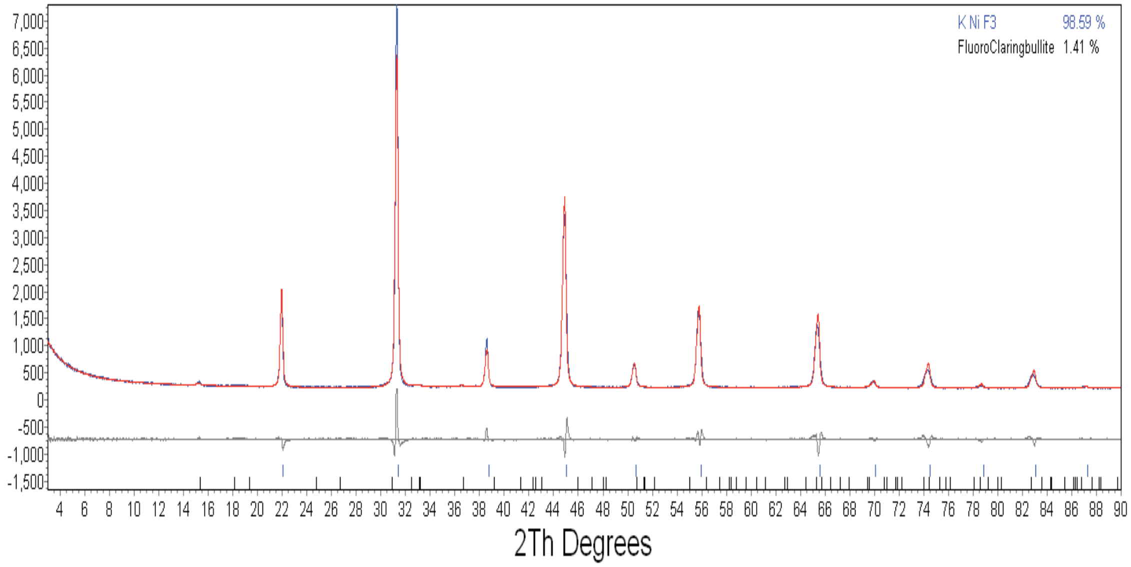

Figure 6.27: Powder X- ray diffraction data and Rietveld refinement for 1402 $KCu_{0.2}Ni_{0.8}F_3$

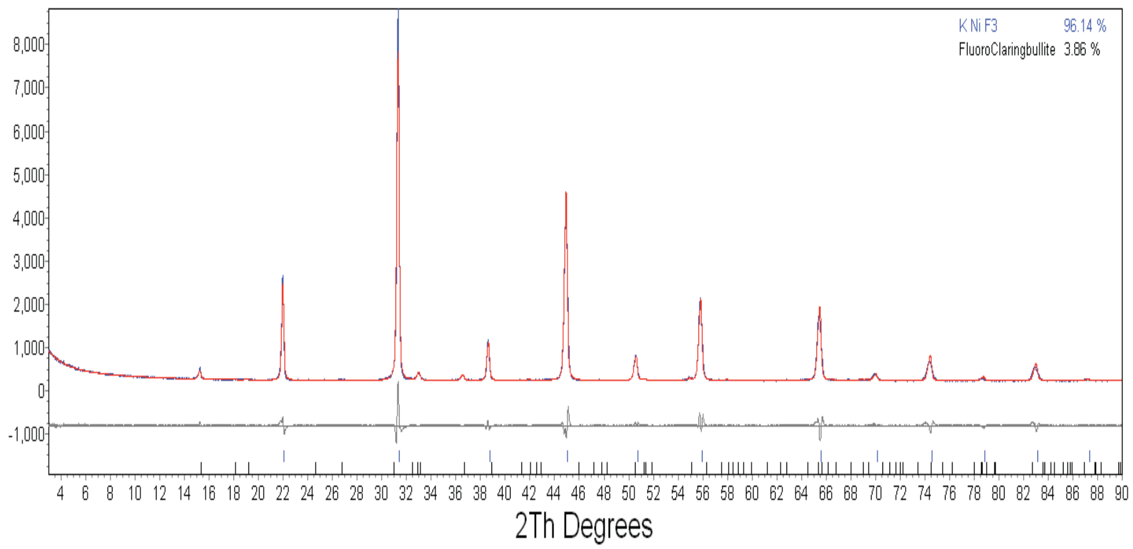

Figure 6.28: Powder X- ray diffraction data and Rietveld refinement for 1403 $KCu_{0.3}Ni_{0.7}F_3$. Blue curve is experimental, red curve is calculated.

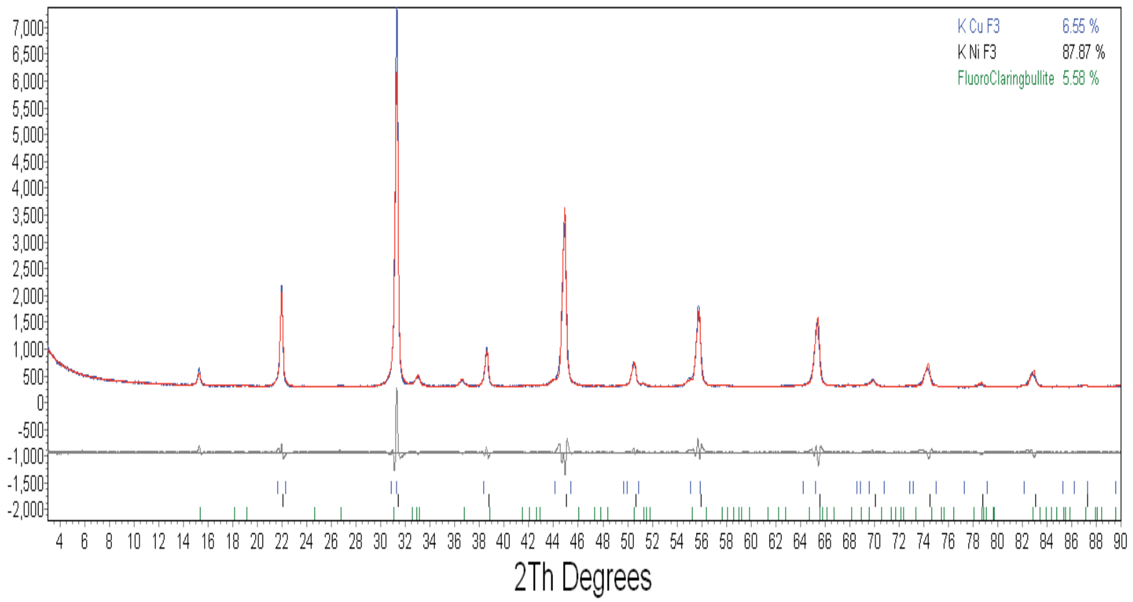

Figure 6.29: Powder X- ray diffraction data and Rietveld refinement for 1404 $KCu_{0.4}Ni_{0.6}F_3$

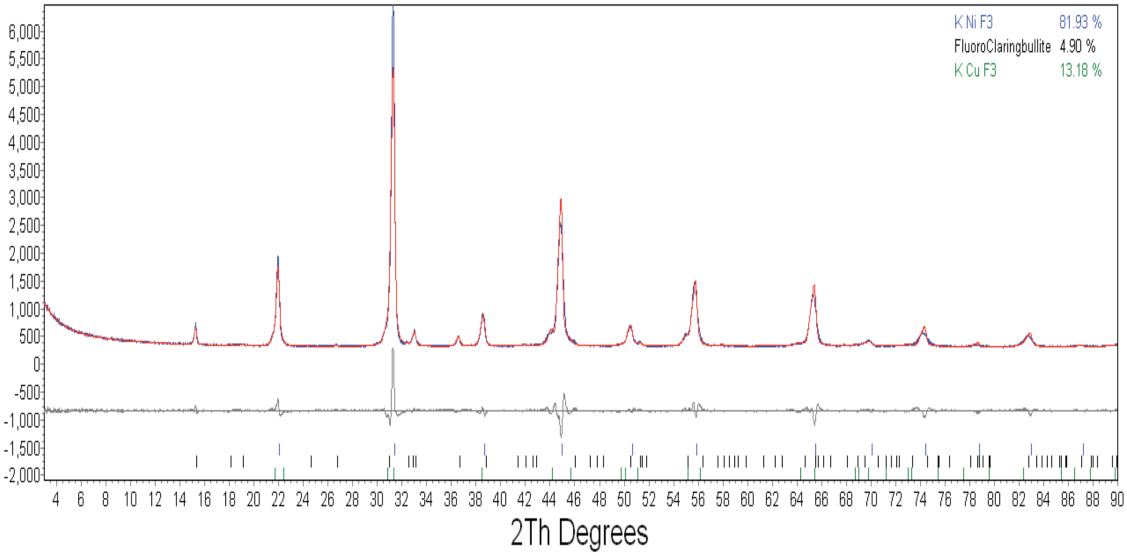

Figure 6.30: Powder X- ray diffraction data and Rietveld refinement for 1405 $KCu_{0.5}Ni_{0.5}F_3$. Blue curve is experimental, red curve is calculated.

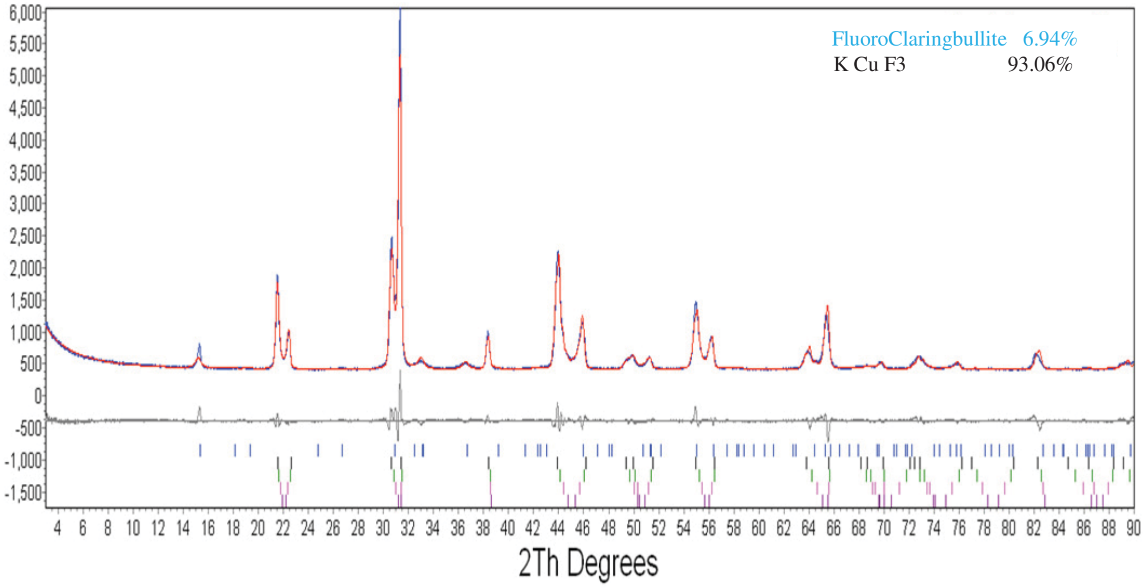

Figure 6.31: Powder X- ray diffraction data and Rietveld refinement for 1406 $KCu_{0.6}Ni_{0.4}F_3$

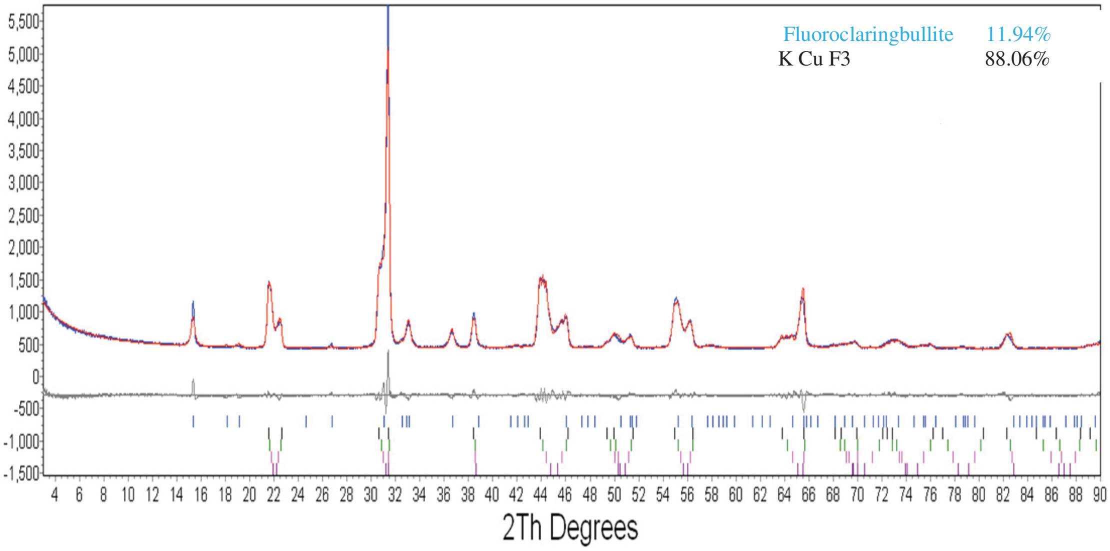

Figure 6.32: Powder X- ray diffraction data and Rietveld refinement for 1407 $KCu_{0.7}Ni_{0.3}F_3$. Blue curve is experimental, red curve is calculated.

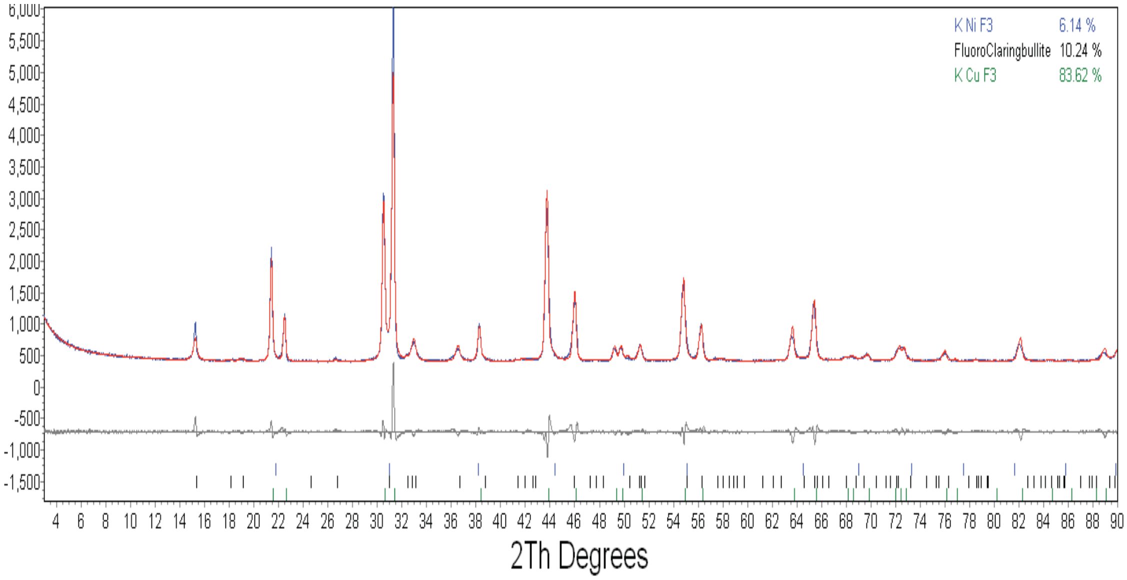

Figure 6.33: Powder X- ray diffraction data and Rietveld refinement for 1408 $KCu_{0.8}Ni_{0.2}F_3$

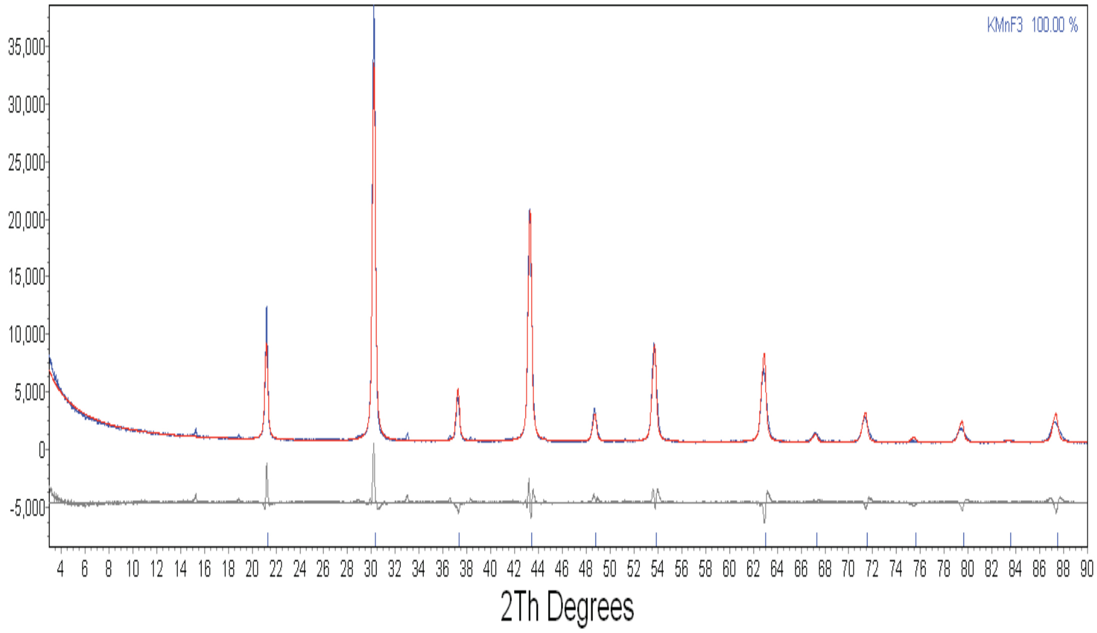

Figure 6.34: Powder X- ray diffraction data and Rietveld refinement for 1501 $KCu_{0.1}Mn_{0.9}F_{3.}$ Blue curve is experimental, red curve is calculated.

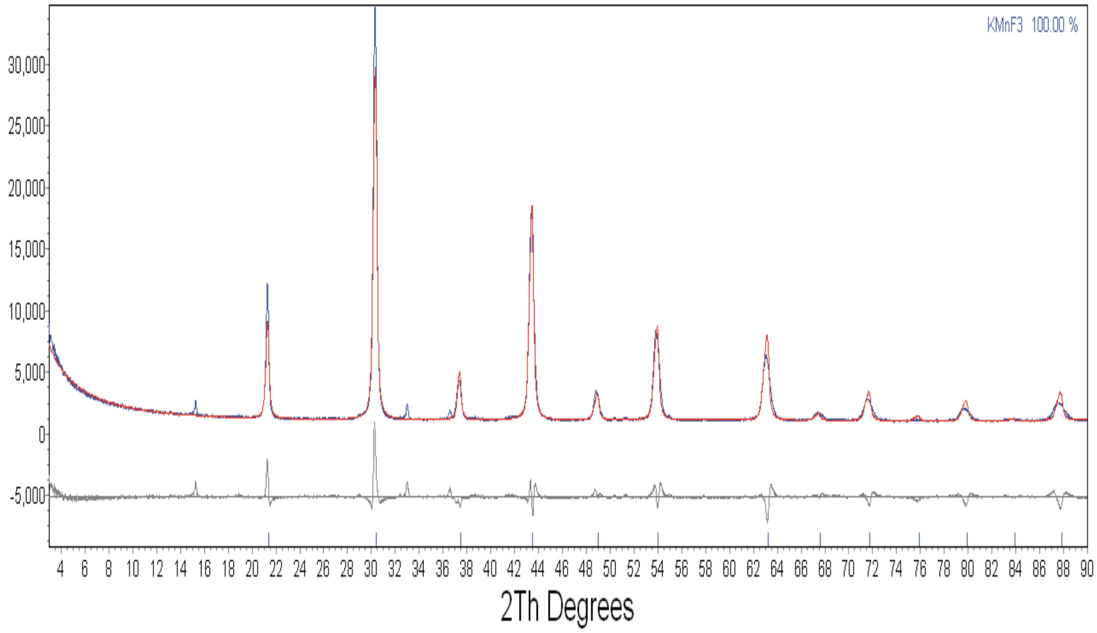

Figure 6.35: Powder X- ray diffraction data and Rietveld refinement for 1502 $KCu_{0.2}Mn_{0.8}F_3$

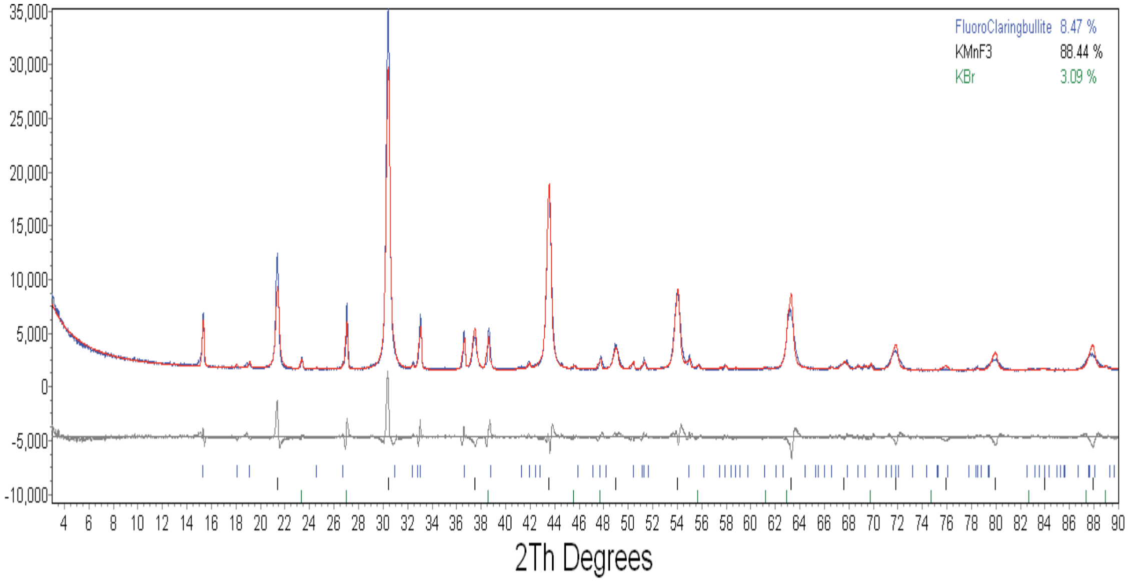

Figure 6.36: Powder X- ray diffraction data and Rietveld refinement for 1503 $KCu_{0.3}Mn_{0.7}F_3$. Blue curve is experimental, red curve is calculated.

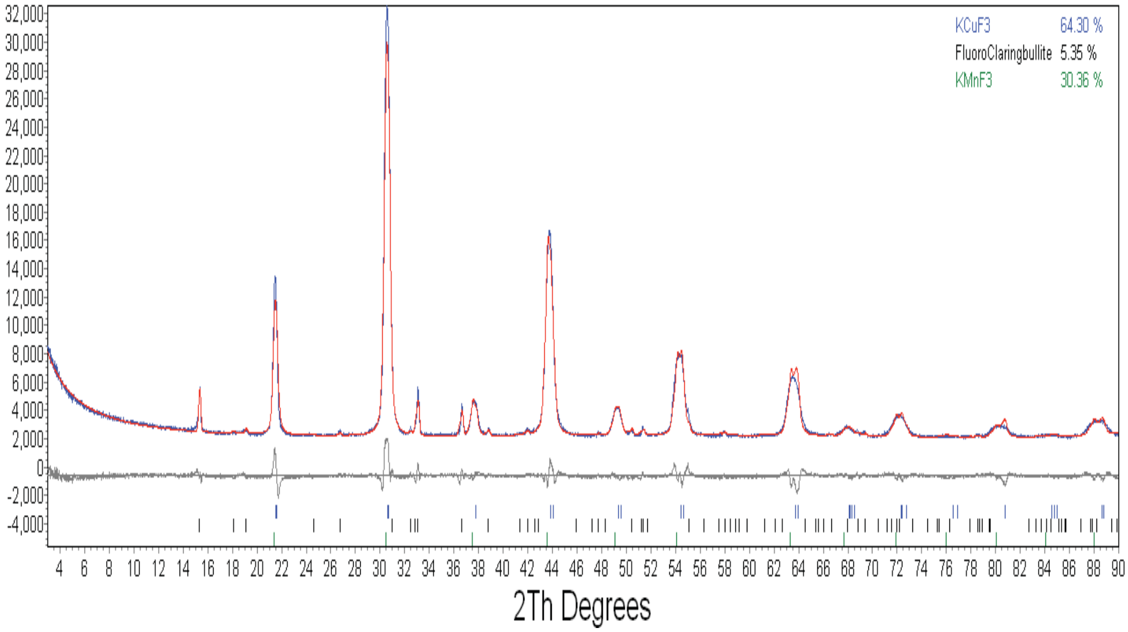

Figure 6.37: Powder X- ray diffraction data and Rietveld refinement for 1504 $KCu_{0.4}Mn_{0.6}F_3$

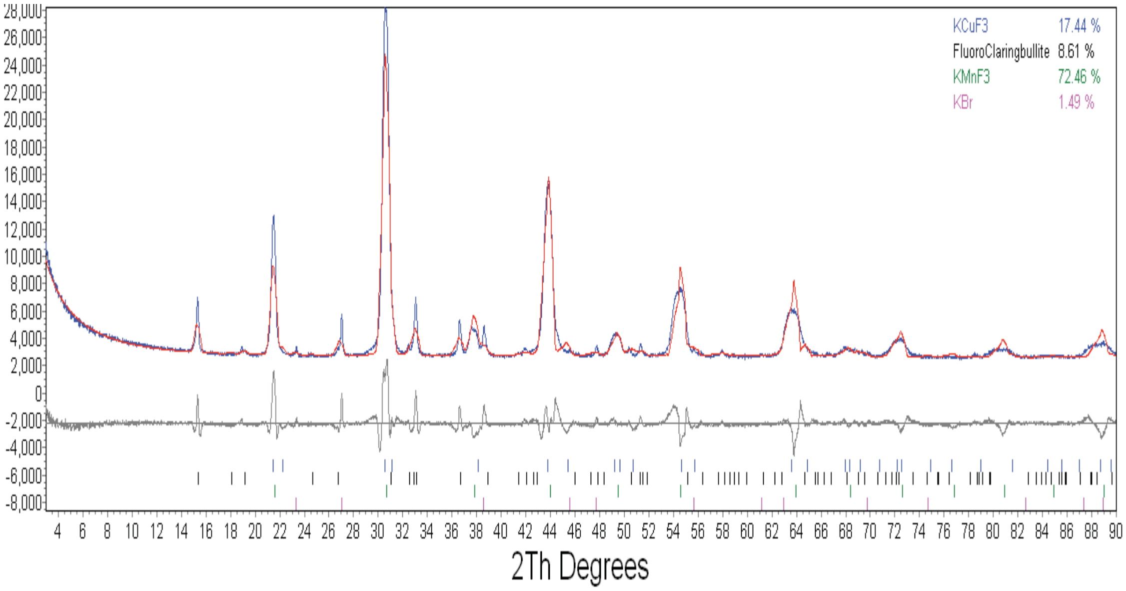

Figure 6.38: Powder X- ray diffraction data and Rietveld refinement for 1505 $KCu_{0.5}Mn_{0.5}F_3$. Blue curve is experimental, red curve is calculated.

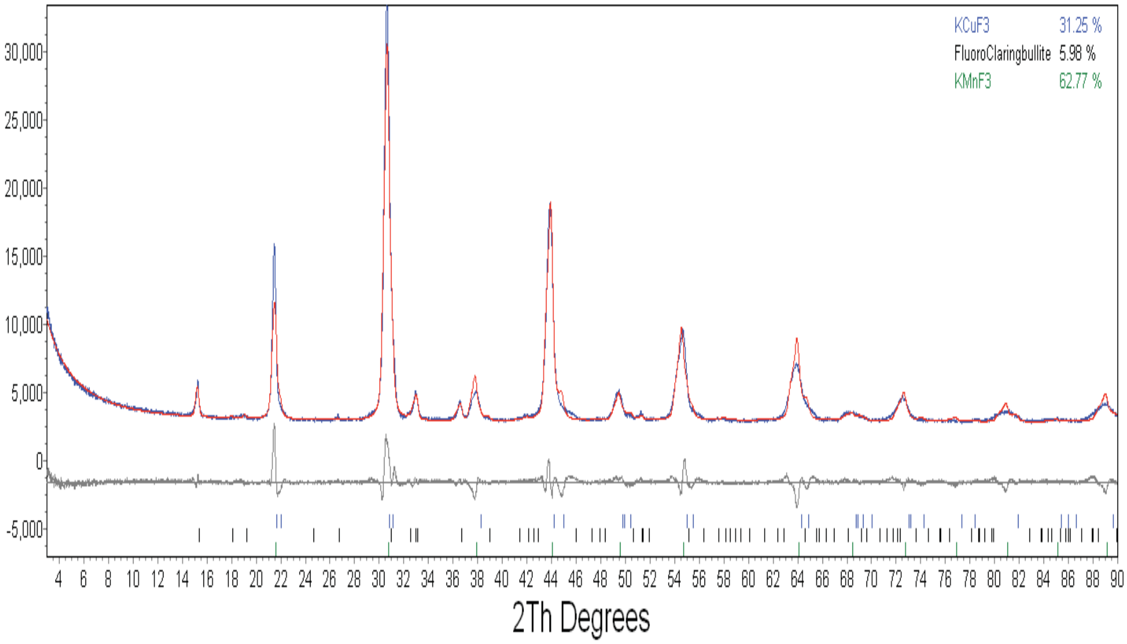

Figure 6.39: Powder X- ray diffraction data and Rietveld refinement for 1506 $KCu_{0.6}Mn_{0.4}F_3$

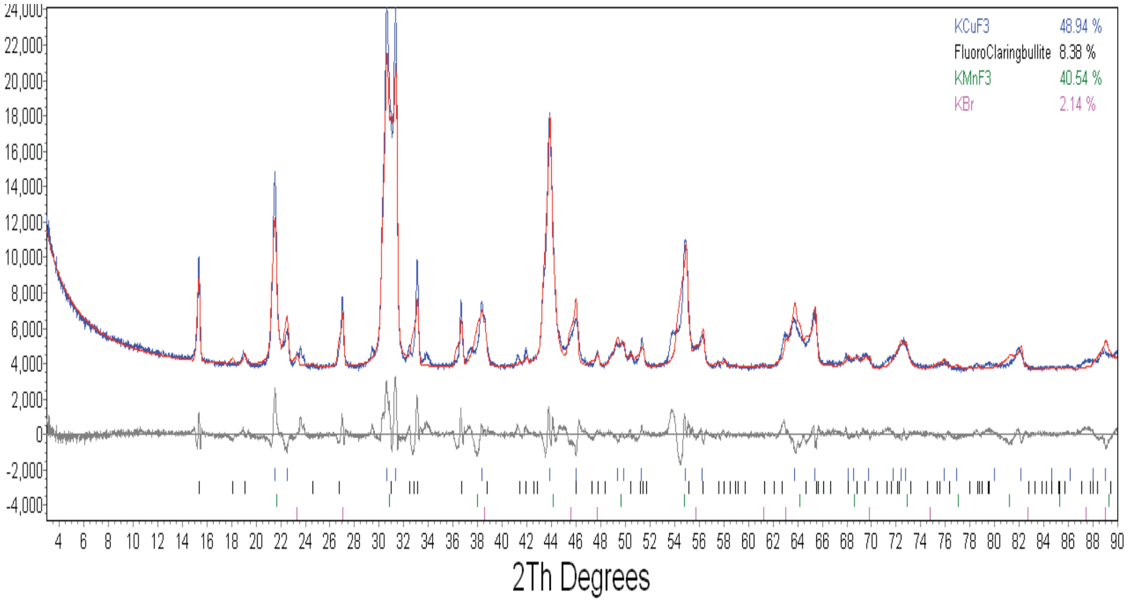

Figure 6.40: Powder X- ray diffraction data and Rietveld refinement for 1507 $KCu_{0.7}Mn_{0.3}F_3$. Blue curve is experimental, red curve is calculated.

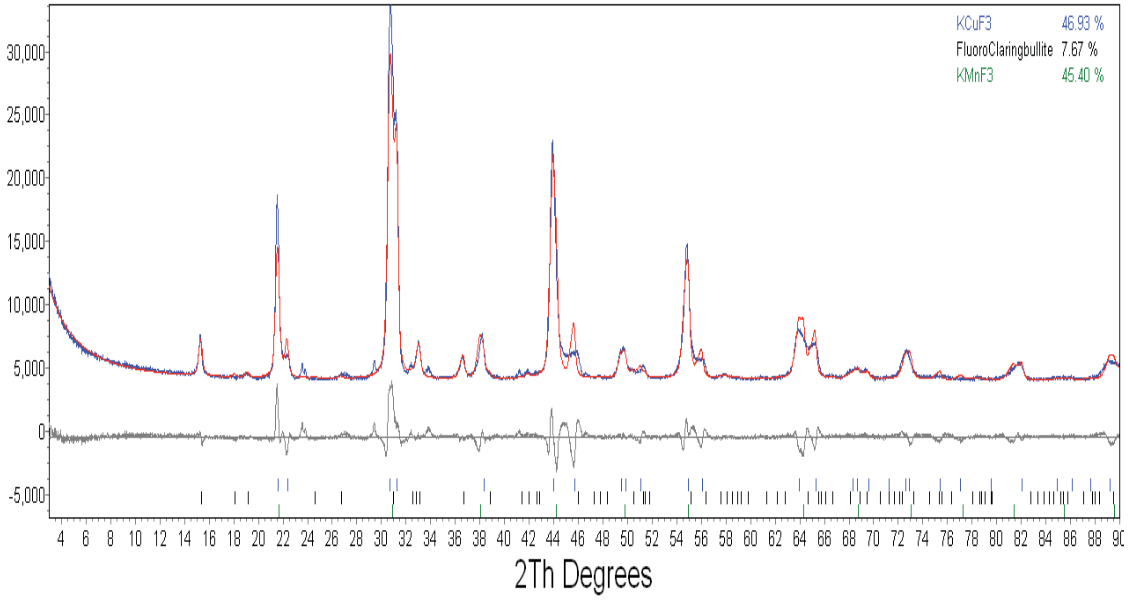

Figure 6.41: Powder X- ray diffraction data and Rietveld refinement for 1508 $KCu_{0.8}Mn_{0.2}F_3$

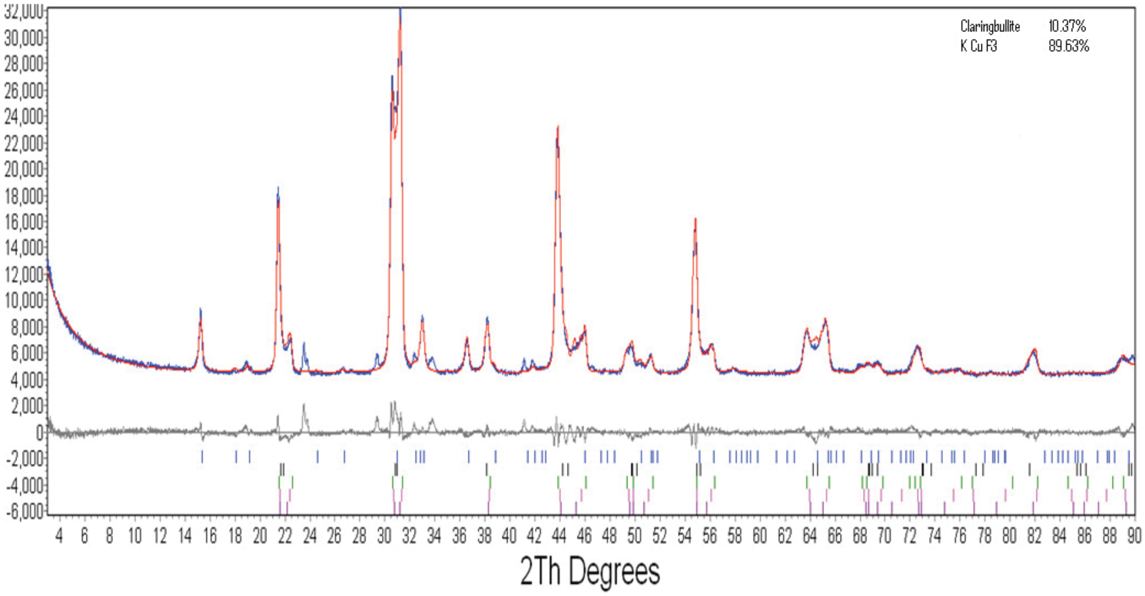

Figure 6.42: Powder X- ray diffraction data and Rietveld refinement for 1509 $KCu_{0.9}Mn_{0.1}F_3$. Blue curve is experimental, red curve is calculated.

It was found in these samples that the same types of impurities were present as observed in the previous syntheses using metal chloride precursors. However, it was seen in these latter samples that not only was a claringbullite phase found in the tetragonal phases, but it was also present in the cubic phases along with KBr in some samples. In addition, although we had previously assigned the impurity as claringbullite, which has the chemical formula $Cu_4(OH)_7Cl$, it was found for these samples that the impurity that is present is actually fluoroclaringbullite. In fluoroclaringbullite the chloride ion is replaced by a fluoride ion making it isostructural to claringbullite, meaning that substituting bromide ions in place of chloride ions in the synthesis cannot prevent formation of impurity using this synthesis procedure.

For the case of the $K(Cu_xNi_{1-x})F_3$ system, it is seen in Figs. 6.26-6.28 that a single cubic phase is observed with x = 0.21 to 0.34 and in Figs. 6.29 & 30 for x = 0.49 & 0.57, a tetragonal phase appears which is mixed with cubic material. In Figs. 6.31-32 at x = 0.89 to 0.86 it is observed that refinement using a tetragonal phase gives the best fit. In Fig. 6.33 at x = 0.96 it is observed that a tetragonal phase with a mixed cubic material reappears after the previous two compounds showed tetragonal phases, this can be due to error in synthesis. (Note that a phase for x = 0.9 was not prepared by this section from Fall 2010, due to a small class size). For the case of $K(Cu_xMn_{1-x})F_3$ systems, the Rietveld refinement results shown in Figs. 6.34-6.36 for x = 0.09 to 0.22 indicate that a single cubic phase is observed. For $K(Cu_xMn_{1-x})F_3$ the cubic phase is only held until x= 0.22, then at x = 0.32 to 0.78 (Figs. 6.37- 6.41) a mixed tetragonal and cubic phase material is observed. A single tetragonal phase is only observed for the x = 0.9 phase (i.e. see Fig. 6.42). Comparisons of some of the results for the Spring vs. Fall 2010 samples are given in Table 6.5.

Table 6.5

Comparison of Results for Spring vs. Fall 2010 Results

	Spring 2010 $KCu_xNi_{(1-x)}F_3$	**Fall 2010 $KCu_xNi_{(1-x)}F_3$**	**Spring 2010 $KCu_xMn_{(1-x)}F_3$**	**Fall 2010 $KCu_xMn_{(1-x)}F_3$**
First Appearance of Mixed Cubic and Tetragonal Phase	x = 0.71	x = 0.49	x = 0.44	x = 0.32
First Appearance of Single Tetragonal Phase	Not observed	x = 0.86	x = 0.88	x = 0.90

The major discrepancy evident in Table 6.5 from the comparison of phase data obtained from Rietveld refinements for the Spring and Fall 2010 samples is the relatively large difference in the amounts of Cu that can be dissolved in the cubic $KNiF_3$ lattices for the Spring 2010 vs. Fall 2010 semesters. The same trend (but to a lesser extent) is seen for the Mn sample. Whether or not this is due to some systematic error in analysis for one of the semesters, or is an artifact of the use of metal chlorides vs. bromides in the synthesis is not known.

Previously in a $K(Cu_xCo_{1-x})F_3$ series made by students of Rachel Kusnic, the tetragonal phase (along with cubic) first appeared at x = 0.72[43], similar to the value of x = 0.71 observed for the Cu-Ni system in Spring 2010. By comparison, for the Mn-containing samples, the tetragonal phase appears at a relatively lower value, e.g. x = 0.44 for the Spring 2010 sample. The only paper published to date on any system related to those described in this chapter was by Burns[42] *et al.* on the $K(Cu_xMg_{1-x})F_3$ series. In this study, samples were prepared via solid state reactions of stoichiometric mixtures of binary fluoride precursors. No dual phase mixtures were observed, but the tetragonal phase first appeared at about x = 0.6.

In general, a reasonable trend to expect for these systems would be that the smaller the cubic KMF_3 lattice, the smaller the amount of Cu^{2+} that can be dissolved before cooperative Jahn-Teller effects are observed. That is, in a larger cell, Cu^{2+} ions are further apart so that it would seem likely that a higher concentration of them is needed before long-range interactions affect the lattice geometry. Given that the cubic cell parameters for KMF_3 phases for M = Mn, Co, Ni, and Mg are 4.193 Å, 4.089 Å, 4.020 Å, and 3.986 Å, respectively, while the corresponding Cu composition at first appearance of tetragonal phase are x = 0.44 or 0.32, 0.72, 0.71 or 0.49, and 0.60, respectively, it is clear that the general trend as stated is not followed. However, note that the trend is actually followed for the Mg, Ni (for Spring 2010 value of x = 0.71 only), and Co systems if the Mn data is ignored. Recall from the discussion of Spring 2010 results above, considering that the lattice dimensions of $KCuF_3$ of a = b = 4.14 Å and c = 3.93 Å[39], it can be assumed that as a cubic cell dimension approaches the value of 4.14 Å, then conditions may become optimal for the cooperative J-T interactions to occur in the a-b plane. For phases such as $KMnF_3$ with cell parameters above this value, the implication is that Cu can be dissolved in the lattice only until the lattice dimensions are reduced to around this optimal value of 4.14 Å. Thus two separate trends are actually expected: (1) increasing values of x (= Cu content) can be dissolved in cubic KMF_3 lattices with parameters increasing *up to* an optimal value of 4.14 Å, and (2) increasing values of x are expected to dissolve in cubic lattices with cell parameters increasing *away from* the optimal value. Thus, the Mn result does not follow the general trend in the series discussed here, because it is beginning a new trend.

Subsequent Refinements of Fall 2010 data: COFSP Project

As previously stated in the Introduction section, the REEL project is implemented only in Ohio and is funded through the National Science Foundation Undergraduate Research Centers Program(NSF-URC). Also implemented at YSU is the Choose Ohio First Scholarship Program (COFSP). In Spring 2011, the students of the COFSP performed subsequent refinements to the $K(Cu_xNi_{1-x})F_3$ samples from Fall 2010. The results from this study are summarized in Table 6.6, and PXRD patterns and Rietveld refinements of some of the samples are given in Fig 6.43.

Table 6.6

Summary of COFSP Project Results

Target Composition *$KCu_xNi_{1-x}F_3$		**Crystal system**	**Refined Unit Cell Lengths Determined from X-ray Powder Diffraction Data**	**% Match From Rietveld Refinement**
x	**1-x**		**(Å)**	**Mass %
0.0	1.0	Cubic	4.01877	100
0.1	0.9	Cubic	4.01945	100
0.2	0.8	Cubic	4.02323	99
0.3	0.7	Cubic	4.02086	98
0.4	0.6	Cubic	4.02430	90
		Tetragonal	a = 5.7902 c = 7.938	7.4
0.5	0.5	Cubic	4.02632	81.60
		Tetragonal	a = 5.7902 c = 7.938	13.54
0.6	0.4	Tetragonal Phases A, B, C, & D	A: a = 5.830; c = 7.855 B: a = 5.798; c = 7.880 C: a = 5.7629; c = 7.940 D: a = 5.7275; c = 8.000	A: 10.33 B: 60.02 C: 7.62 D: 16.07
0.7	0.3	Tetragonal Phases A, B, C, & D	(Identical to values above for x = 0.6)	A: 18.05 B: 26.67 C: 21.89 D: 21.97
0.8	0.2	Tetragonal Phases A, B, C, & D	(Identical to values above for x = 0.6)	A: 73.50 B: 11.62 C: 3.71 D: 1.06
1.0	0.0	Tetragonal	a = 4.11140 c = 3.94135	90.24

* Sample for x = 0.9 was not prepared.

** The impurity phase fluoroclaringbullite, $Cu_4(OH)_7F$, is present in all phases except those for x = 0.0 & 0.1

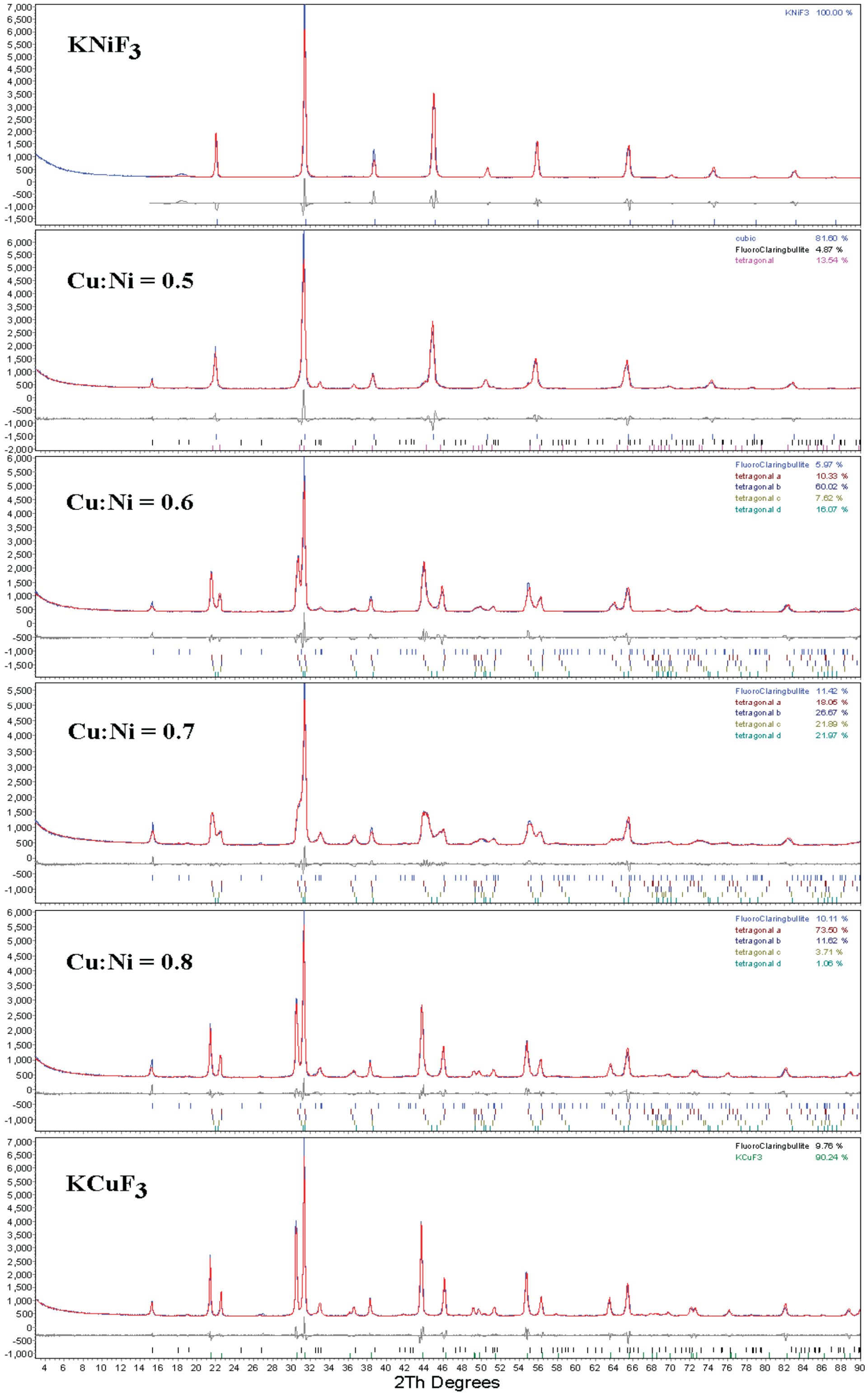

Figure 6.43: Powder X- ray diffraction data and Rietveld refinement for COFSP refinement of $KCu_xNi_{1-x}F_3$

An interesting result that emerged in these refinements is that precipitation of a continuous range of tetragonal compositions (rather than the single phase composition expected) was modeled in the $K(Cu_xNi_{1-x})F_3$ systems for which x was large enough (i.e. Cu-rich enough) such that a tetragonal product precipitated. As can be observed in Table 6.6, this occurs for x =0.6, 0.7 and 0.8. It can be noted by inspection of the PXRD pattern of, e.g. $K(Cu_{0.7}Ni_{0.3})F_3$ (shown enlarged in Fig. 6.44) that the peaks for this sample are relatively broader than those for the end members shown in the patterns above and below it, but do not have the shape expected from broadening due to small particle size. Rather, they appear to consist of several peaks very close together with different intensities. Thus, in order to account for the peak profiles observed in experimental data for some COFSP samples, it was deemed necessary to refine four different tetragonal phases spanning a range of a & c cell parameters.

Presumably, the different cell parameters result from different phase compositions precipitating out in the same mixture. These different but closely related compositions would have very similar energies, so that co-precipitation would be quite feasible. While it is possible that such continuous phases may have precipitated out in the Spring 2010 samples, inspection of the PXRD peaks for those samples suggests that it does not appear to be as prevalent. Whether or not this is some artifact of the use of bromides rather than chlorides

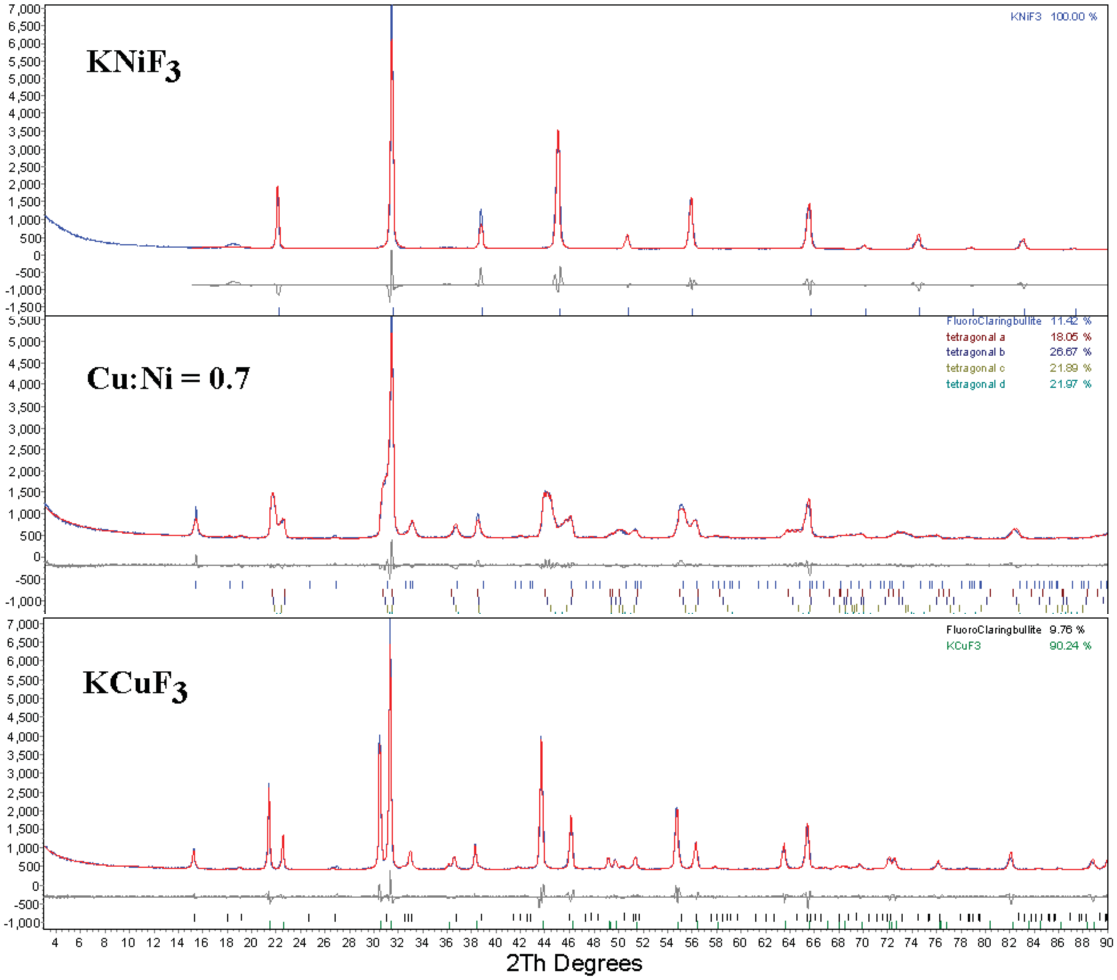

Figure 6.44: Rietveld refinement data for K($Cu_{0.7}Ni_{0.3}$)F_3 shown is expanded here to better enable inspection of peak profiles (see text).

for the latter compounds, or some subtle variation in sample preparation or other conditions in the lab between the three groups of students, is not known.

Table 6.7 compares the results of refinements of the Spring and Fall 2010 $K(Cu_xNi_{1-x})F_3$ samples to the COFSP refinements of the same samples previously analyzed in Fall 2010. As summarized in the Table, for the Fall 2010 samples there were mixed tetragonal and cubic phases observed at x = 0.42, 0.56 and 0.82 and a single tetragonal phase observed at x = 0.64 and 0.71. However for the COFSP $K(Cu_xNi_{1-x})F_3$ samples there were mixed tetragonal and cubic phases also observed at x = 0.42 and 0.56, but for x = 0.64-0.82 the samples were refined to four different tetragonal phases spanning a range of a & c cell parameters. This could possibly mean that the Fall 2010 samples for x = 0.42, 0.56, 0.64 and 0.82 were incorrectly refined as two-phase materials when in reality they are better represented as unusual mixtures consisting of a range of tetragonal phases. This could also be the case with the single tetragonal phases observed at x = 0.64 and 0.71 for the Fall 2010 samples. At this point, the refinements are not rigorous enough to make quantitative comparisons of R values, etc. in order to establish the better model.

Table 6.7

Summary of Three Trials of Rietveld Refinement Data for $KCu_xNi_{1-x}F_3$ Samples

$KCu_xNi_{1-x}F_3$ (Spring 2010, chloride salts) C = cubic, T = tetragonal phase			**$KCu_xNi_{1-x}F_3$ (Fall 2010, bromide salts) C = cubic, T = tetragonal phase**			**$KCu_xNi_{1-x}F_3$ (Fall 2010, COFSP) C = cubic, T = tetragonal phase**		
x	Cell (Å)	% clngb.*	x	Cell (Å)	% clngb.*	x	Cell (Å)	% clngb.**
0.42	**C:** 4.027	0	0.49	**C:** 4.024 (87%) **T:** 4.100, 3.990	5.58	0.49	**C:** 4.024 (90%) **T:** 5.790, 7.938 (7.4)	2.6
0.56	**C:** 4.033	0	0.57	**C:** 4.026 **T:** 4.094, 3.969	4.88	0.57	**C:** 4.026 **T:** 5.7902, 7.938	4.87
0.64	**C:** 4.035	0	0.89	**T:** 4.100, 3.940, equiv to: **T:** 5.798, 7.880	6.94	0.89	A: 5.830, 7.855 (10%) B: 5.798, 7.880 (60%) C: 5.763, 7.940 (8%) D: 5.728, 8.000 (16%)	5.97
0.71	**C:** 4.038 **T:** 4.13, 3.092	0	0.86	**T:** 4.094, 3.947 equiv to: **T:** 5.790, 7.894	11.94	0.86	Same as values for x = 0.64 above	11.42
0.82	**C:** 4.037 **T:** 4.077, 3.976	4.61	0.96	**C:** 4.080 **T:** 4.123, 3.932 equiv to: **T:** 5.831, 7.864	10.24	0.96	Same as values for x = 0.64 above	10.11

* claringbullite, $[Cu_4(OH)_7Cl]$

**fluoroclaringbullite, $[Cu_4(OH)_7$

Chapter 7

Conclusions and Future Work

Manganite Oxyfluoride Synthesis

The primary objective of this research project was to synthesize and investigate the magnetic properties of $Ca_2Mn_2O_5F$. The proposed synthesis of the target compound was broken into 4 steps, including first preparing $CaMnO_3$, followed by ammonolysis of this compound to give the oxygen deficient perovskite-related compound $Ca_2Mn_2O_5$, which in the third step was to be fluorinated to obtain the oxyfluoride, $CaMnO_2F$. The final step was then to react the oxyfluoride with $CaMnO_3$ acquired in step one to give the mixed valent manganite target compound, $Ca_2Mn_2O_5F$. Following several synthesis trials and approaches, $CaMnO_3$ was successfully prepared in this study using a sol-gel method as seen in Figure 5.2, and a citrate sol-gel process as shown in Figure 5.8. Once this first step was successfully completed, step 2 was attempted, however step 2 proved to be more difficult than initially expected. After ammonolysis trials failed, a new technique using urea was attempted. Urea was viewed as a desirable method because it requires a lower temperature and a reduced reaction time compared to the ammonolysis route. However, from the attempt using urea it can be concluded that the initial synthesis of using ammonia gas is the superior method to synthesizing $Ca_2Mn_2O_5$. This is because it was seen that the ammonia produced from the urea in the 30 minutes of heating was too much and reduced the $CaMnO_3$ sample past the desired point and the ammonia reacted with some excess nitrate from the starting material $Mn(NO_3)_2 \cdot 4H_2O$ to produce NH_4NO_3. Due to exhaustive attempts at making $CaMnO_3$ and $Ca_2Mn_2O_5$, only the first two of the proposed four-step synthesis of $Ca_2Mn_2O_5F$ could be attempted in this research project.

Based on the results described herein, it is apparent that future work should focus on the successful synthesis and investigation of $Ca_2Mn_2O_5F$ through continuation of the originally proposed ammonolysis route, or a somewhat modified approach of the urea route. For example, different ratios of $CaMnO_3$ and urea could be used in order to decrease the amount of ammonia that is produced, in turn preventing reduction of $CaMnO_3$ past the desired point. From this research project a successful way of synthesizing $CaMnO_3$ was achieved for future researchers. Ammonolysis can then be attempted again with varying times and temperatures, followed by trials of steps to produce the intermediate and final oxyfluorides.

An alternative, possibly improved approach that could be used to achieve $Ca_2Mn_2O_5F$ was hypothesized as this project was completed. This is a two-step approach involving first synthesizing $CaMnO_3$, and then reacting it with fluoride gas in a fluorination process to achieve the target compound. Fluorination has been used with other solid-state materials to incorporate mixed Mn^{3+}/Mn^{4+} ions by using anion substitution instead of cation substitution. In 2000 L.D Aikens *et al.* synthesized $LaSrMnO_4F$ by heating the sample in a 10%F_2/90%N_2 gas mixture for 2 hours at 200 °C[44]. Also in 2009 David A. Headspith *et al.* synthesized

$Ce_2MnN_3F_2$ by heating a sample in a nickel boat placed in a nickel or stainless steel tube, while the system was flushed with nitrogen as a temperature of 95-115°C was achieved.[45] At the required reaction temperature, the gas was switched to 10%F_2/90%N_2 and the sample was heated. The system was then flushed with nitrogen and cooled to room temperature. In both of these syntheses the reactions were carried out at low temperature and lower time frames in gas mixtures of 10%F_2/90%N_2. A disadvantage may be lack of control of stoichiometry, leading to an undesired product. Nonetheless, in the future a new research project can be attempted reducing the steps from four to two, including synthesizing $CaMnO_3$ and then fluorinating $CaMnO_3$ with a 10%F_2/90%N_2 to achieve $Ca_2Mn_2O_5F$. Hopefully with a faster synthesis plan that is successful, more time can be dedicated to investigating the possible magnetic properties that $Ca_2Mn_2O_5F$ may possess.

Project REEL Analysis

The results represent the first known preparation of the series of $K(Cu_xNi_{1-x})F_3$ and $K(Cu_xMn_{1-x})F_3$ phases for $0 \leq x \geq 1.0$. From these results it was shown that the sample colors and unit cell dimensions can be tuned by varying Cu vs. Ni/Mn content. The solubility of Cu in the $KNiF_3$ and $KMnF_3$ lattices and ranges of two-phase regions (cubic and tetragonal) that were observed in the $K(Cu_xNi_{1-x})F_3$ and $K(Cu_xMn_{1-x})F_3$ series were compared to the $K(Cu_xCo_{1-x})F_3$ series synthesized by a previous class and a $K(Cu_xMg_{1-x})F_3$ series published in the literature. Two general trends were discussed to account for the specific data indicating the maximum amount of Cu that can be dissolved in a cubic KMF_3 lattice before the tetragonal phase appears. These trends depend upon whether the cell parameter of the pure cubic phase is above or below an optimal interaction distance based on $KCuF_3$ cell parameters.

There is an abundance of future work that can be done related to this project. For example, one of the main problems to solve is to determine how to eliminate the impurities of KCl, KBr and fluoroclaringbullite in the precipitated fluorides. The KCl/KBr impurities could likely be eliminated with the addition of more solvent and longer times when filtering the final product. However, the only way to eliminate fluoroclaringbullite may be through a different synthesis approach, e.g. solid-state reaction of binary fluoride precursors.

Future work could also include deriving equations relating metal-fluoride bond lengths to cell parameters in order to estimate compositions of the tetragonal components of the mixed phase systems assigned in the refinements. At present these values cannot be determined. Other related future work could involve preparing samples with intermediate compositions such as $KCu_{0.55}Ni_{0.45}F_3$ or $KCu_{0.65}Ni_{0.35}F_3$ to better determine where exactly the tetragonal phase mixes with the cubic phase and when the compound contains only the tetragonal phase. As with all of the REEL projects, different metals can be mixed to determine what other phases can be prepared and what other colors can be formed. Finally, as a result of Project REEL, the general chemistry student participates gained experience in a variety of materials research techniques, as hopefully had a meaningful research experience as well.

References

1. Sun CC., *J Pharm Sci.* 2009 May;98(5):1671-87

2. http://mscunila.blogspot.com/2009_04_01_archive.html (accessed August 2011)

3. Hench, L., Jon K. West, *Chem. Rev.*, **1990**, *90* (1), pp 33–72

4. Jorge, M.E. Melo, Correia dos Santos, A., Nunes, M.R., *International Journal of Inorganic Materials* **3**, 915-921 (2001).

5. Barron, Andrew R., Smith, Carissa, *Crystal Structure* http://cnx.org/content/m16927/1.10/

6. Garland, C.W., *et al.* Experiments in Physical Chemistry 7th edition (2003)

7. http://www.nobelprize.org/educational/physics/x-rays/what-6.html (accessed October 2011)

8. Ramirez, A.P., *J. Phys: Condens. Mater.*, **9**, 8171-8194 (1997)

9. Rietveld,H.M.(1969). *J. Appl. Crystallogr.*,**2**,65-71

10. Shugar, Gershon J., Ballinger, Jack T., *Chemical Technicians' Ready Reference Handbook* (1996)

11. Zhou, Q. and Kennedy, B., *J. of Physics and Chemistry of Solids.,* **67**, 1595-1598 (2006).

12. Lufaso, M.W., Ph D. Dissertation, The Ohio State University, Columbus, Oh 2002

13. Cava, R.J. *et al.*, *Physical Review Letters.*, **58** 1676- 1679 (1987)

14. Kagata, H. and Kato, J., *Jpn. J. Appl. Phys.* **33** (1994) pp. 5463-5465

15. DiDomenico Jr., M. and Wemple, S.H., *Phys. Rev.* **166**, 565–576 (1968)

16. Yang, Z., Huang, Y., *et al. Materials Research Bulletin* **41** (2006) 274-281

17. http://www.iue.tuwien.ac.at/phd/dragosits/node14.html (accessed October 2011)

18. Dasu, Anita, M.S. Thesis, Youngstown State University, Youngstown, OH, Aug. 2008.

19. Dagotto, E. *et al.*, *Physics Reports* **344** 1-153 (2001)

20. Zener, Clarence, Phys. Rev. **82**, 403–405 (1951)

21. Double-exchange mechanism. (2011, October 29). In *Wikipedia, The Free Encyclopedia*

22. Aliaga, H., *et al*. *J. Physics: Condensed Matter, High temperature susceptibility in electron doped Ca1-xYxMnO3: Double Exchange vs Superexchange* (2002)

23. Anderson, P.W., *Physical Review* **79** (1950)

24. *Nature Chemistry* **2**, 362–368 (2010)

25. Needs, R.L., and Weller, M.T., *Journal of Solid State Chemistry* **139**, 422-423 (1998)

26. Berry, F.J., Ren, X., Heap, R., Slater, P., and Thomas, M.F., *Solid State Communications* **134** 621-624 (2005)

27. Tong, W*., et al*., *Chem. Mater.* **2009**, *21*, 2139-2148

28. Monesi, C., *et al*., *Physical Review B* **72,** 174104 (2005)

29. Poeppelmeier, K.R., *et al*. *Journal of Solid State Chemistry* **44** 89-98 (1982)

30. Longo, J.M., *et al*. *Mat. Res. Bull.* **13** 1359-1369 (1978)

31. Schaber, P.M. *et al. Thermochimica Acta* **424** 131-142 (2004)

32. Halperin, B.; Englman, R., Phys. Rev. B 3, 1698–1708 (1971)

33. Wagner, T.R. Research Experiences to Enhance Learning. Presented at Youngstown State University, Youngstown Ohio

34. Huheey, James E. <u>Inorganic Chemistry: Principles of Structure & Reactivity</u>, 3rd ed. Harper & Row, 1983

35. Towler, M.D., Dovesi, R., and Saunders, V.R., *Physical Review B*, **52**, 10150-10159 (1995).

36. Binggeli, N. and Altarelli, M., Physical Review B, 70, 085117-1 to 085117-10 (2004).

37. Brand, S.J., Hernandez, K.J., Ragan, N.A, Scheckelhoff, C.T., Tatebe, C.J., Wilson, S.M., Lovelace-Cameron, S.R., Wagner, T.R. and Zeller, M. QUEST conference poster April 2011

38. http://www.instruction.greenriver.edu/knutsen/chem150/allurard.html (accessed October 2011)

39. Langley, R.H., *Journal of Chemical Education* **61** (7) 1984

40. Bruker AXS, *TOPAS: General profile and structure analysis*. *software for powder diffraction data*. Karlsruhe; 2003

41. R. D. Shannon *Acta Cryst.* (1976) A32, 751-767.

42. Burns, P. C., Hawthorne, F. C., Hofmeister, A. M., Moret, S. L., *Phys. Chem. Minerals* **23** (1996) 141-150

43. Kusnic, Rachel, M.S. Thesis, Youngstown State University, Youngstown, OH, Aug. 2007.

44. Aikens, L.D., *et al. Chem. Commun.*, 2000, 2129–2130

45. Headspith, David A., *et al., Dalton Trans.*, 2009, 9273–9279